



**JIMMA UNIVERSITY
JIMMA INSTITUTE OF TECHNOLOGY
SCHOOL OF GRADUATE STUDIES
FACULTY OF MECHANICAL ENGINEERING
SUSTAINABLE ENERGY ENGINEERING STREAM**

**ENERGY POTENTIAL ASSESSMENT AND TECHNO-ECONOMIC
ANALYSIS OF MICRO-HYDRO INTEGRATED WITH PHOTOVOLTAIC
FOR RURAL ELECTRIFICATION: CASE STUDY OF GODA WARKE
VILLAGE**

A Thesis submitted to the School of Graduate Studies, Jimma University, Jimma Institute of Technology, Faculty of Mechanical Engineering in Partial Fulfillment of the Requirements for the Degree Master of Science in Sustainable Energy Engineering.

By
Ephrem Assefa Feyissa

July, 2022
Jimma, Ethiopia

JIMMA UNIVERSITY
JIMMA INSTITUTE OF TECHNOLOGY
FACULTY OF MECHANICAL ENGINEERING
SUSTAINABLE ENERGY ENGINEERING STREAM

ENERGY POTENTIAL ASSESSMENT AND TECHNO-ECONOMIC
ANALYSIS OF MICRO-HYDRO INTEGRATED WITH PHOTOVOLTAIC
FOR RURAL ELECTRIFICATION: CASE STUDY OF GODA WARKE
VILLAGE

A Thesis submitted to the School of Graduate Studies, Jimma University, Jimma
Institute of Technology, Faculty of Mechanical Engineering in Partial Fulfilment of the
Requirements for the Degree Master of Science in Sustainable Energy Engineering.

By
Ephrem Assefa Feyissa


July, 2022
Jimma, Ethiopia

DECLARATION

I declare that this research entitled “Energy Potential assessment and techno-economic analysis of Micro-hydro integrated with photo-voltaic for rural electrification: a case study of Goda Warke Village” is my original work and has not been submitted as a requirement for the award of any degree in Jimma University or elsewhere.

Ephrem Assefa Feyissa _____ 28/07/2022
Name Signature Date

As research Advisor, I hereby certify that I have read and evaluated this thesis paper prepared under my guidance, by, Ephrem Assefa Feyissa entitled “Energy Potential assessment and Techno-economic analysis of Micro-hydro integrated with Photo-voltaic for rural electrification: a case study of Goda Warke Village” and recommend and would be accepted as a fulfilling requirement for the Degree Master of Science in Sustainable Energy Engineering


Dr. Ing. Getachew Shunki Tibba
Main Advisor  _____ 28/07/2022
Signature Date

Mr. Tarekegn Limore (MSc.)
Co-Advisor _____ _____
Signature Date

JIMMA UNIVERSITY
JIMMA INSTITUTE OF TECHNOLOGY
FACULTY OF MECHANICAL ENGINEERING
SUSTAINABLE ENERGY ENGINEERING STREAM

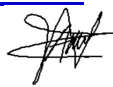
Approval sheet

This is to certify that thesis entitled “Energy Potential assessment and techno-economic analysis of Micro-hydro integrated with photo-voltaic” submitted by Ephrem Assefa to Faculty of Mechanical Engineering, Jimma Institute of Technology for the award of the degree of Master of Science in Sustainable Energy Engineering is carried out by him under our supervision. This thesis is being submitted having met all the requirements, and hereby approved.

<u>Dr. Ing. Getachew Shunki Tibba (PhD)</u>		<u>28/07/2022</u>
Main Advisor	Signature	Date

<u>Mr. Tarekegn Limore (MSc.)</u>	_____	_____
Co-Advisor	Signature	Date

Board of Examiners

<u>Dr. Abdulkadir Aman (PhD)</u>		<u>28/07/2022</u>
External examiner	Signature	Date

<u>Mr. Fikru Gebre (MSc.)</u>	_____	_____
Internal examiner	Signature	Date

<u>Mr. Abraha Kahsay (MSc.)</u>	_____	_____
Chairperson	Signature	Date

ABSTRACT

Rural areas have a high resource of hydropower energy generation system. However, using such systems has the seasonal changes and bad topographical position of the river flowing. Even though Ethiopia has abundant hydropower resources, the rural population has no access to electricity. The utilization of small-scale hydropower in rural areas of the country requires stream flow data of the rural Rivers. However, most of the Ethiopian rural River watersheds are ungauged and poorly monitored due to their remote location. This study focuses on energy potential assessment and techno-economic analysis of micro-hydro integrated with photovoltaic for rural electrification for a case study of Goda Warke village located in Yaya Gulele district. The diesel generator is added to the proposed system as a backup system. The Natural Resource Soil Conservation Service Curve Number (NRSCS-CN) technique is used to estimate the monthly discharge of the Girar River, which is located in the study area. An average Girar river discharge and solar radiation resource of the areas are $0.975\text{m}^3/\text{s}$ and $5.39\text{ KWh}/\text{m}^2/\text{day}$, respectively. The estimated load of the study village is $1269.79\text{ KWh}/\text{day}$. HOMER simulation shows that Hydro/PV/DG/Battery and Hydro/PV/Battery are the best optimum systems in terms of Net Present Cost (NPC). The hydropower potential in the optimum system is 338 KW , with an effective head of 50 m and a levelized cost of energy (LCOE) of $0.0057\text{ USD}/\text{KWh}$. Solar PV has a mean power output of $250\text{ KWh}/\text{day}$ with a LCOE of $0.049\text{ USD}/\text{KWh}$ and a PV penetration of 58.2% . Most of the electric load in the area is covered by micro-hydropower, with capacity factor of 47.5% . The diesel fuel price (DFP), pipe head loss, and village load growth are the sensitive variables on NPC and the cost of energy (COE). When DFP is $0.7\text{ USD}/\text{KWh}$, hydro/PV/battery is more economical with an NPC of $\$1.28\text{ million}$.

Keywords: *Discharge, Energy potential, Micro-hydro and Photovoltaic, Soil Conservation Service Curve number, Sensitivity variable.*

ACKNOWLEDGEMENT

Above all, I would like to acknowledge the Almighty God for his guidance and wisdom throughout my journey. I owe my deepest gratitude to my advisor, Dr. Ing. Getachew Shunki, and co-advisor, Mr. Tarekegn Limore, for their heartfelt advice and dedication to sharing their knowledge. I would like to thank you very much from the depth of my heart. I strongly admire your devotion to filling the generational knowledge gap. It was a great privilege for me to spend time with you, and I gained enormous experience. My most profound appreciation also goes to my friends and colleagues at Bule Hora University for their valuable comments and support. It is my utmost honour to show appreciation to all my lecturers who have made their tireless effort to put knowledge into practice for me during my study period at Jimma Institute of Technology. Last but not the least, I would like to express my deepest gratitude, humble respect, and special thanks to my parents for being with me all the time by moral.

Table of Contents

DECLARATION	i
ABSTRACT.....	iii
ACKNOWLEDGEMENT	iv
LIST OF FIGURES.....	ix
LIST OF TABLES.....	xi
ACRONOMYS	xii
CHAPTER 1	1
1. INTRODUCTION	1
1.1. Background of Study.....	1
1.1.1. Ethiopian Energy Demand Status	1
1.1.2. Small Scale Hydro-Power Development and Classification in Ethiopia.....	2
1.2. Statement of the Problem	3
1.3. Motivation of the Study.....	4
1.4. Objective	4
1.4.1. General Objective	4
1.4.2. Specific Objective.....	4
1.5. Scope of the Study.....	5
1.6. Significance of the Study	5
CHAPTER 2	6
2. LITERATURE REVIEW	6
2.1. Flow Rate Estimation of Ungauged River Catchment	6
2.2. Hydropower Energy Resource assessment of study area.....	7
2.2.1. Hydropower Resource of Study area.....	7
2.2.2. Design parameters of a MHP system	8
2.2.3. Discharge estimation of ungauged catchment using SCS-CN method	18
2.3. Solar Resource Assessment.....	20

2.3.1. Solar Resource potential of Ethiopia	20
2.3.2. Estimation of Monthly solar radiation on tilted surfaces	21
2.3.3. Optimum working condition and meteorology effect of study area on PV components of Hybrid System	24
2.4. Optimization methods of Hybrid Renewable Energy Power Generation System	27
2.4.1. HOMER Software Optimization Method	27
2.4.2. Algorithm Optimization using coding in MATLAB	29
2.5. Hybrid system components and Techno-economic analysis	30
2.5.1. Small Scale Energy Storage System	30
2.5.2. Photovoltaic Cell, Module, Panel and Arrays.....	31
2.5.3. Photovoltaic Costs	31
2.5.4. Hybrid components cost	32
2.5.5. System operation control mechanism	34
2.6. Economic feasibility analysis.....	35
2.6.1. Comparison of standalone hybrid system with grid-extension.....	37
2.7. Summary of Review of previous studies.....	38
2.8. Research gap	40
CHAPTER 3	41
3. METHODOLOGY	41
3.1. Location of Study Area	41
3.2. Research Design Process.....	42
3.3. Primary and Secondary Data collection	44
3.4. Materials and Tools.....	44
3.5. Load assessment of Study area.....	46
3.5.1. Load Assessment	46
3.5.2. Community Load.....	48
3.5.2. Study area load Profile	52

3.5.2.1. Electricity demand forecasting	52
3.5.2.2. Population and energy demand.....	53
3.5.2.3. Customer penetration.....	53
3.6. Discharge estimation flow chart of ungauged catchment of Girar River.....	53
3.6. Hybrid system connection schemes layout	55
3.6.1. Pre-HOMER analysis.....	55
CHAPTER 4	57
4. RESULT AND DISCUSSION	57
4.1. Rainfall intensity in study area (mm).....	57
4.2. Discharge estimation of Girar River	59
4.2.1. Stream order and stream networking	59
4.2.2. Analysis of Catchment area (Drainage area)	60
4.2.3. Hydrologic soil Group (HSG) of the catchments	63
4.2.4. Analysis of Slopes and contours	65
4.2.5. Monthly Stream flow rate estimation	66
4.3. Micro-Hydropower Potential of study area.....	69
4.3.1. Estimation Gross Head	69
4.4. Solar energy Potential assessment.....	70
4.4.1. Estimation of solar radiation	70
4.4.2. Mapping of solar radiation in study area	72
4.4.3. Estimation of optimum operating tilt angle and effects of ambient temperature on Photovoltaic performance.....	74
4.4.3.1. Tilt Angle	74
4.5. Economic assessment, Optimization and sensitivity analysis.....	79
4.5.1. Optimized Simulation Results	79
4.5.1.1. Hydropower Output.....	82
4.5.1.2. Photovoltaic power Output.....	82

4.5.1.3.	Diesel Generator output	83
4.5.1.4.	Storage system output	84
4.5.1.5.	Convertor power Output.....	85
4.5.2.	Sensitivity Analysis	86
CHAPTER 5	90
5.1.	Conclusion.....	90
5.2.	Recommendation.....	91
Reference	92
Appendix-A: Load Assessment and calculated Meteorological data	102
Appendix-B: Software simulation inputs and analysis flow process.....		118

LIST OF FIGURES

Figure 2.1: Location of Girar River, source [https://elevationmap.net/lemi-yaya-gulele].	8
Figure 2.2: Location of suitable area for hydro power generation system on Girar River.	9
Figure 2.3: Moody diagram[53].	10
Figure 2.4: Net head remained after pipe losses [54]	11
Figure 2.5: Micro hydro Turbine selection chart [60].	14
Figure 2.6: Efficiency of various turbines based on discharge [63].	16
Figure 2.7: PV demand in Ethiopia[68].	21
Figure 2.8: Extra-terrestrial solar radiation on horizontal surface through a year.	22
Figure 2.9: Photovoltaic cells, modules, panels and arrays [81].	31
Figure 2.10: Simulink model for hybrid system [31]	34
Figure 3.1: Location map of study area.	41
Figure 3.2: Research Design and process flow chart	43
Figure 3.3: Types of Software tools employed in this work.	44
Figure 3.4: Flow chart of HOMER software analysis.	45
Figure 3.5: Load profile of Study area.	52
Figure 3.6: Flow chart of discharge estimation in ungauged catchments.	54
Figure 3.7: Connection schemes of hybrid system	55
Figure 3.8: Schematic representation of proposed hybrid system by HOMER pro.	56
Figure 4.1: Recorded rainfall amount in Yaya Gulele district from 2012-2018.	57
Figure 4.2: Estimated Average rainfall amount in steady area	58
Figure 4.3: Potential Evapo-Transpiration amount in mm	59
Figure 4.4: Stream ordering and flow direction of rivers and streams in study area.	60
Figure 4.5: a) Degree of basin catchments in study area b) catchment area of Girar and Aleltu River.	61
Figure 4.6: Land Use Land Cover classification of Girar River Catchment	62
Figure 4.7: Hydrologic soil group in Girar catchments	64
Figure 4.8: Elevation and Contours passing through the catchment	65
Figure 4.9: Estimated discharge of Girar catchments.	67
Figure 4.10: Flow duration curve based on rank order technique	68
Figure 4.11: Gross head measurement using contour lines based on DEM.	69
Figure 4.12: Variation of Sunshine hour in months of the year.	70
Figure 4.13: Solar radiation components of tilted surface.	71

Figure 4.14: Monthly average Global solar radiation of study area.	72
Figure 4.15: Areal solar radiation distribution of Yaya Gulele district in 2021.....	73
Figure 4.16: The optimum tilt angle in shiny season of the year.....	74
Figure 4.17: The Optimum tilt angle in rainy and partially cloudy seasons of the year.....	75
Figure 4.18: Power loss due to increase in cell temperature.....	76
Figure 4.19: Power loss variation with cell temperature and tilt angle.	77
Figure 4.20: Power loss of PV module with variation of tilt angle at constant wind speed	78
Figure 4.21: a) Optimal system type at DFP=0.5 \$/KWh and b) at DFP = 0.07\$/KWh	80
Figure 4.22: AC primary load in peak month (July).....	80
Figure 4.23: Electricity production of a) Micro-Hydro/PV/DG and b) Micro-Hydro/PV System through months in a year.....	81
Figure 4.24: Hydropower production capacity in days of the year.....	82
Figure 4.25: Electric energy production by PV system through days in a year.....	83
Figure 4.26: Scatter plot of relation between PV power output with Global irradiance	83
Figure 4.27: Diesel generator Power output throughout the year.....	84
Figure 4.28: Diesel fuel consumption in L/hr.....	84
Figure 4.29: Operating time of Diesel Generator	84
Figure 4.30: Charging and discharging time of the battery system	85
Figure 4.31: Bi-directional convertor system operating profile.....	86
Figure 4.32: Optimal system plot superimposed with RF at a diesel fuel price of 0.7 \$USD/L	87
Figure 4.33: Surface plot of hydro efficiency versus other sensitivity parameters, superimposed with COE, at DFP of 0.5 \$/KWh.....	87
Figure 4.34: a) Hydro/PV/DG/Battery cost summary by components b) Cash flow	88
Figure 4.35: Comparison of Grid extension with the Optimum system	89

LIST OF TABLES

Table 1.1: The nature of household's dependent on lighting source other than national grid electricity [7].	2
Table 1.2: Hydro power classification in Ethiopia[9].	3
Table 2.1: Turbine type and typical net head range [35].	13
Table 2.2: Range of specific speed [33][37].	15
Table 2.3: Selection of Generator type [40].	17
Table 2.4: Solar radiations calculated from meteorology data at the sunshine hour of Goda Warke village for horizontal surface.	23
Table 2.5: Calculated long term Beam, diffuse and diffuse-reflected radiation of study area on tilted surface.	24
Table 2.6: Parameters of loss calculation for the PV system.	26
Table 2.7: Less expensive and affordable solar panel in market of 2021[68].	32
Table 2.8: Costs and specification of hybrid components	33
Table 3.1: Household electric demand estimation.	48
Table 3.2: Estimated electric demand for small clinic and business centre.	49
Table 3.3: Estimated load demand of school sectors	49
Table 3.4: Estimated load of other community sectors.	50
Table 3.5: Load consumption profile	51
Table 3.6: Sensitivity variables with assigned values.	56
Table 4.1: Percentage of Land use and land cover classification of catchment area	63
Table 4.2: Percentage of Soil type and HSG classification of catchment area.	63
Table 4.3: LULC percentage of Girar River Catchment and corresponding HSG with curve number.	64
Table 4.4: Flow rate arrangement in ascending order and ranking.	67
Table 4.5: Optimum tilt angle of months with the maximum irradiance that can be absorbed.	75
Table 4.6: Optimized output category of simulation	79
Table 4.7: summary of converter system	85

ACRONOMYS

AC	Alternative Current
ACC	Annual Capital Cost
ANN	Artificial Neural Network
AOC	Annual Operation and Maintenance Cost
ARC	Annual Replacement Cost
ArcGIS	Aeronautical Reconnaissance Coverage Geographic Information
ASRTM	Automatic shuttle radar topographic mission
BGED	Breakeven Grid Extension Distance
CFL	Compact Fluorescence
CN	Curve Number
COE	Cost of energy
CRF	Capital Recovery Factor
DC	Direct Current
DEM	Digital Elevation Model
DFP	Diesel Fuel Price
DG	Diesel Generator
EEP	Ethiopian Electric Power
EES	Engineering Equation Solver
ERDAS	Earth Resource Development Assessment System
ESS	Energy Storage System
FDC	Flow duration curve
FTC	Farmer training centre
GIS	Geographic Information System
GTP	Growth and Transformation plan
HES	Hybrid Energy System
HOMER	Hybrid Optimization of Multiple Electric Renewable
HPBS	Hybrid Pumped Battery Storage
HRES	Hybrid Renewable Energy System
HSG	Hydrologic soil Group
IES	Integrated Energy Storage System
KVA	Kilovolt Ampere
KWP	Kinematic Wave Parameter
LCC	Life Cycle Cost

LCOE	Levelized cost of energy
LED	Light Emitting Diode
LULC	Land Use and Land Cover
MIPM	Medium irrigation project methods
MoWE	Ministry of Water and Energy
NASA	National Aeronautics and Space Administration
NEP.2	National Electrification Programme.2
NGO	Non-Governmental Organization
NMA	National Meteorological Agency.
NOTC	Nominal operating cell temperature
NPC	Net Present Cost
NREL	National Renewable Energy Laboratory
NRSCS	Natural Resource and Soil Conservation Service
NSGA	Non-dominated Sorting Genetic Algorithms
NSWOA	Non-dominated Sorting Whale Optimization Algorithm
O&M	Operation and Maintenance Cost
PET	Potential Evapo-Transpiration
PHS	Pumped Hydro-Storage
PID	Proportional Integrative and Derivative
PSO	Particle Swarm Optimization
PV	Photo-voltaic
RF	Renewable Fraction
SAC	System Annualized Cost
SCS	Soil Conservation Service
SFF	Sinking Fund Factor
SOC	State of Charge
SRTM	Shuttle Radar Topographic Mission
SSA	Sub-Saharan Africa
STC	Standard Test Condition
SWOT	Surface Water and Ocean Topography
USD	United states dollar

CHAPTER 1

1. INTRODUCTION

1.1. Background of Study

For a long time, water dropping from a great height has been used as a source of energy. Waterwheels were frequently employed with the discovery of hydro turbines at the turn of the nineteenth century. It is the world's oldest renewable energy technology for converting mechanical energy and generating electricity. Hydropower has been a well-known power production technique since the invention of hydraulic turbines in the 19th century [1]. Through delivering material-assisted education, health centres, and reducing indoor air pollution, modern energy access contributes to national growth strategies, income-generating initiatives, and environmental sustainability.

Most rural areas, especially those with flowing river systems, have hydropower energy potential. However, the major drawbacks of using such systems are seasonal shifts and poor topographical positioning of river flowing basins. When there is shortage of rain in the winter, the water flow is low, and the hydropower plant produces little energy while PV is the inverse [2]. However, because of its flexibility, hydro power can be used to replace fluctuating photovoltaic (PV) power [3]. The combination of hydro power plants and solar PV power plants is considered as an efficient and promising power generation approach for rural electrification [4].

1.1.1. Ethiopian Energy Demand Status

Electricity access varies substantially between urban and rural locations in Ethiopia. Electricity is available to 87 percent of the population in urban areas, but less than 5 percent in rural communities, which is incredibly low. Although electricity is frequently delivered more in urban areas, 83 percent of the country's population lives in rural areas, which performs heating, lighting and cooking activities by traditional utilization of biomass energy sources [5].

Ethiopia's energy sector continues to rely significantly on traditional way using biomass energy because of inadequate supply of electricity to fulfill expanding demand. Forecasting energy demand for a long-term is crucial for directing the country's energy supply system growth plans. The most challenging task facing Ethiopia is providing basic power to the rural

communities households located at a distance of more than 7 Km from the national power grid that do not have access to electricity [5][6].

Non-grid-based households are divided into three distinct groupings based on their proximity to national mid-voltage lines. These are short-term household, mid-term households and long-term off-grid households. These groups provide a clearer insight into the types of off-grid solutions which may be appropriate for some groups of households that rely on their ability to pay, based on non-grid lighting sources [7]. The national electrification coverage rate of Ethiopia is less than 20%. The lowest rating of connection charges for grid electricity is between USD 50 up to USD 100 [8]. This is an average pre-electrification fee collected from customers for grid electrification method.

Table 1.1: The nature of household's dependent on lighting source other than national grid electricity [7].

Group	Distance from national medium voltage grid lines	Year to be connected	Percent of national households	households dependent on non-grid lighting sources
Short term	2.5 km	2025	31 %	45 %
Mid term	2.5-25 km	2025-2030	36%	52 %
Long term	>25 km	More than 2030	2%	3 %

1.1.2. Small Scale Hydro-Power Development and Classification in Ethiopia

Small-scale hydropower accounts for 10% of Ethiopia's hydropower potential. Due to inaccessibility, topographical position and the proximity to the grid and service facilities, the potential for the technological viability is reduced by more than half to around 5 %. The government is focusing on the expansion of massive hydropower to fulfil the nation's energy requirements. Therefore, because of these factors, hydro power potential in the country was not exploited much [9].

The hydropower generating classes range from larger power plants that deliver electricity to many consumer groups, including industries and businesses, to small-scale and micro power plants for a small number of villages or homes. Although there are different criteria for classifying hydroelectric power plants in different countries, there is currently no international standard [1][9]. Ethiopia has a hydropower system classification scheme that differs from other countries as shown in Table 1.2.

Table 1.2: Hydro power classification in Ethiopia[9].

Terminology	Capacity	Unit
Large	>30	MW
Medium	10-30	MW
Small	1-10	MW
Mini	501-1000	KW
Micro	11-500	KW
Pico	≤ 10	KW

1.2. Statement of the Problem

Even though Ethiopia is abundant in renewable energy resources, a lack of energy supplies in rural areas of Ethiopia has become a serious problem. The main reason is that, the location of these areas from the national grid and the sparsely populated community living there. In addition, the high cost of transmission and very low load factor in those areas are not able to support extension of the national grid because of the economic capacity of the country[10].

In rural area, 90% of households energy demand is covered by energy sources like fuelwood, cow dung for cooking, heating, and kerosene lamps for lighting, which causes problems associated with health risks and environmental impacts such as deforestation due to demand of firewood and charcoal [7].

The Ministry of Water and Energy (MoWE) of Ethiopia established National Electrification Programme 2 (NEP.2) with the motto of “Lighting to all” in 2019 for remote area electrification [11] based on available renewable resources in the area [12] such as; Solar photovoltaic, Small scale wind turbines, Biogas, and Small scale hydro-power. However, the energy resource potential in remote area needs further study Since, there is no adequate organized stream flow data of rural Rivers which is a challenge for potential assessment and techno-economics study [13]. Most of the Ethiopian rural River watersheds are ungauged and poorly monitored due to their remote location [14]. The utilization of small-scale hydropower in rural areas of the country requires stream flow data of the rural Rivers.

Goda Warke village is one of rural community, which does not have electricity access and depends on the traditional energy source. The village was well known by burning of charcoal as the main sources of energy and income in Yaya Gulele district.

Considering those bottlenecks, Micro-hydro/PV hybrid system is proposed in this work as a possible means of power generation system in a case study of Goda Warke village through a detailed assessment of the renewable energy resource potential in the area.

Girar River is located in Goda Warke Village at a distance of 1 km which is considered as a hybrid system with Photovoltaic (based on solar radiation resource of the area) to meet the energy access shortage of the Village. In addition, the proposed system plays a vital role by providing feasible evidence for the MoWE of Ethiopia to achieve a rural electrification program, considering the study area.

1.3. Motivation of the Study

The motive of this research is to address a full access of information and pre-feasibility study document concerning renewable energy resource potential (RERP) and economic analysis, for Ministry of water irrigation and Energy (MoWE) of Ethiopia to achieve the planned Rural electrification programme. It is also, used to give feedback for NGO's and other Volunteer Organization interested in the implementation of the proposed system for the undeserved rural communities of Goda Warke village in Yaya Gulale district. Furthermore, the recent growth in the availability of climate-related and donor funding for low carbon and Climate Resilient Green Economy (CRGE) that emphasizes renewable is one of the study's primary motivators [15], [16].

1.4. Objective

1.4.1. General Objective

The main objective of this study is Energy potential assessment and techno-economic analysis of micro-hydro integrated with photovoltaic for rural electrification: a case study of Goda Warke village.

1.4.2. Specific Objective

- ✓ To estimate discharge for ungauged Girar River.
- ✓ To assess solar energy and hydropower potential of the study area based on meteorological parameters.
- ✓ To analyse the effects of tilt angle variation with the ambient temperature of the study area on the performance of the PV system based on respective losses.
- ✓ To perform sensitivity analysis of the optimum system compared to grid extension-related costs linked with NPC and LCOE generation.

1.5. Scope of the Study

The scope of this study is limited to determining energy resource potential and economic assessment of micro-hydro power and PV system combinations in the form of hybrid configurations for a case study of Goda Warke village in Yaya Gulele district. The thesis includes energy (load) demand assessment through data collection during a field survey and investigates the feasibility of the proposed system to achieve the desired purpose in the selected study area based on the meteorological data collected from NMA. The proposed system is sized for load consumption of 1269.79 KWh/day, which has the capacity to electrify 411 households with an average of 4 occupants per household.

In addition, this study analyses relevant parameters to assess the energy potential of hybrid micro hydro/PV systems and recommends necessary actions and measures that configure a system for MoWE to achieve the national rural electrification plan in addition to providing relevant data to accommodate the current and near future electrical energy demand for the village.

1.6. Significance of the Study

The significance of the study is to provide comprehensive information for EEP, MoWE, NGO's and other volunteer organizations on the hybrid renewable energy systems such as micro-hydro and photovoltaic to electrify the rural community of Goda Warke village that has lack of electricity due to location distance from the national grids. This work is a possible solution reference by utilization of solar and hydro energy sources for the electrification of the community of the remote area. In addition, it plays a vital role as a solution to reduce deforestation in the area due to wood fuel and charcoal demands, which are the major causes of climate change and global warming.

The study also provides scientific facts that, the available potential of energy resource in the study area can drastically change the life quality by decreasing indoor air pollution due to the burning of dry cattle dungs, woods for cooking and kerosene for lighting purpose.

CHAPTER 2

2. LITERATURE REVIEW

The previous works are revised and compared in this section, based on the methodology and findings obtained. Flow rate estimation methods, utilized software, methodologies and results of different literatures has been revised to identify research gaps in literatures in order to put the direction to reach on the best results and outcomes of this study. Stream flow estimation is the beginning step in energy potential assessment of ungauged river. The summary of the literatures and the research gaps obtained in the literatures was discussed at the end of this section.

2.1. Flow Rate Estimation of Ungauged River Catchment

Estimation of peak discharge in the selected ungauged river basins can be determined by using three important geomorphic-based hydrological models as manning's equation, kinematic wave parameter (KWP), and SCS curve number (CN) method. [Suwendu Roy et al., \[17\]](#), Estimated the peak flood discharge of the Kunur River Basin, a major tributary of the Ajay River in the lower Gangetic plain using those techniques. They found that the peak discharge during flood season based on daily rainfall data is 239.44, 204.08, and 146.52 using manning's equation, kinematic wave parameter (KWP), and SCS curve number (CN) method, respectively.

[Umuru Garba \[18\]](#) assessed the hydro power potential of the ungauged river of Rukarara and Mushishito in the southern province of Rwanda, using flow data of an analogue site to generate the data of an ungauged river. Characterization and delineation of catchments were done by GIS technology based on elevations, land uses, and rainfall and soils types of the site. He developed a contour map of the study area and proposed position of the component of a hydro-power plant with the net available head using Digital Elevation Model in ArcGIS and topographic map respectively.

The estimate for Po and Sacramento Rivers discharge has been investigated by [H. Oubanas et al., \[19\]](#) using a variation of the traditional variational data assimilations method called "4D-Var" from simulated observed surface water and ocean topography (SWOT) satellite missions. Synthesizing SWOT data products, which have an estimated height and width increase of 200 m along river central lines, vectorises simulated radar returns. Simulated SWOT data generally led to local improvements in pre-bathymetry and roughness estimates allowing river discharge

prediction in times of overpassing, with average relative root-squared error of 12.1% and 11.2%. However, equality issues arising from simultaneous estimates of bed lift and ruggedness may prevent their use for various applications except for the estimated discharge under the present framework.

Many literatures discussed that the Catchment Area Ratio, Rational CIA and the NRSCS-CN are the most commonly used methods for runoff estimation in ungauged basin. However, Rational CIA method is used for relatively small drainage areas less than 1 square miles. In addition this method assumes, the rainfall is distributed uniformly over the drainage area and there is no appreciable storage of water such as reservoirs and impoundments in the drainage area [20].

Catchment area ratio (CAR) method estimates the flow in ungauged catchment where a nearby catchment is gauged and present for use as a reference. Even though it's easy and simple techniques, it assumes the rainfall amount in the nearby catchment as similar intensity [21]. The Majority of literatures used NRSCS-CN due to its feasible and best method of estimation and it is applicable to a wide variety of condition that can be adapted to a number of different situations. NRSCS-CN method is the most robust model that can be used in almost any watershed.

NRSCS-CN method is employed for this study to estimate monthly stream flow of Girar River for the purpose of micro-hydro power generation, considering soil types of the river catchment and hydrologic soil group (HSG) they fall in. The land use and land cover (LULC) of the river catchment is also analysed in ERDAS Imagine and ArcGIS software to determine the weighted CN value.

2.2. Hydropower Energy Resource assessment of study area

2.2.1. Hydropower Resource of Study area

Girar River is the small river located in North shoa crossing through two districts Girar Jarso and Yaya Gulele district respectively. The community living around the river uses it, for irrigation and other purpose. It's located at less than 1 km from the study area Goda warki village to east direction. In this work, micro-hydropower energy generation potential of this river is assessed integrating with photovoltaics to determine the capacity of energy resource in the area for fulfilling energy demand of the selected study Village.

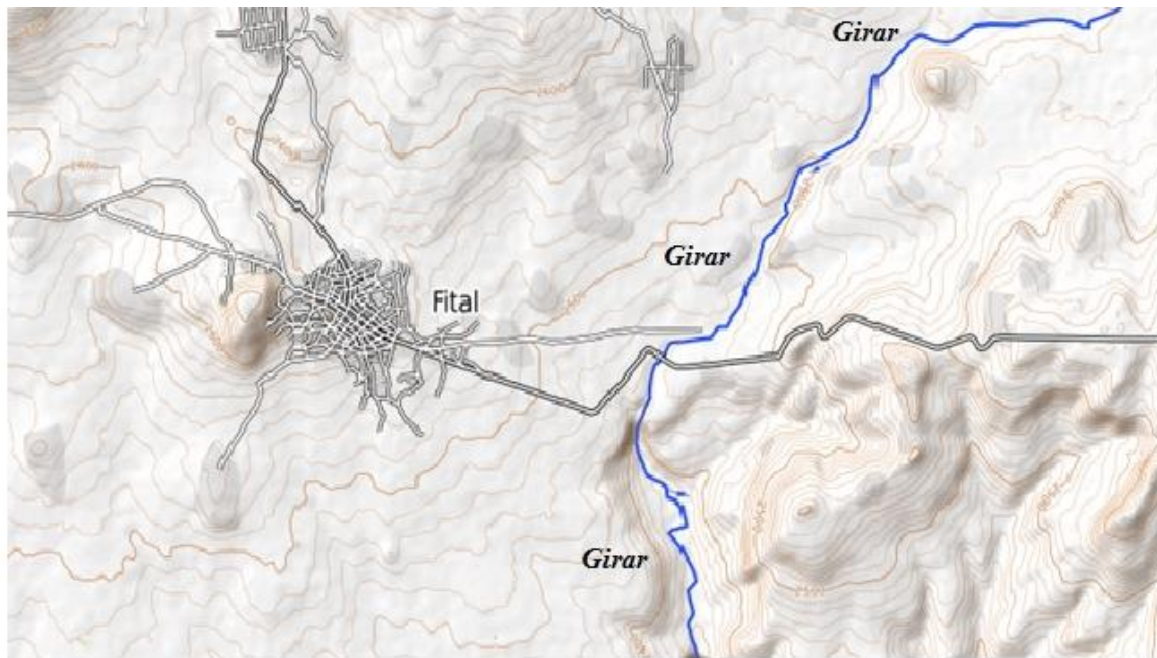


Figure 2.1: Location of Girar River, source [<https://elevationmap.net/lemi-yaya-gulele>].

2.2.1.1. Annual rainfall amount

The study area's elevation varies from 1500 to 2760 meters above sea level. There are two rainy seasons: Belg (February - April) and Meher (June - September). The average annual rainfall ranges from 1400 to 1600 mm, whereas an average annual temperature is from 15 to 19 °C. The climatic conditions of Woreda is classified as 28% High land, 41% mid land and 31% Desert [[22](#)][[23](#)].

2.2.2. Design parameters of a MHP system

2.2.2.1 Head Measurement

The head is the vertical height in meters between the levels at which water enters the penstock and the level where the water leaves the turbine housing (tailrace). The more the head, the quicker the waterfalls and the higher the pressure on the turbine blades. Altimeter, GPS and topographic maps are used to estimate the vertical drop of a stream. Counters generated on topographic maps are employed in this work to determine the net head at the study site.



Figure 2.2: Location of suitable area for hydro power generation system on Girar River.

2.2.2.2. Gross Head and Effective Head

The gross head is an available head to generate power, obtained using topography map after contour generation. The essential available resources, such as head and water volume, are assessed using topography and demographic data [24][25]. The other method is slope calculation, where only an elevation value is assigned to a cell, in which the discharge meets the selection criteria for a river. This provide separate River DEM containing the slope of each cell that gives actual river [26].

Effective head is less than the gross head as shown in Figure 2.4 due to the pressure losses in the penstock. There are different methods for calculating the frictional losses in pipes but Darcy-Weisbach formula is considered as the most accurate pipe friction loss formula [27][28]. The Darcy Weisbach formula is as follows;

$$h_f = f \left(\frac{L_p}{D_p} \right) \left(\frac{v^2}{2g} \right) \quad (2.1)$$

Where h_f = head loss due to friction L_p is pipe length, D_p is pipe diameter, v is flow velocity in m/s and g is acceleration due to gravity whereas f is a dimensionless friction factor known as the Darcy friction factor.

This friction factor can be obtained through various theoretical calculations or charts known as Moody diagrams, named after L.F. Moody and so the factor is sometimes called the Moody friction factor [29]. Moody charts link several key factors that contribute to the overall frictional losses in the system and these are the Reynolds number and the relative roughness.

Reynolds number R_e is defined as

$$R_e = V \times \frac{D_p}{\nu} \quad (2.2)$$

where V is mean speed of flow [m/s]

D_p is nominated characteristic length of the system (in the case of a hydropower penstock, the diameter),

ν is the kinematic viscosity of water = 1.004×10^{-6} (m²/s)

The energy balance is maintained in a pipe (penstock) but energy will be lost in proportion to the inner surface of the pipe as defined by the Reynolds number. The value of the Reynolds number therefore depends on the temperature of the water, the site conditions, the penstock diameter and the water flow which can be calculated from values of V (measured mean speed of the water), D_p (measured diameter of the penstock) and kinematic viscosity of water ν .

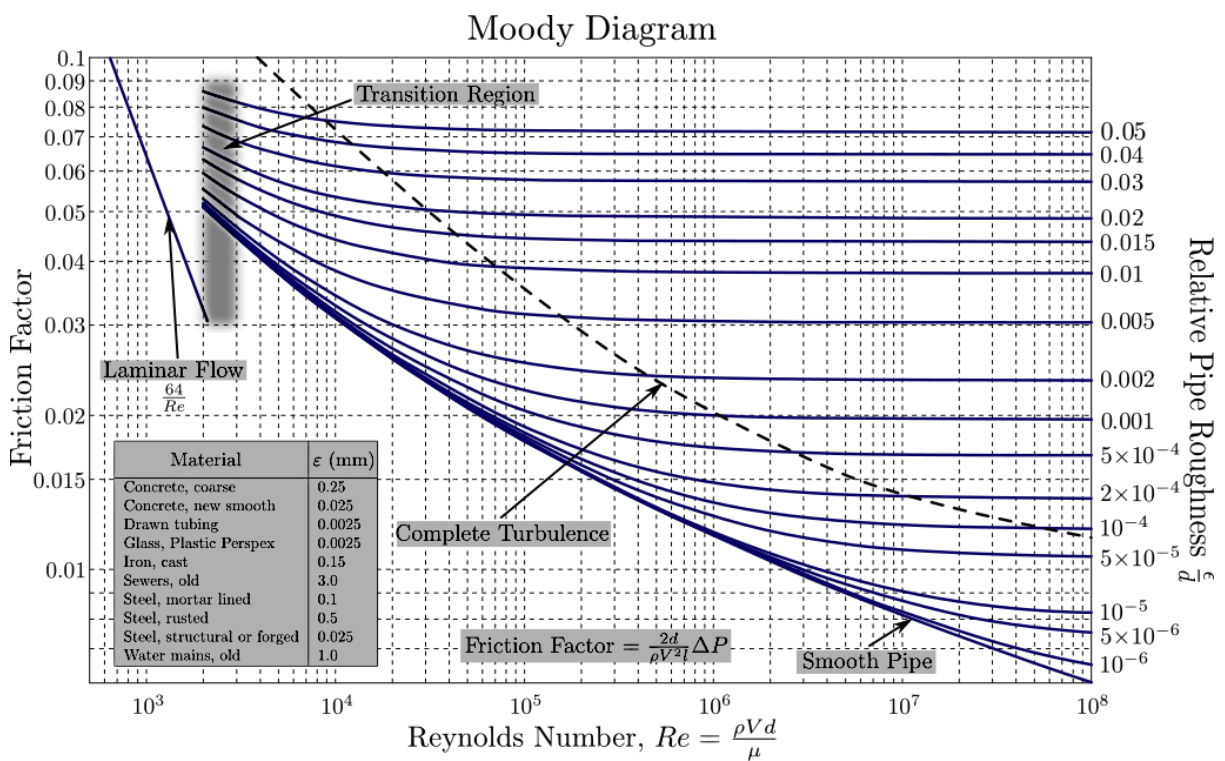


Figure 2.3: Moody diagram[29]

The Moody chart can be split into two flow regimes; laminar and turbulent. Laminar flows occur for values of Reynolds number less than 2000 and this is unlikely to occur for water flow. Instead, water flow is most likely to be turbulent and this occurs for values of Reynolds number in excess of 3000. Both the friction coefficient and the Reynolds number must be determined to calculate the head loss. The friction coefficient depends on the surface roughness height (e) of the pipe relative to the diameter of the pipe (D_p). The friction coefficient can be calculated using the "Moody Diagram" after the relative roughness is determined.

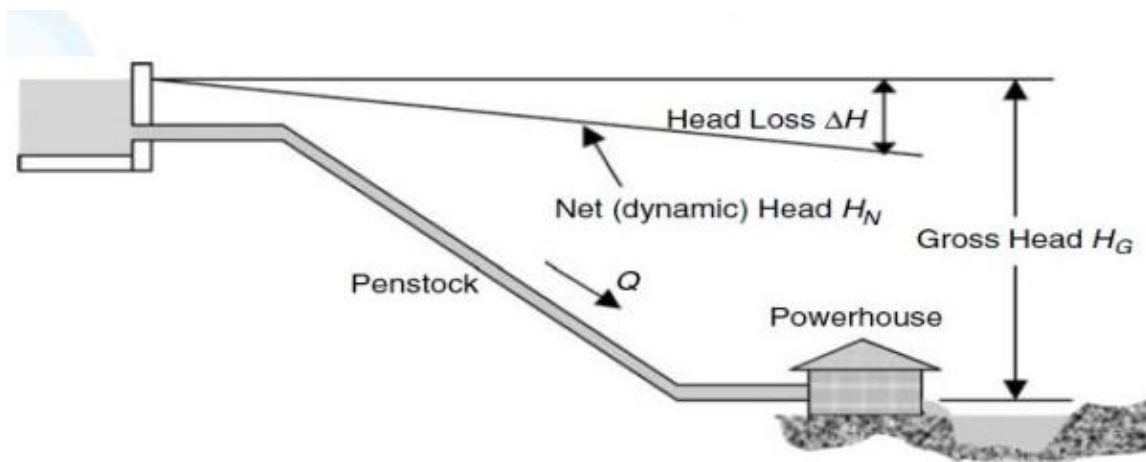


Figure 2.4: Net head remained after pipe losses [30]

2.2.2.3. Calculation of Potential Power

The potential power that can be generated by the micro hydro power plant is frequently assessed based on the site study [31]. The power output of the stream can be estimated using net head and flow measurements. According to equation (2.3), the power created by the available water is proportional to the flow rate of the water, height head (the difference in elevation between the intake and outlet of the water), gravity force, density of water, and efficiency of the hydropower system.

$$P_h = \rho \times QgH_n \quad (2.3)$$

The turbine power derived from hydraulic power is given by

$$\text{Turbine power (KW)} = P_h \times \eta_t \quad (2.4)$$

Where ρ is water specific density [kg/m^3]

Q is flow rate or quantity of water flowing into turbine [m^3/s]

g is gravitational constant [m^2/s]

H_n is net head [m]

η_t is turbine efficiency.

The turbine power output is directly proportional to river flow and the vertical distance that the water falls. Theoretically, a river with twice the amount of flowing water should produce twice much energy, but in reality, there is pipe loss due to the friction of pipes, which decreases the output power. However, there will be some loss of power while the hydropower plant converts the available water energy.

2.2.2.4. Penstock Design

Penstocks pipes conveys water from the diversion weir to the powerhouse. The penstock pipe length, flow rate and gross head are often used to calculate the internal diameter of the penstock (D_p) as shown by equation (2.5) [32].

$$D_p = 2.69 \times \left(n_p^2 \times Q^2 \times \frac{L_p}{H_g} \right)^{0.1875} \quad (2.5)$$

Where

n_p Manning's coefficient of the penstock material type

L_p Penstock length in (m)

H_g Gross head in (m)

The penstock wall thickness is determined by the tensile strength, pipe materials, operating pressure, and pipe diameter. The minimum acceptable wall thickness [33] in millimetre is given by:

$$t_p = \frac{D_p + 508}{400} + 1.2 \text{ (mm)} \quad (2.6)$$

Where t_p minimum penstock thickness in

400 represents tensile strength of welded string

1.2 represents corrosion allowances

2.2.2.5. Selection of Hydraulic Turbine

The type and size of a turbine for a hydropower system differ for one project than the other depending on many factors. Therefore, using these factors as criteria, the type and size of turbine for a particular hydropower system can be determined.

a. Turbine Selection Criteria

The characteristics of any specific site profoundly influence the type, design, and size of the turbine. These important criteria are described as follows:

i. Net Head

The net head is the necessary factors to consider for selecting suitable turbine. In low-head designs, where significant discharges must be managed, the selection is very important. For estimating head values, contour maps are quite useful. If a height of point's needs to be calculated overlapped with contour, the elevation of that contour is the best estimate of the point's elevation. However, if the location lies between contours, linear interpolation can be employed to get the approximated elevation [34].

Table 2.1: Turbine type and typical net head range [35].

Turbine type	Head Range (m)
Kaplan and propeller	$2 \leq H_n \leq 40$
Francis	$25 \leq H_n \leq 350$
Pelton	$50 \leq H_n \leq 1300$
Crossflow	$5 \leq H_n \leq 200$
Turgo	$50 \leq H_n \leq 250$

ii. Quantity of Flow volume and Discharges through the Turbine

In order to identify the set of turbine types appropriate to the flow environment of a site, the flow regime, rated flow, and net head must be known. One option for determining the appropriate turbine types is to employ graphical tools that demonstrate the appropriateness of various turbine designs in terms of head, flow volume, and power output. Figure 2.5 depicts the approximate range of head, flow, and power for several turbine types. This is an approximation based on each manufacturer's precise design.

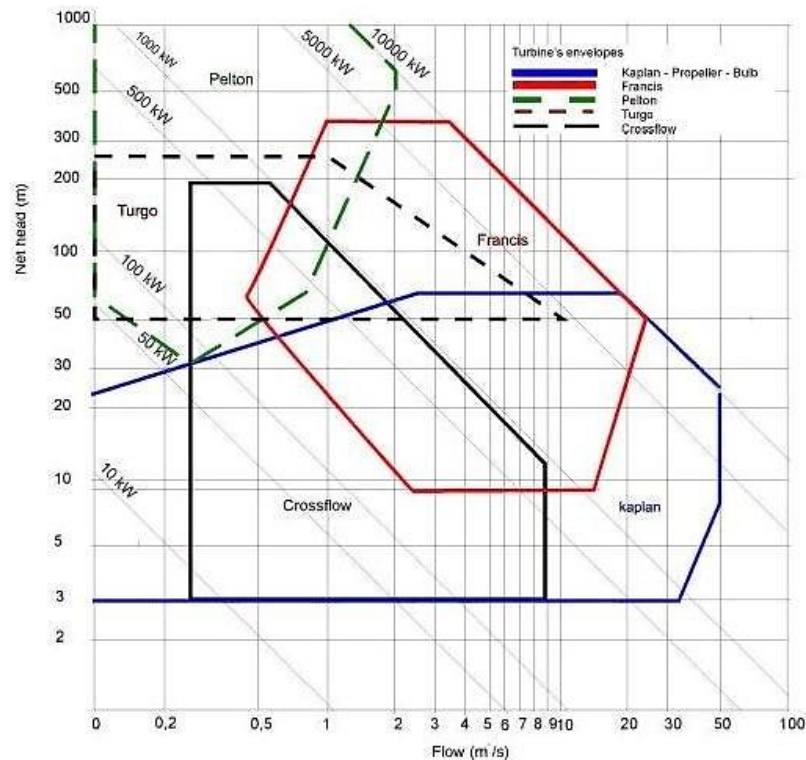


Figure 2.5: Micro hydro Turbine selection chart [36].

Figure 2.5, shows that a propeller turbine is suited for low heads and large flow rates. Cross-flow turbines are suitable for flows of $0.25 \text{ m}^3/\text{s}$ up to $5 \text{ m}^3/\text{s}$, net heads ranging from 3m to 200m, and output power of up to 500 kW. Francis turbines are suitable for flow rates ranging from $0.25 \text{ m}^3/\text{s}$ to $20 \text{ m}^3/\text{s}$, net head ranging from 10m to 300m, and power output ranging from 100kW to 10MW. Pelton wheels are suitable for flows up to $2 \text{ m}^3/\text{s}$, net heads ranging from 30m to 500m, and power output ranging from 50 KW to 10 MW.

All turbine types overlapped on the specified functioning zone suitable for the individual application. Before coming to a decision on which kind to employ, it will be required to calculate installed power and electricity production against costs. It should be noted that "envelopes" differ from manufacture to manufacturer and should only be used as a reference.

ii. Specific speed (Ns)

Specific speed of turbine is a speed of an ideal, geometrically similar turbine, which yields one unit of discharge for one unit of head. Given a flow and head for a specific hydro site, and the rpm (revolution per minute) requirement of the generator it becomes easy to calculate the specific speed. Through comparing the determined net head and specific speed to those in Table 2.2, the turbine type can be selected.

The specific speed is a reliable criterion for choosing the turbine. If it's required to produce electricity in a scheme with H_n (m) net head, using a P (kW) turbine directly coupled to a standard N (rpm) generator we should begin by computing the specific speed according to equation (2.7) .

$$N_s = N \times \frac{\sqrt{P}}{H_n^{1.25}} \quad (2.7)$$

Where N_s is turbine specific head

N is running speed of the turbine (rpm)

H_n is net head (m) and

P is power to be generated in (KW)

After computing the specific speed, it is possible to choose which turbine type to use or to decide whether to use a speed increaser like belts and gears. Using all this tools one can have appropriate selection of the turbine that is to be used for the site at hand.

Table 2.2: Range of specific speed [33][37].

Turbine type	Specific Speed range
Pelton one nozzle	$5 \leq N_s \leq 25$
Pelton two nozzles	$7 \leq N_s \leq 35$
Pelton four nozzles	$10 \leq N_s \leq 50$
Cross-flow (Banki-michell)	$20 \leq N_s \leq 50$
Francis	$50 \leq N_s \leq 350$
Kaplan and propeller	$200 \leq N_s \leq 1550$

To produce a constant frequency from a generator powered by a water turbine, the turbine must run at a constant speed and drive the generator via a set gear ratio. A governor controls the speed of the water turbine by opening and closing a valve or gate to keep the speed constant as the load varies. By adjusting the gate position, both mechanical and electrical hydraulic governors are employed to control the flow of water through the turbine [38].

iii. Turbine Efficiency

The relative efficiencies of different turbine designs, both at their lowered flows and design point are an important aspect in comparing them. Figure 2.6 depicts how the efficiency of selected turbines varies as a function of turbine flow ratio.

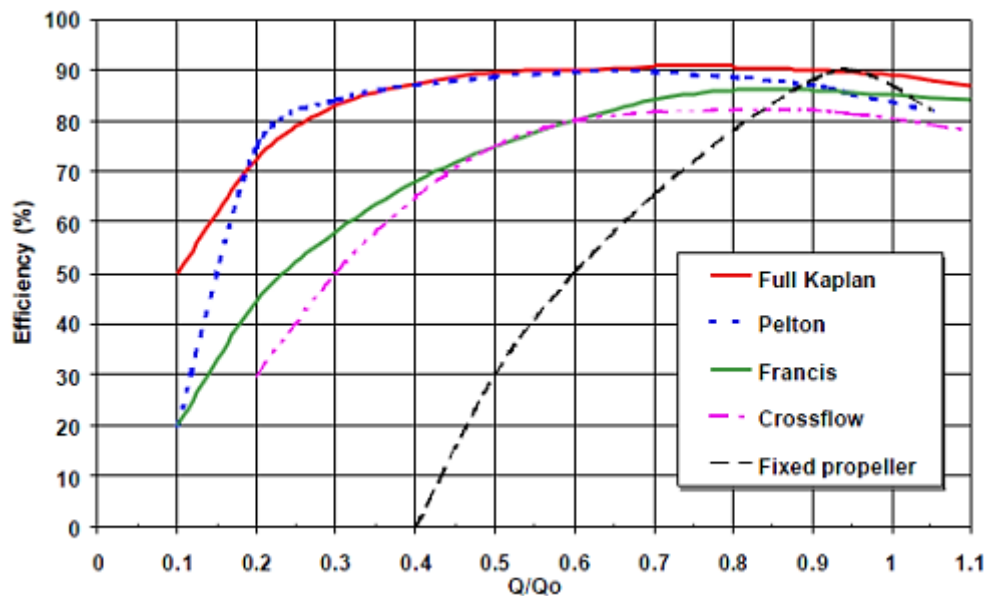


Figure 2.6: Efficiency of various turbines based on discharge [39].

As it observed from the efficiency's comparison in Figure 2.6, the Kaplan turbines has a maximum efficiency of 90%, which achieved when the percentage of turbine flow is between 50 and 90%. It can also be seen that when the percentage flow drops below 30% the efficiency quickly deteriorates. For Pelton turbines when the percentage flow is below 20% the efficiency drops away rapidly though this turbine is capable of reaching efficiencies of 90% when the percentages flow is 60-70%.

However, Francis turbine can be observed to have less maximum efficiency, they have the widest range of application among the various turbines in terms of size and operating heads. It can be noted that when the turbines flow rate drops below 80% the efficiency of the turbine drops off rapidly. Both in the case of the cross- flow turbine and the Francis turbine the efficiency falls away rapidly as they are operated below half their design flow.

2.2.2.6. Generator Selection

Micro-hydro generators are low-speed devices with a high number of poles, a large diameter, and a short rotor. MHP systems employ synchronous generators because they can produce their own operating voltage and maintain frequency when operating in a remote location.

Table 2.3: Selection of Generator type [40].

Size of schemes	Up to 10 KW	10-15 KW	More than 15KW
Generator	Synchronous/induction	Synchronous/induction	Synchronous
Phase	Single or three phase	Three phases	Three phases

The basic factors to consider while selecting a good type of electrical generator are as follows:

- ✓ Type of desired output: A.C. or D.C. constant frequency or variable frequency.
- ✓ Hydraulic turbine operations mode.
- ✓ Type of electrical load: Connection to the national grid, battery storage, or an independent system serving a range of residential or industrial loads.

The designing power factor for a micro-hydro generator can be 0.95. The generator speed is determined by the turbine speed, which is governed by the specific speed of the turbine. The air gap, diameter and length of the stator core are the major dimensions of the generator. The generator's output in (KVA) is determined by these primary dimensions and the machine's speed [37][38]. The general expression for generator output power in (KVA) is as follows:

The generator frequency can be given as

$$f = P \times \frac{n}{2} \quad (2.8)$$

Where f frequency in (HZ), P is number of magnetic poles, n is generator speed in (r.p.s).

The voltage per phase can be given as

$$E_{ph} = 4.44 \times K_w f N_{ph} \Phi_m \text{ (volts)} \quad (2.9)$$

Where K_w is winding factor of the generator

N_{ph} is number of series turns per phase.

Φ_m is maximum magnetic flux per pole (Weber)

The winding factor for a three-phase synchronous machine is 0.95, and the flux per pole is given by [33]:

$$\Phi_m = B \times (\pi \times D/p) \times L \quad (2.10)$$

Where B = average flux density in air gap (weber/m²)

D = stator diameter at the air gap (m)

L =Core Length (m)

The current per phase in ampere (A) is given by:

$$I_{ph} = \frac{(\pi \times D \times a_c)}{(6 \times N_{ph})} \quad (2.11)$$

Also, the output power of the 3-phase, AC generator is given by:

$$S = 3 \times E_{ph} \times I_{ph} \times 10^{-3} \text{ (KVA)} \quad (2.12)$$

$$S = 10.4 \times B \times D^2 \times L \times n \times a_c \times 10^{-3} \quad (2.13)$$

The factor (a_c) for the micro-hydro power generator is between (30000-43000) ampere-conductor per meter of stator periphery, and the air-gap flux density (B) is between (0.54-0.7) weber/m² [33]. After determining the ampere-conductor per meter and flux density in the air-gap, the value of ($D^2 \times L$) for a particular output power may be calculated using equation (2.13).

The generator core's length L may be calculated as:

$$L = 1.2 \times \lambda \text{ (m)} \quad (2.14)$$

Where λ = pole pitch of the machine winding and given as: $\lambda = \pi \times D/p \text{ (m)}$

2.2.3. Discharge estimation of ungauged catchment using SCS-CN method

The soil conservation service curve number (SCS-CN) approach is one of the most well-known methods for forecasting the surface runoff extent from a small watershed due to a rainstorm. The SCS curve number technique is a simple, commonly used, and effective method for estimating the amount of precipitation depth following a rainfall event in a certain location [17][41]. In this approach, the direct runoff from any ungauged basin is calculated using the following equation.

$$P_e = \frac{(P-0.2S)^2}{(P+0.8S)} \quad (2.15)$$

Where P_e estimated direct runoff (inch), P is maximum storm rainfall within a day (inch), and S is the potential maximum retention. Where P_e the predicted direct runoff in mm, P is the maximum storm rainfall during a day in mm, and S is the probable maximum retention in mm. equation (2.16) may be used to compute S from the CN value that is:

$$S = \frac{1000}{CN} - 10 \quad (2.16)$$

The dimensionless curve number CN ranges is between $0 \leq CN \leq 100$. For impervious and water surfaces $CN = 100$ but for natural surfaces $CN < 100$ [28].

Curve numbers have been tabulated in Appendix-A, [Table-A 9](#) by the Soil Conservation Service (SCS) based on soil type and land use. Four soil groups are defined [[27](#)].

Group A: Deep sand, deep loess, aggregated silts.

Group B: Shallow loess, sandy loam.

Group C: Clay loams, shallow sandy loam, soils low in organic content, and soils usually high in clay.

Group D: Soils that inflate a lot when wet, thick plastic clays, and certain saline soils. The values of CN for various land uses on these soil types are presented in the [Table-A 13](#) for a watershed composed of diverse soil types and land uses, a composite CN can be calculated. In this study, the soil properties and types are considered as the combination of type B and D.

The soil categories such as Cambisol, Andosol, Fluvisol, Leptosol, Vertisol and Luvisol are identified and hydrologic soil group is assigned to each category based on US Natural Resource Conservation Service (NRCS) that may fall into four hydrologic soil groups (HSG) (A, B, C and D): high, moderate, slow and very slow infiltration rates respectively.

[Appendix-A, Table-A10](#) discusses soil types with their corresponding HSG. The Ethiopian Road Authority manual is being employed to develop the correlation between soil type and hydrologic soil group in the Girar river watershed [[42](#)]. Equation (2.17) is often used to calculate the peak runoff rate (m^3/s) after computing the direct or excess runoff from any basin (Q).

$$Q = 0.208 \times \left(\frac{A \times P_e}{T_p} \right) \quad (2.17)$$

Where A represents the drainage basin area (km^2), P_e indicates excess rainfall (mm), Q is the peak runoff rate unit hydrograph (m^3/s), and T_p is the time to peak runoff unit hydrograph (h). Time to peak (T_p) is the time elapsed between the start of runoff from a rainfall event across a watershed and the peak of runoff. It's time to peak the runoff unit hydrograph.

The relation between lag time and concentration time for average natural watershed conditions and an approximately uniform distribution of runoff can be calculated from time of concentration T_c using the following equation [[43](#)].

$$T_p = 0.6 \times T_c \quad [hr] \quad (2.18)$$

The SCN-CN is a method developed for watershed lag that covers a wide range of situations, from severely wooded watersheds with steep channels and a high percentage of runoff originating from subsurface flow, through meadows with strong surface runoff retardance, to smooth land surfaces and big paved areas.

$$T_p = \frac{\ell^{0.8} \times (S+1)^{0.7}}{1900 \times Y^{0.5}} \quad (2.19)$$

Therefore

$$T_c = \frac{\ell^{0.8} \times (S+1)^{0.7}}{1140 \times Y^{0.5}} \quad (2.20)$$

The time of concentration T_c is the point at which the whole watershed begins to contribute. This is the time it takes for water to travel from the farthest point on the watershed to the outlet.

Therefore, substituting in the above lag time formula

$$T_c = \frac{\ell^{0.8} \times (S+1)^{0.7}}{1140 \times Y^{0.5}} \quad (2.21)$$

Where T_c is time of concentration [hr], ℓ is flow length in [ft], Y is an average watershed slope in % and S is a maximum potential retention [inch].

$$S = \frac{1000}{CN} - 10 \quad [inch] \quad (2.22)$$

i. Flow length (ℓ): the longest path that water takes from the watershed divide to the outflow.

The longest flow path was employed to represent the hydraulically most distant location in the watershed while creating the regression equation for the lag approach. Aerial images, quadrangle sheets, and GIS approaches can be used to measure flow length. The following equation expresses an empirical relation between flow length and drainage area.

$$\ell = 209 \times A^{0.6} \quad (2.23)$$

Where ℓ is flow length [ft] and A is drainage area in [acres]

ii. Land slope (Y), percent: The average land slope of the watershed can be calculated by using the following equation.

$$Y = \frac{100 \times CI}{A} \quad (2.24)$$

Where C is the total of the lengths of contour lines on the quad sheet that run across the watershed drainage area [m], I is contour interval used [m] and A is the drainage area [m²].

2.3. Solar Resource Assessment

2.3.1. Solar Resource potential of Ethiopia

The amount of exploitable reserve of solar radiation falling daily, in Ethiopia is about 4-6 KWh/m²/day. Among these, only less than 1% of the resource is exploited [13],[44]. Solar electricity appears to be the principal choice for off-grid electrification according to the Growth and Transformation plan (GTP) Strategy where the target is to distribute more than 3 million

solar home systems by 2015. The outlook for the solar electricity sector in Ethiopia is for rapid increase in installation for off-grid applications and later for grid-connected applications. Off grid PV, applications include home and institutional lighting, mobile charging, running audio-visual equipment, refrigeration and diagnostic equipment in health facilities, water pumping, and powering telecom.

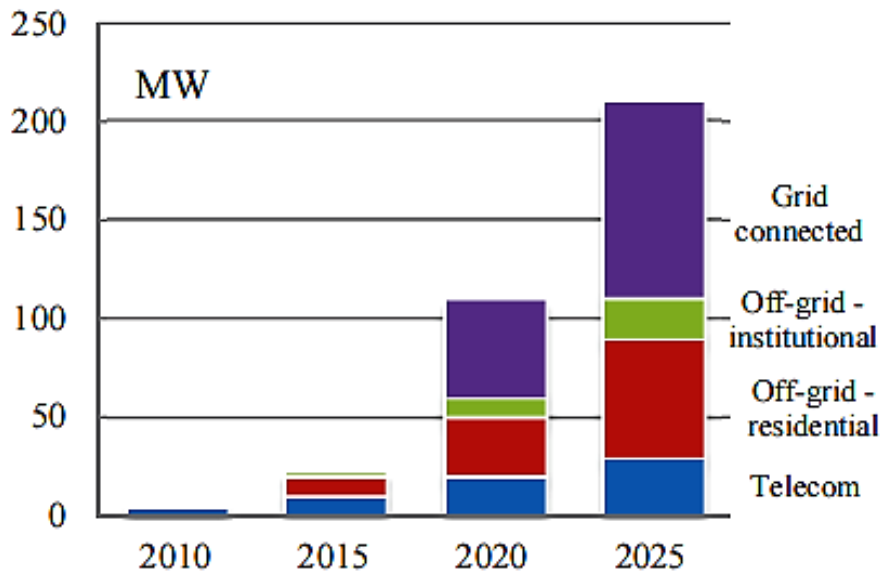


Figure 2.7: PV demand in Ethiopia[44]

2.3.2. Estimation of Monthly solar radiation on tilted surfaces

The Angstrom equation was one of the earliest approaches for estimating solar irradiance on a horizontal surface. It was simple linear model relating average horizontal radiation to clear day radiation and to the sunshine level [45][46].

$$\bar{H}_h = \bar{H}_o \left(a + b \frac{\bar{n}}{\bar{N}} \right) \quad (2.25)$$

$$\bar{K}_T = \frac{\bar{H}_h}{\bar{H}_o} = \left(a + b \frac{\bar{n}}{\bar{N}} \right) \quad (2.26)$$

Where \bar{H}_h and \bar{H}_o are the horizontal terrestrial and horizontal extra-terrestrial radiation levels averaged for a month, \bar{K}_T is clearness index, a and b are regression constants for a given site and \bar{n} and \bar{N} are the monthly average numbers of hours of bright sunshine and day length respectively.

$$a = -0.309 + 0.539 \cos(L) - 0.0639h + 0.29 \times \frac{\bar{n}}{\bar{N}}$$

$$b = 1.527 - 1.027 \cos(L) + 0.0926h - 0.359 \times \frac{\bar{n}}{\bar{N}}$$

Where L is Latitude and h is elevation in km above sea level

$$\bar{H}_o = \frac{24 \times 3600 G_{sc}}{\pi} \times \left(1 + 0.033 \cos \frac{360n}{365}\right) \times \left(\cos(L) \cos \delta \sin \omega + \frac{\pi \omega}{180} \times \sin(L) \sin \delta\right) \quad (2.27)$$

Where G_{sc} is constant 1367 W/m^2 and $\omega = \cos^{-1}(-\tan(L) \times \tan(\delta))$

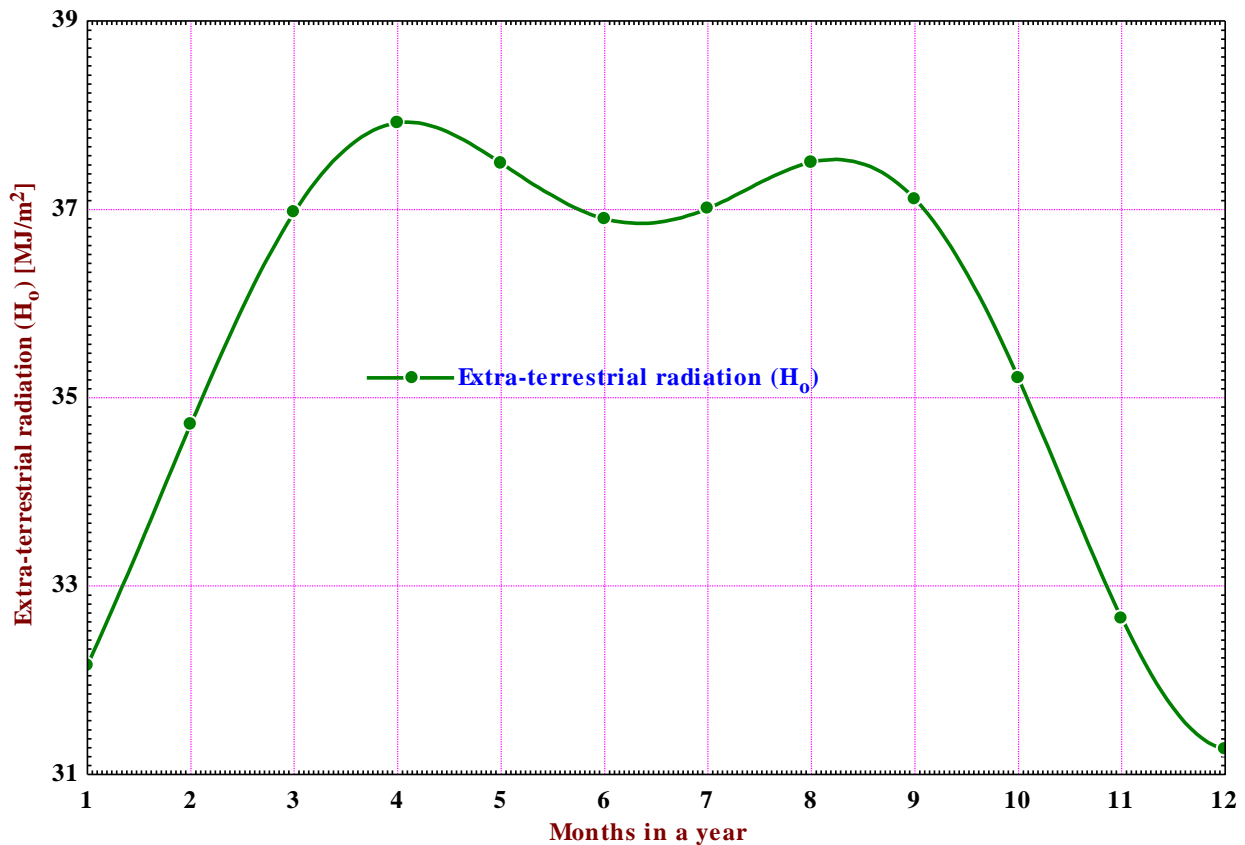


Figure 2.8: Extra-terrestrial solar radiation on horizontal surface through a year

The monthly diffuse \bar{D}_h to monthly total \bar{H}_h ratio can be expressed by the empirical equation

$$\frac{\bar{D}_h}{\bar{H}_h} = 0.775 + 0.347 \left(\omega_{ss} - \frac{\pi}{2}\right) - \left[0.505 + 0.0261 \left(\omega_{ss} - \frac{\pi}{2}\right)\right] \times \cos(2\bar{K}_T - 1.8) \quad (2.28)$$

The monthly average beam component \bar{B}_h on a horizontal surface can be readily calculated by simple subtraction since \bar{D}_h is known;

$$\bar{B}_h = \bar{H}_h - \bar{D}_h \quad (2.30)$$

The optimum tilt angle β_{opt} can be obtained using correlations that has been formulated as the linear, second-degree polynomial, and third-degree polynomial mathematical models, respectively [47]. By using these mathematical formulas, the value of the optimum tilt angle can be assessed.

$$\beta_{opt} = -1.0728(\delta) + 33.28 \quad (2.31)$$

$$\beta_{opt} = -0.0009(\delta)^2 - 1.0727(\delta) + 33.515 \quad (2.32)$$

$$\beta_{opt} = -0.00002(\delta)^3 - 0.0009(\delta)^2 - 1.0647(\delta) + 33.515 \quad (2.33)$$

Table 2.4: Solar radiations calculated from meteorology data at the sunshine hour of Goda Warke village for horizontal surface.

Months	Horizontal extra-terrestrial \bar{H}_o (MJ/m ²)	Horizontal terrestrial \bar{H}_h (MJ/m ²)	Monthly Diffuse radiation \bar{D}_h (MJ/m ²)	Average beam component \bar{B}_h (MJ/m ²)
January	41.02	28.40	7.077	21.32
February	44.72	27.03	6.960	20.07
March	48.25	27.58	7.384	20.19
April	50.38	29.00	8.091	20.91
May	50.56	28.65	8.261	20.39
June	50.39	24.62	7.220	17.40
July	50.27	21.77	6.337	15.43
August	50.56	23.65	6.694	16.96
September	49.36	28.89	7.863	21.03
October	46.06	27.61	7.203	20.41
November	42.16	26.74	6.722	20.02
December	40.19	24.82	6.126	18.69

The beam irradiation tilt factor R_b is a purely geometric quantity that converts instantaneous horizontal beam radiation to beam radiation intercepted by a tilted surface.

$$R_b = \bar{R}_b = \frac{\cos(L-\beta)\cos\delta \times \sin\omega_{sr} \times \sin(L-\beta) \times \sin\delta}{\cos\delta \times \sin\omega_{sr}(\alpha=0) + \omega_{sr}(\alpha=0) \sin L \times \sin\delta} \quad (2.34)$$

Therefore, the long-term beam radiation on tilted surface is given by

$$\bar{B}_c = \bar{B}_h \times \bar{R}_b \quad (2.35)$$

The diffuse radiation tilt factor \bar{R}_d

$$\bar{R}_d = R_d = \cos^2\beta / 2 = \left(\frac{1+\cos\beta}{2} \right) \quad (2.36)$$

Some beam and diffuse energy reflected from the ground can be absorbed by the collector surface in some circumstances where solar panels are positioned near the ground. As a result, the tilt factor is determined using the formula stated by equation (2.37).

$$\bar{R}_r = R_r = \frac{\bar{R}}{\bar{B}_h + \bar{D}_h} = \rho \sin^2 \beta / 2 = \frac{\rho(1 - \cos \beta)}{2} \quad (2.37)$$

Where ρ is diffuse reflectance of the surface, south of the PV collector, which is $\rho \cong 0.2$ for grass and concrete. The value diffuse reflectance (ρ) for different surfaces are given in Appendix-A Table-A 14.

The total long-term radiation intercepted by the surface is

$$\bar{H}_c = \bar{B}_h \bar{R}_b + \bar{D}_h \bar{R}_d + \bar{R}_r (\bar{D}_h + \bar{B}_h) \quad (2.38)$$

$$\bar{H}_c = \bar{B}_h \bar{R}_b + \bar{D}_h \cos^2 \beta / 2 + (\bar{D}_h + \bar{B}_h) \sin^2 \beta / 2 \quad (2.39)$$

Table 2.5: Calculated long term Beam, diffuse and diffuse-reflected radiation of study area on tilted surface.

Months	Beam radiation $\bar{B}_c = \bar{B}_h \bar{R}_b$ (MJ/m ²)	Diffuse radiation $\bar{D}_c = \bar{D}_h \bar{R}_d$ (MJ/m ²)	Diffuse-Reflected $\bar{D}_r = \bar{R}_r (\bar{D}_h + \bar{B}_h)$ (MJ/m ²)	Total \bar{H}_c (MJ/m ²)
January	26.6	5.539	1.234	33.37
February	21.82	5.845	0.866	28.53
March	19.5	6.675	0.529	26.7
April	18.43	7.759	0.238	26.43
May	18.22	8.154	0.740	27.11
June	16.04	7.183	0.252	23.47
July	14.0	6.286	0.355	20.64
August	14.91	6.512	0.128	21.55
September	19.17	7.296	0.416	26.88
October	21.11	6.206	0.764	28.08
November	24.06	5.362	1.082	30.50
December	24.30	4.694	1.160	30.15

2.3.3. Optimum working condition and meteorology effect of study area on PV components of Hybrid System

i. The effect of Tilt angle variation, ambient Temperature and Wind

The electrical properties of PV modules are highly dependent on the cell temperature. In this study, the Faiman-model equation is used, which includes the effect of not only the ambient temperature and irradiance but also the wind speed in the equation of the cell temperature.

$$T_c = T_a + \frac{\bar{H}_c}{U_o + U_1 \cdot v_m} \quad (2.40)$$

Where T_a is the ambient temperature, U_o is the constant heat transfer coefficient, U_1 is the wind speed coefficient of heat transfer, v_m is the wind speed at the height of the modules. The value of $U_o = 30.02 \text{ W/m}^2 \text{ K}$ and $U_1 = 6.28 \text{ W/m}^3 \text{ K}$ are constant coefficient values [48].

The performance of solar cells decreases significantly as the temperature increases. On the contrary, lower temperatures are known to improve the efficiency of the PV modules [49]. The power generation variation due to temperature also depends on the type of the solar panel. Losses caused by the temperature $P_{T_{loss}}$ are calculated using equation (2.41).

$$P_{T_{loss}} = P_{STC} \times \left(\frac{\bar{H}_c}{G_{STC}} \right) \times Q_{deg} \times C_{Temp} \times (T_{c,STC} - T_c) \quad (2.41)$$

Where P_{STC} is the maximum power of the PV system at STC (G_{STC} is the irradiance at the standard test condition (STC) equal to 1000 W/m^2) and C_{Temp} is the temperature coefficient, Q_{deg} Module quality degradation coefficient and \bar{H}_c is plane of array irradiance in W/m^2 . It is assumed that the average quality degradation factors will be 90.35%. As a result, temperature losses will be positive when the module temperature exceeds $T_{c,STC} = 25 \text{ }^\circ\text{C}$; otherwise, temperature losses will be negative.

The modules temperature has a direct relationship with the efficiency of the solar panels. Equation (2.43) connects these parameters [50].

$$\eta = \eta_r [1 - C_{Temp} (T_c - T_{NOCT})] \quad (2.43)$$

Where η is the cell's monthly average efficiency, η_r is the module's efficiency at solar radiation flux of 1 kW/m^2 and at reference temperature, T_{ref} . C_{Temp} is the temperature coefficient which is dependent on the panel's material (e.g.: 0.004 K^{-1} for crystalline silicon modules), and T_c is the monthly average temperature of the cell. Normally, C_{Temp} and T_{NOCT} are provided by the cell's manufacturer.

Therefore the power output is given by a relation;

$$P = \bar{H}_c \times \tau_{pv} \times \eta_r \times A [1 - 0.0045 \times (T_c - 25)] \quad (2.44)$$

Where \bar{H}_c the irradiance on the cell (W/m^2) is, τ_{pv} is the transmissivity of the glass and A is the module's surface area (m^2). For the most widely employed 3.2 and 4 mm thick glass, the visible light transmittance of sunlight is generally 90–92 % [51]. Since Maximum power of the PV module is the product of maximum current and maximum voltage as determined by;

$$P_{max} = V_{max} \times I_{max} \quad (2.45)$$

For a given temperature and insolation level, the maximum output current (I_m) and voltage (V_m) of a PV array can be Estimated as follows.

$$I_{max} = \left[\frac{C_o \cdot \bar{H}_c}{G_{STC}} + C_1 \times \left(\frac{\bar{H}_c}{G_{STC}} \right)^2 \right] \times [I_{mo} + K_{Im}(T_c - 25)] \quad (2.46)$$

$$V_{max} = V_{mo} + C_2 \cdot a \cdot V_t \cdot \ln \left(\frac{\bar{H}_c}{G_{STC}} \right) + \frac{C_3 (a \cdot V_t \cdot \ln(\bar{H}_c / G_{STC}))^2}{N_s} + K_{Vm} \left(\frac{\bar{H}_c}{G_{STC}} \right) (T_c - 25) \quad (2.47)$$

Where

$$V_t = \frac{N_s \cdot k \cdot T_c}{q}$$

$k = 1.3806503 \times 10^{-23} \text{ J}/^\circ\text{C}$ is the Boltzmann constant, $q = 1.602176 \times 10^{-23} \text{ C}$ is the electron charge, T_c and \bar{H}_c are the PV module temperature in $^\circ\text{C}$ and plane of array irradiance in W/m^2 respectively. G_{STC} is the irradiance at the standard test condition (STC) equal to $1000 \text{ W}/\text{m}^2$.

Table 2.6: Parameters of loss calculation for the PV system.

Parameter	Value	Parameter	Value
a	1.452	k_{vm}	$-0.42 \text{ } \%/^\circ\text{C}$
C_o	1.002	k_{tm}	$-0.09 \text{ } \%/^\circ\text{C}$
C_1	-0.002	N_s	7
C_2	-0.5279	V_{mo}	33.2 V
C_3	-9.615	I_{mo}	2.41 A

The quantity of dust deposited on the panels is also affected by the tilt angle of the panels. As previously proven in a prior research [52],[53], lower tilt angles result in more dust deposition. One of the causes is that the gravitational impact influences dust deposition. Modules with tilt angles below 15 degrees showed increased water retention on the panels, which when mixed with the dust present created a "sticky substance" that, in addition to not being blown off by wind, resulted in the collection of extra dust particles [54].

When PV modules with tilt angles of 0° , 20° (the most common installation angle), and 33.5° are compared, According to [55], modules installed at 33.5° had over 50% reduced soiling losses than panels set at 0° . Rain would combine with earth to generate mud, which would settle on top of the panels with a horizontal (0 degree) tilt angle.

When incoming light strikes a water particle, it might scatter or be absorbed. Scattering reduces direct normal irradiance while increasing global horizontal irradiance, whereas absorption decreases total irradiance, both of which interfere with irradiance reaching the cell and hence

impact efficiency [56]. The greater the value of β , the larger the dust particles can roll off from the surface of the panels or slide to the lower regions of the panels due to the higher impact of gravitational forces, which rise with the sine of angle β .

2.4. Sizing and Optimization methods of Hybrid Renewable Energy Power Generation

2.4.1. HOMER Software Optimization Method

In the typical Iraqi rural village and Uttarakhand state in India [Ali Saleh et al.](#), and [Ankit et al.](#), [57][58], studied the techno-economic and environmental analysis of various hybrid systems respectively. [Ali Saleh et al.](#), [57] HOMER to optimize systems using the Multi-year Module and they has been found that PV/hydro/diesel/battery HES is the most economical option with a net present cost (NPC) of 113201 dollars. The production of PV electricity decreases 9.1 percent while the generation of diesel, CO₂ and load are increased by 90.8%, 91.7% and 8.8%, respectively, throughout the project's life time of 20 year.

Similarly [Ankit et al.](#), [58] used HOMER software for Size optimization and sensitivity analysis of techno-economic feasibility of micro hydro–photovoltaic–biomass and biogas–diesel–battery hybrid energy system (HES) in off-grid mode to meet electricity demand of five villages those lacks electricity. The best configuration setup is selected as optimum from three configuration depending on economy and environment as the main driving factors, for the study area, which comprises total NPC \$5, 33,654, COE \$0.197/kW h, RF 94%, and CO₂ emission 15,930 kg/yr.

The most cost-effective system was suggested by [Ramadoni et al.](#), and [Tarlochan et al.](#), [59][60], taking into account the load profile and resources estimation and the sensitivity analysis carried out with the use of HOMER software for various hybrid systems. [Ramadoni et al.](#), [59] designed the plan of power generation from an irrigation water as a hybrid micro-hydro and solar photovoltaic system of up to 6,800 L/s of 11.9 m high in the rural areas of Central Java, Indonesia. They found that Micro-hydro can produce an output power of 555 kW which is cost up to 100 years with a replacement cost of USD 925,000 and a replacement cost of US\$500 is also charged for USD 1,132,426 solar panel with a power capacity of 0.3 kW.

[Tarlochan et al.](#), [60] investigated the possible use of Hydro, small scale generation units, solar PVs, both with and without energy storage solutions, for hybrid electricity systems. They found a hybrid system with the lowest electricity costs (\$0.147/unit). Hydro turbines supply about 29% of the production and Gen turbines supply around 71%. Gen-sets absorb and deliver reliable power for the season variability of renewables. A hybrid mix of hydro, generator set,

solar power and the battery provide a cleaner option, although at a higher electric charge (\$0.29 per unit).

Siamak Hosienzade et al., [2] used the system integration method principle for combining hydroelectric power stations with solar power for 1,6MW/yr power consumption, with an estimated hydraulic turbine capacity of 60 kW and a service life of 30 years. They have also modelled photovoltaic in-Home Software with clearness for cloudy and sunny days 0.25 and 0.75 respectively. They found that photovoltaic hydropower of 61 kW was the best and least costly combination for the Sarrood geographic conditions to compensate the power shortage.

Getnet et al., [1] used the single model with a modified Angstrom-type equation and an empirical method to calculate the flow rate of an ungauged river by estimating the average daily global solar radiation on a horizontal surface in a study site. They have found average solar insolation of 5.13 kWh/m²/day with a minimum flow rate of water found in the dry season is 0.838 m³/sec in December, while the Net-Head was at 10.5 m in the area of the study. They considered catchment area ratio method in their study to determine the discharge of ungauged river in the study area. Nevertheless, this method considers the rainfall intensity of the different area as a similar value. NRSCS-CN method is the most feasible method of discharge estimation in ungauged catchments.

Odou et al.,[61] and Tilahun et al.,[10] analysed a hybrid system with combination of PV/DG/Battery and Hydro/PV/DG/Battery respectively. Odou et al.,[61] obtained least cost PV/DG/Battery (of 150 kW/62.5 kVA/637 kWh) solar hybrid optimal system which can reduce battery requirements by 70% compared to PV/battery system and achieves 97% CO₂ emissions reduction compared to a conventional DG. While Tilahun et al.,[10] found optimum system with COE of \$0.133/kWh and the renewable fraction of the hybrid system is 99%. However, they do not considered mapping of solar radiation in their selected study area to determine possible area of PV installation.

2.4.1.1. The Application of HOMER Software in Simulation of Micro-grids

The HOMER Micro-power Optimization Model is a computer model created by the National Renewable Energy Laboratory (NREL) in the United States to support in the design of micro power systems and to simplify the comparison of electric generation technologies across a broad range of applications. HOMER performs three principal tasks such as simulation, optimization, and sensitivity analysis. HOMER simulates the performance of a certain micro-grid system configuration every hour of the year to assess its technical feasibility and life-cycle

cost. During the optimization phase, HOMER simulates a large number of possible system configurations in order to find the one that meets the technical criteria with having the lowest life-cycle cost. Throughout the sensitivity analysis phase, HOMER runs various optimizations under a range of input assumptions to analyze the consequences of ambiguity or changes in model inputs [62].

HOMER pro software is used in this study for hybrid system configuration, sensitivity analysis and economic evaluation of the optimized hybrid system. The analysis of this software is classified into three stages such as, Input stage, analysis stage and end result. Figure 3.4 shows detail application of HOMER pro software in this work.

2.4.2. Algorithm Optimization using coding in MATLAB

S.Kumar et al., and Muhammad et al., [63][64], Carried out particle swarm optimization (PSO) method for mathematical optimization of the model and designing of HRES (Hybrid renewable energy resource). S.Kumar et al., [63] used an artificial neural network (ANN) for solar resource assessment and hydrology estimation techniques for discharge estimation with an energy index ratio of 1. They found that the site has an estimated discharge of $0.625 \text{ m}^3/\text{s}$ with an available head of 9 m. They have combined micro-hydro with solar PV and diesel generator. The result shows a high renewable fraction of around 96.99% with a low value of CO_2 emissions of 9514.56 kg/yr.

Muhammad et al., [64] compares the different combinations of renewable energy (solar, wind) and storage technology (battery, hydro-pumped, hybrid) for off-grid energy supply. In particular, they discuss the performance and results of their mathematical model in four configurations (that is single RE source system, two RE source systems, one storage system, and double storage system) based on two scenarios. Their mathematical model was optimized by the Particle Swarm Optimization (self-discharge equal to 0 percent and 1 percent). They found that the hybrid pumped battery storage (HPBS) energy management strategy involves a low power supply shortage, while pumped hydro-storage (PHS) is an essential part of energy storage system that provides a large power production and deficit.

The multi-target optimization model was established by Fang-Fang Li et al., and Xing Li et al., [3][65] to maximize power generation and reduce energy consumption gaps using NSGA (non-dominated sorting genetic algorithms) frameworks to optimize hybrid energy generation models. The model aims to maximize the annual electricity generation while reducing production fluctuations [60]. A mean annual discharge in the Longyangxia River of $650 \text{ m}^3/\text{s}$

found by Fang-Fang Li et al [3]. During the implementation of the NSGA-II, population is set to 200, the iteration stops 500 times, the probability of crossover of simulated binary crossover (SBX) is 0.90, and the probability of mutation of a polynomial mutation is 0.10.

Xing Li et al., [65] used a long-term multi-objective optimization model where a waterfall is a compensation system of a hydro-photovoltaic-wind system. The aim of the model is to increase the total annual power generation of the electrical system and to smooth output fluctuations. A modified type of the non-dominated sorting whale optimization algorithm (modified NSWOA) provides the solution set for the designed model. They set a size of 100, a size of 50, and maximum iteration of 10000 and a probability of polynomial mutation of 0.01. They also found the power generation capacity of a PV, wind and hydroelectric stations, each of whom is 8000 MW, 2500 MW and 14,820 MW respectively. The results show that wind and PV can well be offset by the hydropower. The hybrid power generation system can take into consideration for stability and total capacity.

2.5. Hybrid system components and Techno-economic analysis

2.5.1. Small Scale Energy Storage System

In order to mitigate supply fluctuations and increase power Quality, renewable energy with storage systems is integrated. The Micro-grid Storage System also has advantages for voltage control and operating reserves. For example, an ESS system can be used to manage energy and to enhance the stability and economy of a micro grid storage system that stores excess energy generation and operates the electrical system during power interruptions. Chun Sing Lai et al., [66] use a state-of-the-art model to present GIES (pumping-heat storage) and NGIES (lithium-ion battery) systems and compare their economic and financial merits with the United Kingdom's wind power generation. The outcome of deterministic, risk, and sensitivity studies show that the most influencing factor is in IES economics capital cost, whereas the energy storage cost is the most influencing factor in non-GIES economics.

An Integrated Energy Storage System (GIES) is a form of storage system which saves energy and the transformation almost simultaneously between primary and secondary forms of energy at the same time.

2.5.2. Photovoltaic Cell, Module, Panel and Arrays

Photovoltaic cells are electrically coupled in series, parallel, or mixed circuits to create larger voltages, currents, and power levels. Photovoltaic modules are the basic building elements of PV systems, consisting of PV cell circuits sealed in an environmentally protective laminate. Photovoltaic panels are made up of one or more PV modules that are pre-wired and ready to be installed in the field. A solar array is a full power-generating equipment made up of any number of PV modules and panels [67].

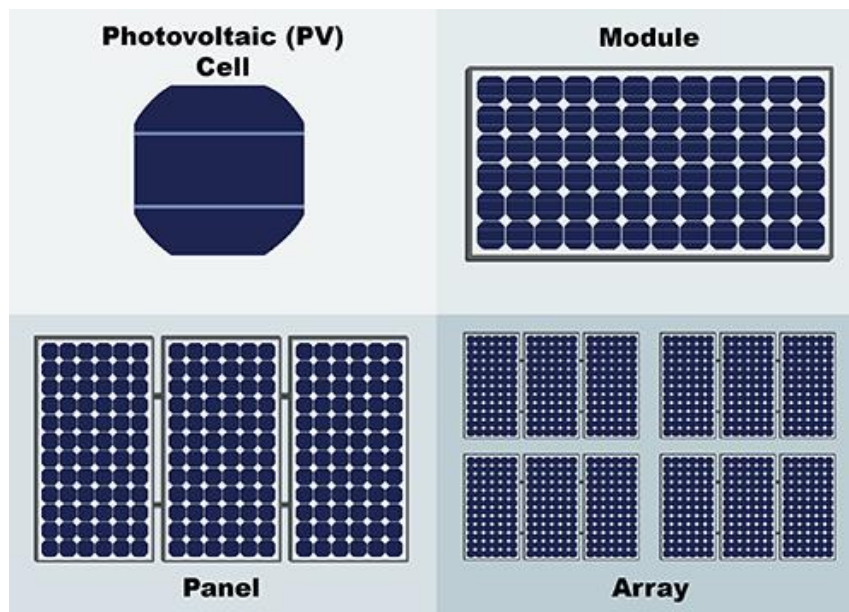


Figure 2.9: Photovoltaic cells, modules, panels and arrays [67].

2.5.3. Photovoltaic Costs

The price of photovoltaic modules fluctuates with invention, demand and supply issues. Photovoltaic solar panel cost has been reduced dramatically in the past ten years and it is assumed to continue its down slope of the future. The cost of an investment in a PV system is driven mostly by the initial up-front investment or capital expenditure. Additional costs encountered during a systems lifetime are comparatively low. The most affordable home solar panels on the market in 2021 are shown in the table below [68].

Table 2.7: Less expensive and affordable solar panel in market of 2021[68].

Most affordable solar panel	Price per panel	Power rating	Price per watt	Efficiency rating	Warranty
LONGI LR6-60-HPB-350	\$225 (11475 ETB)	350W	\$0.60 (30.6 ETB)	20.3%	Limited 25 year warranty
Hanwha-Q Cell 340WQ.PEAK	\$240 (12240 ETB)	340W	\$0.70 (35.7 ETB)	19%	25 year warranty
DUO Canadian Solar Model CS1H-315MS	\$225 (11475 ETB)	315W	\$0.71 (36.21 ETB)	18.68%	25-year output warranty

2.5.4. Hybrid components cost

Micro hydro installation costs around US\$1,200 (61200 ETB) per installed KW in Ethiopia. The investment cost of a micro hydro power plant is expected to be \$1136 (57936 ETB) per KW, with replacement cost equal to 50% of the capital cost and O&M cost equal to 10% of the capital cost. In addition, the initial capital cost of micro hydro power plants with new technologies are internationally estimated in between US\$1500 (76500 ETB) to \$2500 (1275000 ETB)/kW [10][69].

The capital cost and transportation of Bertoli Brand generators with power generation capacity of 24, 40 and 48 kW are \$20545 (1047795 ETB), \$22,419 (1143369 ETB) and \$27,024 (1378224 ETB). The price per kW was determined using the average unit price inferred from each generator cost and reached to \$660/KW or 33660/KW. The replacement cost is assumed to be constant, and the O&M cost is equal to 3% of the capital cost. The current fuel price is \$0.8 (40 ETB) per litre, and the minimum load ratio is set to 30%. The optimised capacities are: 0, 40, 45, 50, 60, 70, and 80 kW [61].

Table 2.8: Costs and specification of hybrid components

		Description	Specification	
PV System [61]		Capacity (KW)	1 KW	10 KW
		Capital (\$)	2000	11000
			(102000 ETB)	(561000 ETB)
		Replacement cost (\$)	2000	11000
		O&M cost (\$/yr)	40 (2040 ETB)	220 (11220 ETB)
		Life time (yr)	25 year	
Diesel generator [61]		Capacity (KW)	1,24,40,48	
		Capital Cost (\$)	660, 20542, 22419, 27024	
		Replacement cost (\$)	660, 20542, 22419, 27024	
		O &M (\$/hr)	0.03, 0.72, 1.2, 1.44	
		Life time (hr)	15000	
Converter [61]		Capacity (KW)	1	
		Capital (\$)	1000 (51000 ETB)	
		Replacement cost (\$)	1000 (51000 ETB)	
		O&M cost (\$/yr)	20 (1020 ETB)	
		Life time (yr)	15	
Hydro [10]		Capacity (KW)	1	
		Capital (\$)	1300 (66300 ETB)	
		Replacement cost (\$)	600 (33150 ETB)	
		O&M cost (\$/yr)	130 (6630 ETB)	
		Life time (yr)	40	
Battery [70]		Capacity (KW)	1	24
		Capital (\$)	1000	23947
			(51000 ETB)	(1221297 ETB)
		Replacement cost (\$)	1000	23947
		O&M cost (\$/yr)	20 (1020 ETB)	479 (24429 ETB)
		Life time (yr)	20	
Grid [61][8]		Capacity cost (\$/km)	15500	(790500 ETB)
		O&M cost (\$/yr/Km)	310	(15810 ETB)
		Grid power price (\$/KWh)	0.22	(11.22 ETB)

Therefore, to meet the total load demand of the study area (338 KW), 150 KW of PV power output is required. Diesel Generator (50 KW) is added in the system for comparison purpose considering the variation of fuel price. When the fuel price is 0.5 USD/KWh (25.5 ETB/KW/h), DG is used to support PV system and the requirement of PV is reduced to 150 KW. Hence, the capital cost of LONGI LR6-60-HPB-350 PV module is considered as 0.6 \$/W (30.6 ETB/W), the total capital cost and replacement cost of PV system becomes \$157200 (8017200 ETB) for each and O&M cost is estimated to be \$10480 (534480 ETB) according to [61][68].

2.5.5. System operation control mechanism

2.5.5.1. Stand-alone Micro-hydro Controlling System

Anuradha et al., [71] Proposed PV/hydro hybrid system linked with RLC load. A PV system and micro-hydro system is connected in parallel with grid system and which is called hybrid energy system and is interfaced with RLC load. They modelled and simulate a common electrical three-phase RLC load, which supplied by hydro-servo system and hydro turbine system using MATLAB Simulink software. They also used zero series load ($R_{se}=0$) and no leakage to ground ($R_{sh}=0$) for a PV cell and high quality silicon cell with varying R_s from 0.05 to 0.1 ohm and that R_{sh} from 200 to 300 ohm.

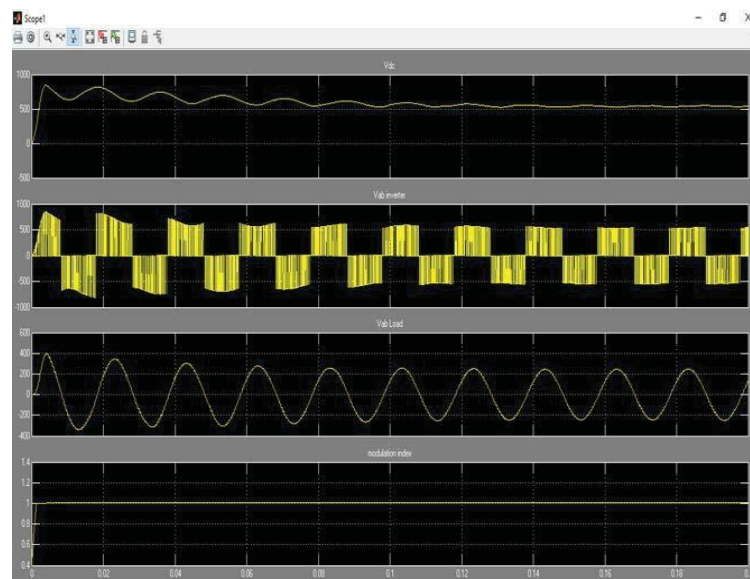


Figure 2.10: Simulink model for hybrid system [71]

Lack of a reservoir at the headrace of micro-hydropower plant results in variable water flow to the turbine. In addition, consumer load connected to the generator varies with time. The variation in water flow to the turbine and consumer load changes result in variation in generator output power and frequency. Asad Ali et al., [72] proposed 100 kW and 440 V Simulink model a three-phase synchronous generator (SG) feeding a 60 kW base load. Voltage and frequency

controller for micro hydro power plant (MHPP) measures frequency of the generator through phase-locked loop (PLL) block.

The frequency is then compared with a reference frequency, i.e., 50 Hz and the variance between reference frequency and measured frequency proportional integral and derivative (PID) control block.

The water flow power (P_w) depends on the water density (ρ), water turbine swept area (A) and the speed of water flow cube (V^3) as shown in the equation (2.48) and (2.49).

$$P_w = 1/2 \times \rho \times A \times V^3 \quad (2.48)$$

and

$$C_p = \frac{T_t \times U_s}{0.5 \times A \times V^3} \quad (2.49)$$

Where C_p is power co-efficient of performance and U_s is rotor speed of turbine. Rotational speed of turbine T_t depends on the power of water flow (P) and rotor speed of water turbine U_s .

The HOMER software simulates each system using both the LF (load following) and the CC (cycle charging) dispatch strategies and selects the best method for each system. When the LF method is implemented, the generators will only produce enough electricity to meet the load demand. Meanwhile, for the CC strategy, the generators will be operating at full capacity, with any extra electricity utilized to charge the battery bank. This work's HOMER optimized simulation corresponds to the CC dispatch approach.

2.6. Economic feasibility analysis

Different techniques and approaches are applied to investigate the best economics to achieve an optimized design of hybrid renewable energy system components. The essential objectives to optimize HRES are Levelized cost of energy (LCOE), net present cost (NPC), system annualized cost (SAC), operation and maintenance cost (O&M cost) and overall system cost. In addition the Life cycle cost (LCC) of the HRES accounts for all costs associated with an overall system life time, considering inflation and discount rate [73][74].

The minimum energy cost can be estimated as annual system cost (ASC) from equation:

$$ASC = ACC + ARC + AOC \quad (2.50)$$

Where ACC , ARC and AOC are annual capital cost, annual replacement cost and annual operation and maintenance costs.

A yearly capital cost (ACC) indicates the yearly capital cost of the components that do not need to be replaced throughout the project lifecycle:

$$ACC = C_{cap} \times CRF(i, n) \quad (2.51)$$

Where C_{cap} and CRF are the component investment cost and capital recovery factor respectively. CRF Combines project lifetime (n) with yearly interest percentage as shown below.

$$CRF(i, n) = \frac{i(1+i)^n}{(1+i)^n - 1} \quad (2.52)$$

Where i is the rate in which the loan is paid-back (i_{loan}) and it's affected by inflation rate f .

$$i = \frac{i_{loan} - f}{f} \quad (2.53)$$

The annual replacement cost of the system is components that require to be replaced before the end of the project lifetime, as shown in below. Its calculation depends on elements replacement cost (C_{rep}) and sinking fund factor (SFF) as follows.

$$ARC = C_{rep} \times SFF(i, n_{rep}) \quad (2.54)$$

$$SFF(i, n_{rep}) = \frac{i}{(1+i)^{n_{rep}} - 1} \quad (2.55)$$

Sinking fund factor coefficient is used in estimating the values of a series of equal annual cash flow in the future.

The components of the HRES configuration are required to be maintained periodically and are needed a payment of their operation.

$$AOC = AOC_1(1 + f)^n \quad (2.56)$$

Where AOC_1 the first year cost is spent for the entire system components.

The total net present cost (NPC) and levelized cost of energy can be calculated as follows.

$$NPC = \frac{C_{t,ann}}{CRF(i, n)} \quad (2.57)$$

$$LCOE = \frac{C_{t,ann}}{E_{t,ann}} \quad (2.58)$$

Where $C_{t,ann}$ and $E_{t,ann}$ are total annualized cost of configuration and total energy drawn by the load KWh/yr respectively.

$$C_{t,ann} = C_{cap} + \sum_{i=1}^n C_{OM,i} \quad (2.59)$$

Where, n is the number of all the components in the system and $C_{OM,i}$ is the annual operation and maintenance (O&M) cost for the component of the system [75].

The renewable energy shared by the system sources to the load is estimated based on RF (renewable fraction). RF is a fraction of the energy consumed by the load that is developed by renewable energy system.

$$\%RF = \left(1 - \frac{E_{non-ren,ann}}{E_{t,ann}}\right) \times 100 \quad (2.60)$$

Where $E_{non-ren,ann}$ is defined as the energy equipped by non-renewable resources in one year in KWh/yr .

The number of years required for the invested capital to be offset by resulting benefits is determined by payback period.

$$\text{simple pay back period } (P_B) = \frac{\text{Initial investment}}{\text{Annual cash inflow}} \quad (2.61)$$

Simple payback period Calculated for a proposal compared with some predetermined target period of different scenario.

2.6.1. Comparison of standalone hybrid system with grid-extension

The cost of optimised off-grid system is compared with grid extension analysis using the advanced grid module of HOMER in the form of Breakeven Grid Extension Distance (BGED). The BGED is the location distance from the grid when the total NPC of grid extension equals the total NPC of the off-grid system. The following equation is used to compute BGED [61].

$$D_{grid} = \frac{C_{NPC} \times CRF(i, R_{proj}) - C_{power} \times E_{demand}}{C_{Cap} \times CRF(i, R_{proj}) + C_{om}} \quad (2.62)$$

Where C_{Cap} is capital cost of grid extension (\$/km), C_{om} is O&M cost of grid extension (\$/yr/km), C_{power} is cost of power from the grid (\$/kWh), E_{demand} is total annual electrical demand (kWh/yr) and C_{NPC} is total NPC of the standalone power system (\$).

The cost for the smallest rated consumer service is often of the order of USD 100 to 300 in African sub-Saharan country. These costs are in stark comparison to connection rates in South and East Asia and South America, which range from USD 10 to USD 75 [8]. Recently in 2021, the price of electricity in Ethiopia is 0.1 USD/KWh for households and 0.2 USD/KWh for business, which includes all components of the electricity bill such as the cost of power, distribution and taxes [76].

2.7. Summary of Review of previous studies

Author	Topic	Methodology	Result	Gap
Saimak Hosienzadeh et al. [2] (2020)	✓ Application of hybrid system in solution of low power generation at hot season for micro hydro system.	✓ HOMER software is utilized to determine the best technical and economical hybrid system	✓ Found the best and the least cost combination of (61 kW hydro power, 20 kW photovoltaic, 7.5 kW wind turbine, 20 kW inverter and 10 4-way battery packs).	✓ Does not perform solar radiation mapping to show possible installation area for PV array in study area.
Ali saleh et al [57] (2019).	✓ Optimization and sensitivity analysis of standalone hybrid energy systems for rural electrification: A case study of Iraq	✓ Used HOMER software which is utilized for the optimization of the systems using the multi-year module.	✓ Found that the PV/ hydro/ diesel/battery HES is the most economical option with a net present cost (NPC) of \$113201.	✓ Sensitivity analysis using parameters such as pipe loss, load growth, and PV capital cost is not considered in detail.
Oluwarotimi Delano Thierry Odou et al.,[61] 2020	✓ Hybrid off-grid renewable power system for sustainable rural electrification in Benin.	✓ Used Hybrid Optimization of Multiple Energy Resources (HOMER) software to perform optimization, simulation and sensitivity analysis.	✓ Obtained least cost PV/DG/Battery (of 150 kW/62.5 kVA/637 kWh) solar hybrid optimal system which can reduce battery requirements by 70% compared to PV/battery system and achieves 97% CO ₂ emissions reduction compared to a conventional DG.	<ul style="list-style-type: none"> ✓ Does not perform solar radiation mapping to show possible installation area for PV array in study area. ✓ Dimensions like institutional and socio-cultural aspects, which play a crucial role could be considered.

Tilahun Nigussie et al. [10] 2017	✓ Feasibility study for power generation using off- grid energy system from Micro-hydro/PV/DG/Battery for rural area of Ethiopia: The case of Melkey Hera village.	✓ Used HOMER software for optimum and best techno-economic selection. Flow rate data of the site was taken from MoWE and the gross head was measured using portable GPS.	✓ Energy obtained from hydropower, accounts 79%, the PV module covers 20%, and diesel generator is 1% of total load. The system has COE of \$0.133/kWh and the renewable fraction of the hybrid system is 99%.	✓ The effect of site meteorological parameters (i.e. temperatures) on PV power generation potential were not included in potential assessment.
Muhammed shahzed Jave et al [64]. 2021	✓ Economic analysis and optimization of a renewable energy based Economic analysis and optimization of a renewable energy based island	✓ Mathematical modelling optimization using Particle Swarm Optimization PSO is developed and implemented in MATLAB	✓ Configurations of solar/ wind/ battery/PHS were considered, and two scenarios were examined based on ESS self-discharge (0% and 1%). the optimal COE increased from 0.196 \$/kWh to 0.222 \$/kWh as storage self-discharge is 1%.	<ul style="list-style-type: none"> ✓ ESS self-discharge is taken as constant which is (0&1) % however it should be considered because it affected by the temperature. ✓ Environmental parameters i.e. battery emission PHS land requirement are not considered in optimization.

2.8. Research gap

Optimum hybrid (micro-hydro and PV) configuration requires further study on sensitivity analysis by considering parameters like pipe head loss, Diesel fuel price, community load growth, capacity shortage and pricing PV capital cost that have effects on Net present cost of the optimum system based on Goda Warke village. The Net present Cost is sensitive to these parameters which determines the selection of best economic configuration of hybrid system [57]. The effects of meteorological parameter (Temperature and wind) of the site on performance of PV array and PV land requirement does not considered in design of hybrid system configuration. In addition, the possible area for Photovoltaic array installation in selected study site with highest solar irradiance does not shown by mapping of solar radiation in recent literatures [10] [64].

CHAPTER 3

3. METHODOLOGY

This section deals with the location of study area, data collection methods, the flow sequence of thesis and the materials (software) utilized to reach on best result and conclusion of this work. In general, the methods and approach used in this study have discussed in detail as follows.

3.1. Location of Study Area

Yaya Gulele is one of the woredas in the Oromia region of Ethiopia located about 115 Km North-West of the capital city, Addis Ababa. It is part of former Yaya Gulale and Debre Libanos and separated recently from Debre Libanos in North Shoa zone. This woreda is bordered on the south by Mulo and Sululta, on southwest by muger river wich separates it from west shoa, on the north by Girar Jarso, on north east by Debre libanos on east by Wuchale. Towns in Yaya Gulele includes Fital. Administratively, it is divided into 17 rural and one urban Kebele administrative. The total population of the Woreda was estimated to be about 75,000 with an average population density about 279 persons per km² [77][78][79].

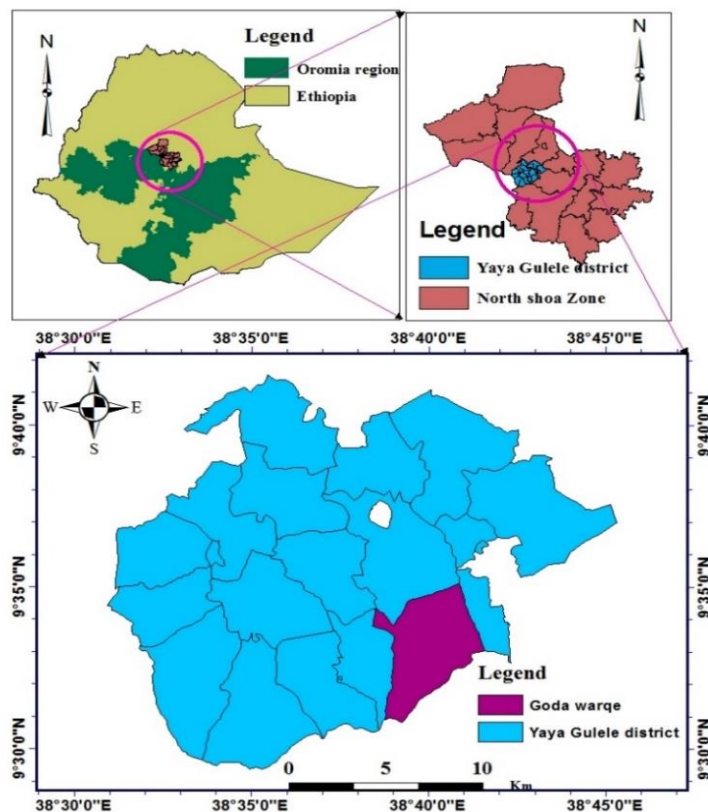


Figure 3.1: Location map of study area

3.2. Research Design Process

The research design is based on Meteorological data of the selected site in terms of which flow rate estimation, rainfall data, sunshine hour (solar resource data) and techno-economic evaluation is assessed. The economic analysis and sensitivity analysis are conducted by using hybrid system simulation software's such as HOMER pro software. The methodology used in this work is software analysis, using collected load demand data from the study site.

The energy resource potential assessment of the selected site was done by using ArcGIS software using Digital elevation model (DEM) and analytical hydrological model. Monthly flow rate of the local river is determined by using the rainfall data collected from meteorological station and NRSCS-CN method is applied in order to estimate the stream flow of ungauged river in study area for hydro potential assessment. The preferring criteria of this method over the other methods was clearly described in literature review section of this work.

The sunshine hour and Global horizontal solar radiation falling per day in study area is estimated from meteorological data collected from National Meteorological Agency (NMA). The estimated value was compared with NASA and software estimated value such as New-LoClim software. In order to identify whether the energy resource in the study area has potential of energy generation, load assessment was done in Goda Warki village located in Yaya Gulele district. The number of households, governmental institution and worshipping institution in the study village are assessed through data collection to determine load assessment and energy consumption pattern.

Based on the load profile of the study village, Sizing of the system was done using HOMER. Micro hydro sizing includes, flow rate, design head, type of hydraulic turbine, generator and calculation of catchment area. Whereas solar photovoltaic sizing includes parameters such as number of panels, orientation and inclination angle. Finally, the Hybrid Micro-hydro/PV power generation system will be modelled with energy storage system. Configuration setup and economic analysis is performed using in HOMER software considering sensitivity parameters such as net head, pipe head loss, electric load consumption, hydro turbine efficiency and fuel price.

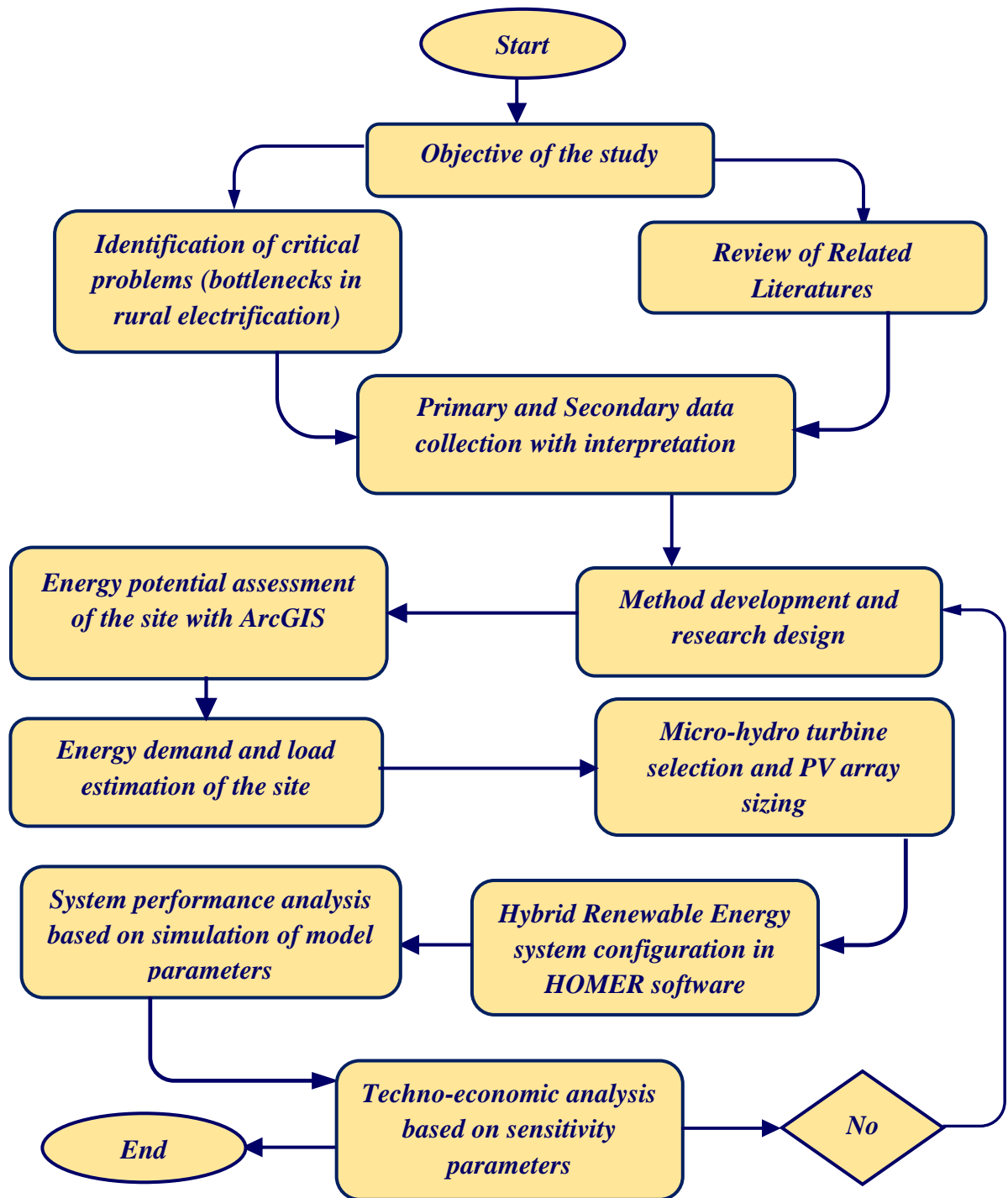


Figure 3.2: Research Design and process flow chart

3.3. Primary and Secondary Data collection

The primary data are collected from study village during field survey. It includes number of households, number of populations, worshipping place and government institution such as kebele administration, farmer training centre (FTC), clinic and schools. The number of households in study area are classified into high class, medium class and low-class households based on the interval of the land owned tax they are paying as shown in [Table 3.1](#) as well as [Table-A 1](#), [Table-A 2](#) and [Table-A 3](#) in Appendix -A. These data are obtained from Office of Agricultural and Natural Resource Conservation of Yaya Gulele district, cooperation with Goda Warke kebele administration. The collected data are used in estimation of load assessments of steady area.

The secondary data are meteorological data of the study area, which consists of rainfall amount, and sunshine hour data. These data are used in this work for potential assessment of energy resource in steady area which is limited to micro-hydro and solar PV. The collected data is converted to monthly average value as presented in [Table-A 9](#) and [Table-A 11](#) in [Appendix-A](#). The Assessment was employed based on the estimated load of Goda Warke village as a case study.

3.4. Materials and Tools

Different software tools are used in this work for different purposes. ArcGIS and ERDAS Imagine software are applied to determine catchment area of the ungauged river as well as LULC analysis in case of monthly discharge estimation and for drawing the map of a study area. EES software is utilized for analytical works and graphical representation of desired parameters. The New-LoClim software estimates some meteorological parameters based on the geographical location of the study area.



Figure 3.3: Types of Software tools employed in this work

There are some software tools available for hybrid system design and analysis. Such as Hybrid2, HOMER, REET Screen, and In My Back Yard (IMBY) [10]. HOMER has some unique characteristics, such as a broader range of renewable resource input with their potential combinations under varied conditions and has a broad selection of system architecture and dispatch in comparison to similar software computing approaches such as RETScreen, PVSOL, Hybrid2, TRANSYS, SAMS, RAPSYS, and MATLAB [62][80].

HOMER is the most versatile system in terms of systems that can simulate, offer more complete information, and do sensitivity analysis with minimum input [81]. It carries out three major tasks such as simulation, optimization, and sensitivity analysis for recommending the best system design [82] which provides the best-optimized model architecture based on Net Present Cost (NPC) and a given inputs.

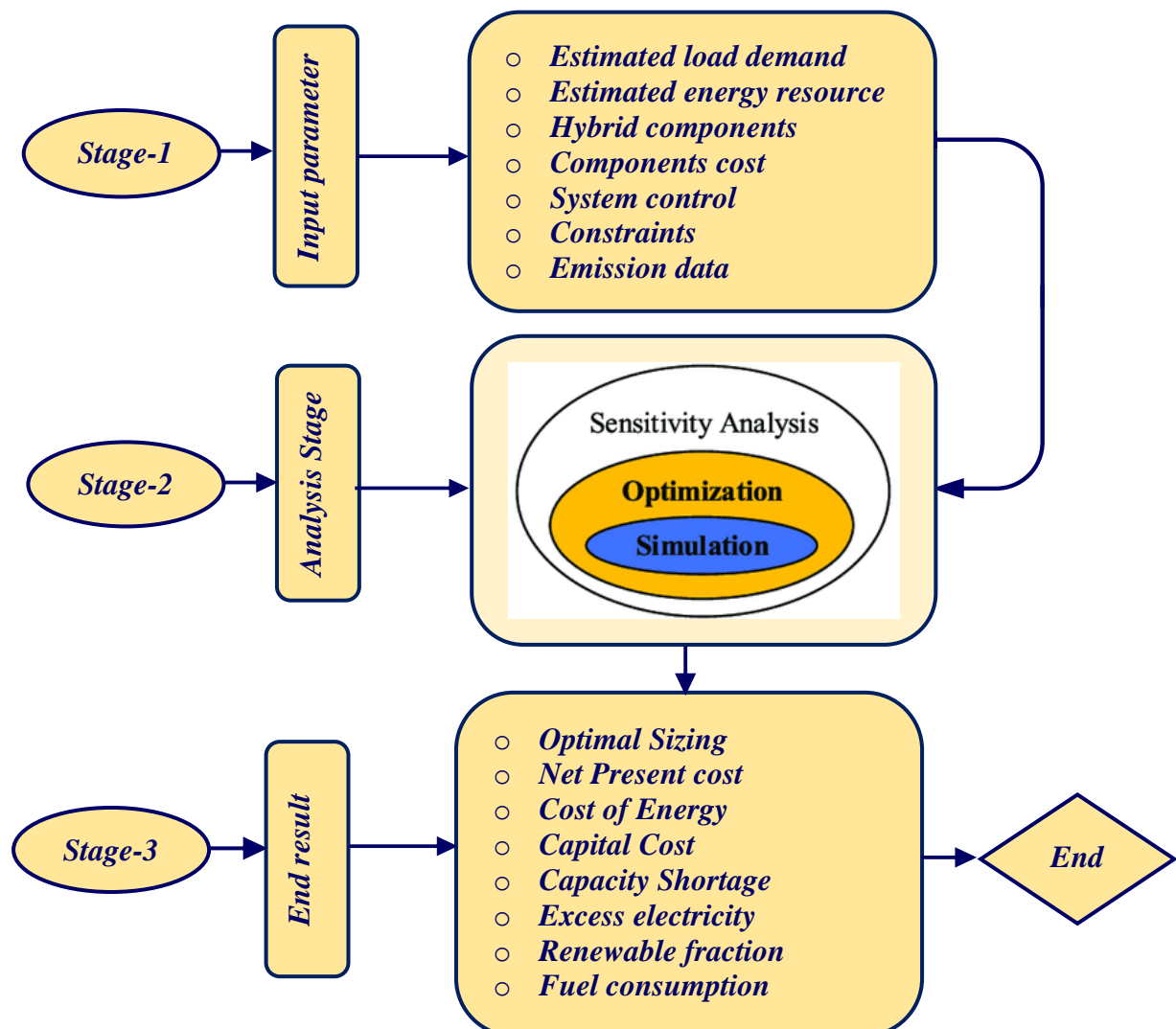


Figure 3.4: Flow chart of HOMER software analysis.

3.5. Load assessment of Study area

The consumption of electricity in a community depends on a number of influences such as the income of its residents and a valid tariff (price per KWh or monthly cost), the cost of competing or substitute services (wood, kerosene), the cost of appliances, and other socioeconomic, economic and cultural factors. Detailed planning methods must take all of these factors into account. However, despite the need to take all of these factors into account, researchers and planners face challenges such as the inability to obtain accurate information and a shortage of recorded data, particularly in rural areas. An onsite survey was conducted in the community, to assess the power demand. A modified version of the standard load Assessment questionnaire created by a GIZ program [83] was used for this study. During field survey in study village the number of populations is 411 households, three elementary school, one Orthodox Church with in Goda Warke village.

Actual load forecasting consists of projecting peak demand requirements for the entire groups of users with the time of project lifetime. In this study, power estimated is based on consumption loads and patterns inferred from each household. It was taken based on the number of room he/she had and his/her affordability to use radio and colour television. In general, Goda Warke village's typical rural domestic consumption is predicated on the assumption of lights, television, radio and charging appliances. The detail analysis is presented in [Table-A 4 in Appendix-A](#).

3.5.1. Load Assessment

The village load is estimated assuming that all households and public sectors utilize efficient appliances and energy saving LED light bulbs. Traditional cooking methods utilizing firewood and charcoal are replaced by one cooking stoves per household. It is assumed that, the electrified household will use energy saving bulbs for indoor lights (depends on number rooms of the household). The setting of the sun is an influencing aspect with the use of light bulbs. Since Ethiopia is right along the equator, the time for dusk is very constant throughout the year. The internal/indoor light bulbs are turned on at around 18:00 and turned off at around 24:00. It is assumed that all of the security/street lights turn on daily from 19:00 until 6:00.

Households in the study area are classified into three classes, Low class households, medium class households and high-class households based on their income capacity. Low class household's accounts 161 household, medium class households 178 household and high class are 72 household. The total number of households in study area is 411.

The best way to compare energy consumption and the cost of running different appliances is to look at their power consumption, which is measure of how much power they use in Watts. An important point is also to bear in mind the length of time for which the device will be used. All values are estimated based on the operating hours in use and wattage of the appliances [84].

i. Load Estimation of Household Sector

In load estimation of households, different assumption was made based on family classes and probability to use household appliances for better estimation of load consumption. The probability of using Colour TV for each family classes are estimated as, 25 percent, 75 percent and 100 percent for low class, medium class and high-class family respectively. It was assumed that only high-class family use fridge in home frequently for food preservation.

It is also assumed that 100% of the households use a tape recorder type radio. Radios and TV sets are used during varying hours of the day, but morning and evening hours are most common. News is a popular listening program, especially in the morning hours, thus it is assumed that most radios will be switched on early mornings for news broadcasts. It is also assumed that the popularity of TV sets will rise rapidly, with at-least 50% of the households owning a television set.

$$\text{Demand power} = \text{No. appliance} \times \text{No. household} \times \text{Wattage} \quad (3.1)$$

The load assessment for the household classes are clearly explained in detail including types of appliances, rated power, operating times and number of appliances in [Table-A 1](#), [Table-A 2](#) and [Table-A 3](#) in [Appendix-A](#), for High, Medium and Low class family respectively.

Table 3.1: Household electric demand estimation.

Household category	Number of households	Appliance	Possibility of using appliance (%)	Quantity	Rated power in (W)	Demand (KW)
High class	72	TV	100	1	120	8.64
		Radio	100	1	10	0.72
		Mobile charge	100	2	5	0.72
		Light bulb	100	4	11	2.12
		Fridge	75	1	100	5.4
		Stove	100	1	1200	86.4
		Medium class	178	TV	75	1
Radio	100			1	10	1.78
Mobile Charger	100			2	5	1.78
Light bulb	100			3	11	5.84
Stove	100			1	1200	213.6
Low class	161			TV	25	1
		Radio	100	1	10	1.61
		Mobile Charger	100	2	5	1.61
		Light bulb	100	2	11	3.542
		Stove	100	1	1200	193.2

3.5.2. Community Load

i. Load Demand Estimation of Small Business Centre and Clinic

In small business centre, barber, beauty salon and sewing machines are considered based on wattage required for operation while Fridge, indoor and outdoor lighting are for small clinic centre.

Table 3.2: Estimated electric demand for small clinic and business centre

Sector Name	Appliance	Quantity	Rated Power in (W)	Demand (KW)
Small Clinic	Lighting indoor	6	11	0.066
	Lighting outdoor	6	11	0.066
	Fridge	2	100	0.2
Small business centre	Singer Machine	6	100	0.6
	Barber (hair clipper)	6	15	0.09
	Hair roller	2	400	0.08
	Hair dryer	2	2500	5
	Hair straighter	2	300	0.6
	Lighting	10	11	0.11
Total				6.81

ii. Load Demand Estimation of Schools and Religious Centre

In study area three school are located. Two schools are grade one up to eight and the remaining is from grade one up to four. 11W LED energy saver light bulbs are suggested for indoor and outdoor illumination. It has also assumed that one desktop with inkjet printer is present in each school with wattage of 450W and 30W respectively. The load demand estimation of each school was presented in a [Table 3.3](#) as follows.

Table 3.3: Estimated load demand of school sectors

Sector Name	Appliance	Quantity	Rated Power in (W)	Demand in (KW)
Idino and Goda Warke (Grade 1-8)	Lighting indoor	16 bulbs	11	0.176
	Lighting outdoor	16 bulbs	11	0.176
	Desktop	2	450	0.9
	Copy machine	2	30	0.06
	Inkjet printer	2	30	0.06
	Megaphone	2	11	0.022
Tamene school (Grade 1-4)	Lighting indoor	4	11	0.044
	Lighting outdoor	4	11	0.044
	Desktop	1	450	0.45
	Copy machine	1	30	0.3
	Inkjet printer	1	30	0.3
	Megaphone	1	10	0.01
Total				2.542

Churches, street lights, and a farmer training center (FTC) are considered for load forecasting in the case of calculation of load demand for worship places and other sectors. For indoor and outdoor lighting purpose and street lighting 11W LED energy saver light bulbs and 100W incandescent light bulbs are considered respectively.

Table 3.4: Estimated load of other community sectors.

Sector name	Appliances	Quantity	Rated Power in (W)	Demand in (KW)
Orthodox church	Lighting indoor	8	11	0.088
	Lighting outdoor	6	11	0.066
	Megaphone	1	82	0.082
Street Light	Lighting (100 W incandescent light bulb)	50	100	5
Farmer Training Centre (FTC)	Indoor lighting	4	11	0.044
	Outdoor lighting	3	11	0.033
Total				5.324

Energy consumption in each sector is determined based on energy demands in each sector and the operating time of appliances used in the sector.

$$\text{Energy consumed per day (KWhr/day)} = \text{Energy demand} \times \text{operating hours per day} \quad (3.2)$$

The daily load assessment data was classified as residential, community and Commercial load, with respective time sequence of daily electric consumption. The school, Clinic, worshipping place and farmer training centre loads are a community load. The load consumption based on home appliances of the community such as lighting and cooking load are grouped as a residential load. The time of load consumption was counted based on international time counting method with 24 hrs format, starting from morning at 7:00 AM-6:00 AM as shown in Table 3.5, Table-A 4, Table-A 5 and Table-A 6 in Appendix-A.

Table 3.5: Load consumption profile

Time	Residential Load consumption	Community Load Consumption	Commercial Load Consumption	Total Load
7:00	85.022	0.476	0	85.498
8:00	82.742	0.96	0.11	83.812
9:00	87.942	0.84	2.09	90.872
10:00	71.582	0.39	9.59	81.562
11:00	72.272	0.84	9.59	82.702
12:00	75.082	0.75	9.59	85.422
13:00	74.102	0.39	2.09	76.582
14:00	68.782	0.84	2.09	51.712
15:00	46.04	0.87	9.59	56.50
16:00	45.87	0.66	9.59	56.12
17:00	84.48	0.78	2.09	87.35
18:00	64.502	0.46	9.7	74.662
19:00	73.932	5.59	2.2	81.722
20:00	73.932	5.93	2.2	82.062
21:00	46.742	5.79		52.532
22:00	14.05	5.57		19.62
23:00	0.49	5.57		6.06
24:00	0.49	5.57		6.06
1:00	0.23	5.74		5.97
2:00	0.23	5.74		5.97
3:00	0.23	5.74		5.97
4:00	0.23	5.74		5.97
5:00	0.23	5.74		5.97
6:00	58.47	0.62		79.09
Total	1127.674	71.596	70.52	1269.8

3.5.2. Study area load Profile

In this study, the load of the selected village is divided into three categories: residential load, community load, and commercial load. The residential load includes lighting and cooking loads, whereas community load includes school's load, religious centre, clinic, farmer training centre. Small business centres are considered as commercial load. A load profile of the study site is illustrated in Figure 3.5 based on the electric demand data entered into HOMER with a random day-to-day variability of 10% and time step of 20%. The power system serves for 24 hours per day and the hourly load consumption shifts throughout the day with peak demand of 155.36 KW, average load of 52.91 KW, average energy consumption of 1269.79 kWh/day and load factor of 34 %.

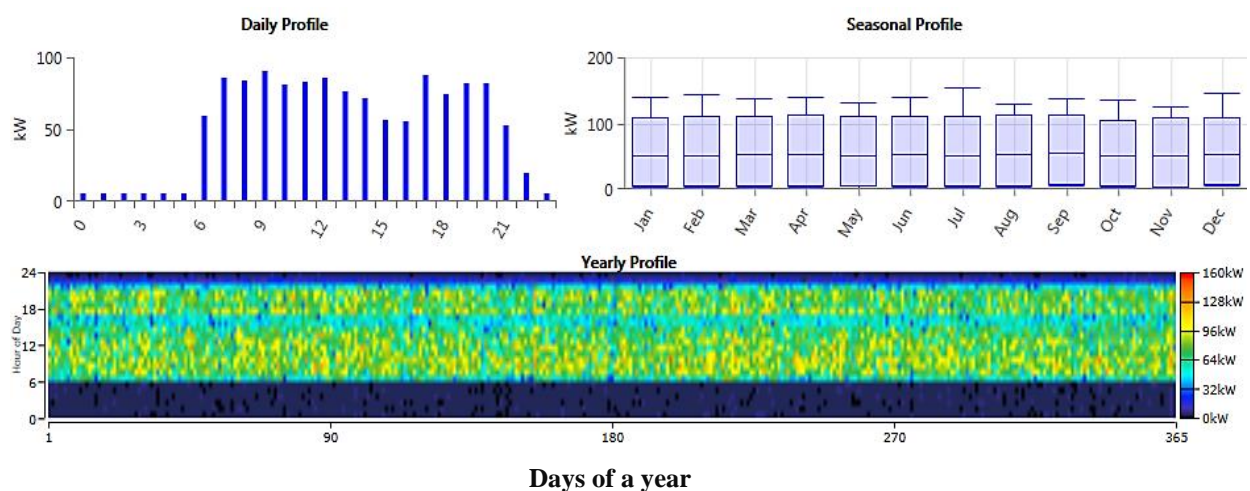


Figure 3.5: Load profile of Study area

3.5.2.1. Electricity demand forecasting

An end-use technique is employed in this study to anticipate demand increase in a distant location served by a hybrid power system. This technique states that the community's present energy demand is first calculated based on end-device energy consumption, and the energy demand is then forecasted during the project's lifetime based on household increase owing to population growth and system penetration [10].

Forecasting the load growth of the study area is essential for operating and planning of energy utilization from hybrid system. Therefore, the end use approach is used in this study to forecast the energy demand projected throughout the project life time based on the growth of households in the study site using equation (3.3). The forecasted load growth was discussed in Appendix-A Table-A 8.

$$E_i = E_o + S \times (h_i - h_o) \times E \quad (3.3)$$

Where E_i is the i^{th} year annual average energy demand in KWh/day

E is Annual average energy consumption in $KWh/day/household$

S is customer penetration rate

E_o is annual average electricity demand in KWh/day in base year

h_o is the number of households in base year

h_i is the number households in the i^{th} year

3.5.2.2. Population and energy demand

The total electricity consumption is heavily influenced by growth in population. However, the electricity demand is supplied for households, the increase individual population increases the number of households and energy consumption. According to data [85][86], the average rural population growth rate of Ethiopia is about 2.6 %. The figure is assumed constant throughout the project life time and used to determine the population of the study area in the next 25 year. The population size of the study area in 2021 is about 1644 (411 HH). This population figure is projected by an annual growth rate of 2.6 % as shown in Table-A 7 in Appendix-A, until the end of the forecasted period and converted to total number of households using a given number of 4 occupants per household. Equation (3.4) is used for population growth forecasting.

$$P_n = P_o \times \left(1 + \frac{r}{100}\right)^n \quad (3.4)$$

Where P_n is population at n^{th} year, P_o is current population, r is annual population growth rate in %.

3.5.2.3. Customer penetration

Customer penetration indicates the number of newly growing households that are connected to the system annual to be electrified. It's the ratio of number of populations to be electrified in the base year to the total number of population number in project life [87] [88].

$$\text{Customer penetration (CP)} = \frac{P_o}{P_n} \times 100 \quad (3.5)$$

3.6. Discharge estimation flow chart of ungauged catchment of Girar River

The discharge of Girar River is estimated based on ArcGIS Satellite image remote sensing method with SRTM (shuttle radar topographic mission) Image of 30 m resolution and band composite of 0.01% cloud cover.

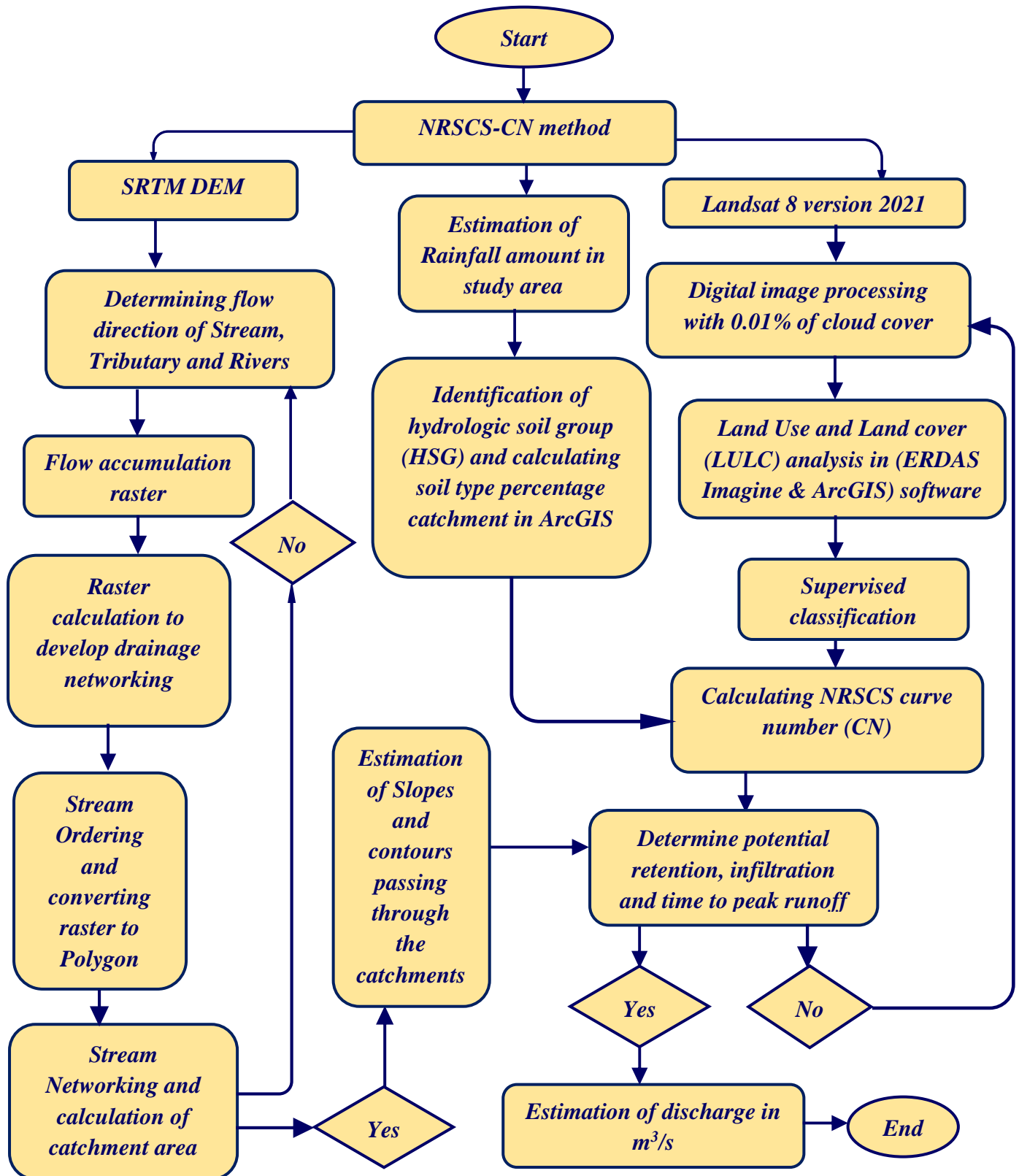


Figure 3.6: Flow chart of discharge estimation in ungauged catchments.

3.6. Hybrid system connection schemes layout

The hybrid-system connection schemes classified into three major types depending on the kind of voltage system and the bus that interconnect the sources. The most common hybrid system connection schemes are AC bus line, DC bus line, and mixed bus line. In this study AC and DC buses are used in hybrid configuration system as shown in Figure 3.7.

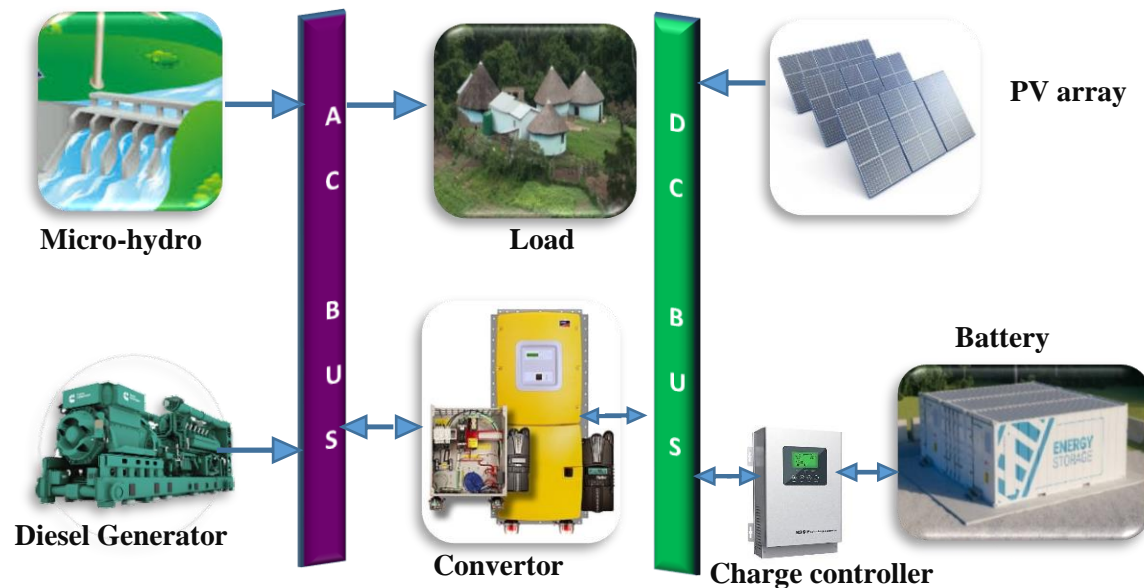


Figure 3.7: Connection schemes of hybrid system

3.6.1. Pre-HOMER analysis

Before starting simulation with HOMER Pro, different input variables are considered. The first Input parameters are selection of study area and components of the hybrid system. The second input is energy resource. Solar and hydro resource, given in Table 2.4 and Table-A 11 are used for this works respectively. The components costs are selected based reviewed literatures, considering average cost and affordability of the components in the recent market. The cost of components used for this works are stated in Table 2.7 and Table 2.8.

In addition, sensitivity variables are considered to study techno-economic analysis. The various values are assigned to these variables to determine their influences on the optimized proposed system and energy potential assessment of the study area.

Table 3.6: Sensitivity variables with assigned values

Sensitivity variables	Assigned values	Units
Net head	50, 52, 54, 56, 58	M
Average stream flow	918, 950, 980, 990, 1000	L/s
Electric load consumption	1289.8, 1300, 1350, 1400	KWh/day
Pipe head loss	5, 10, 15, 20, 25	%
Diesel fuel cost	0.5, 0.6, 0.7, 0.8, 1	\$/KWh
MHP plant efficiency	75, 80, 85, 90, 95	%

In Ethiopia the mean inflation rate is 7.5 % in a year of 2005-2010 according to [89]. Recent study on [90], considered 10.51 % of energy inflation rate for optimization and sizing of HRES on lake Tana. Inflation rate of 11 % with 8% discount rate is considered in this work for simulation. The Sensitivity analysis by [91], said that Ethiopia should invest more in renewable energy resource based power generation such as solar PV. The future capacity for solar PV increases significantly to 2.49 GW -9.24 GW with this low discount rate in 2040-2045.

The technology option, component pricing, component specification, and resource availability should be under consideration when modeling hybrid components. As a result, the availability of renewable resources at a place might vary significantly from site to site, which is an important consideration in constructing the hybrid system. Figure 3.8 depicts the hybrid power generating systems modeled in HOMER utilizing load, resources, component size, cost, and technical parameters. The micro-hydro power generation is linked to an AC bus, whereas the PV and batteries require a DC bus and a converter.

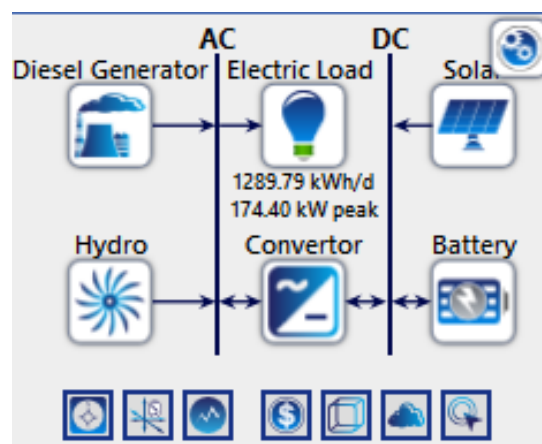


Figure 3.8: Schematic representation of proposed hybrid system by HOMER pro.

CHAPTER 4

4. RESULT AND DISCUSSION

4.1. Rainfall intensity in study area (mm)

In study area, the maximum rainfall amount is received for three months during summer season which is June, July and August. During this time the potential evapotranspiration (PET) is very low due to moderate shining of the sun in cloudy season. The rainfall amount (precipitation) of the area were estimated by data collected from National meteorological agency (NMA) and the result is compared with NASA and New-LoClim 1.10 software. Seven years monthly rainfall data was collected from national meteorological agency from 2012-2018 in [Figure 4.1](#). The average of each year was used in this study for comparison with precipitation obtained from NASA and New-LoClim 1.10 software as depicted in [Figure 4.2](#).

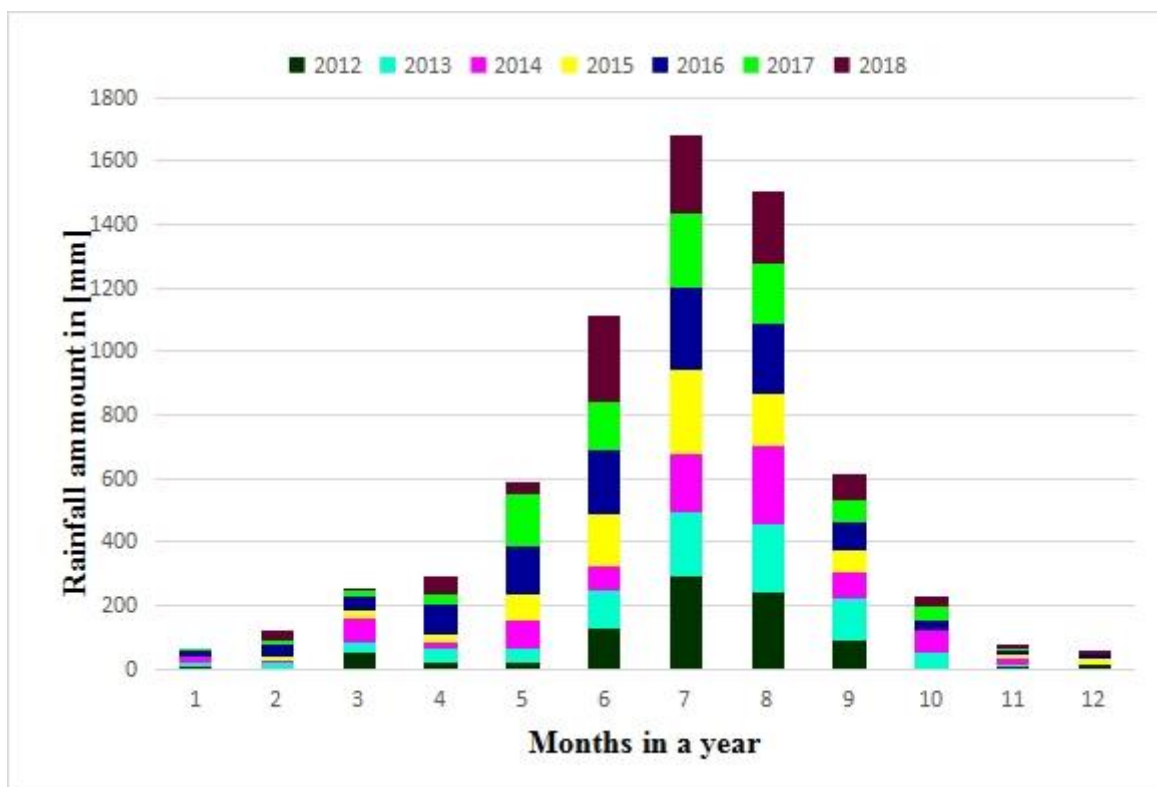


Figure 4.1: Recorded rainfall amount in Yaya Gulele district from 2012-2018.

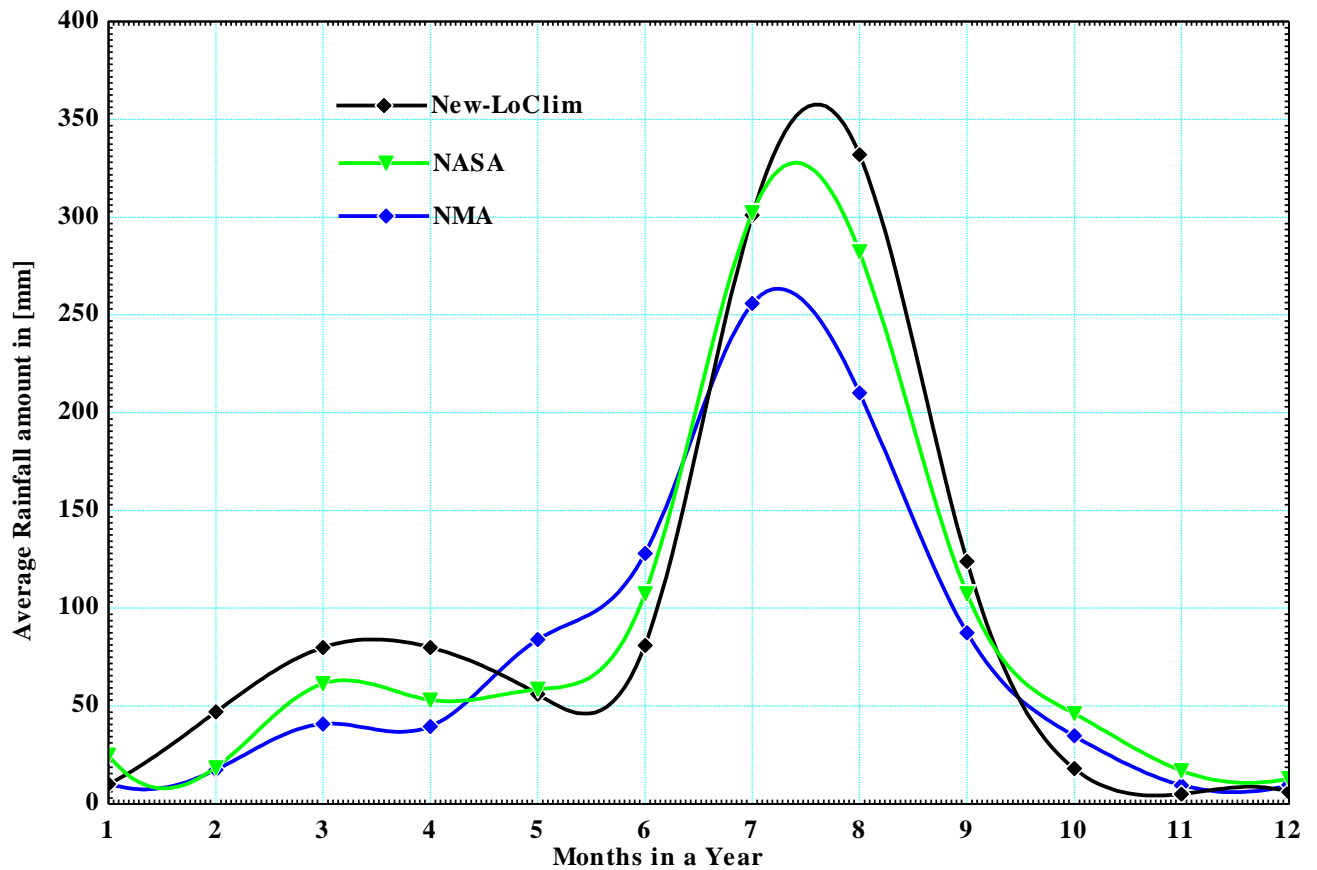


Figure 4.2: Estimated Average rainfall amount in steady area

In addition, potential evapotranspiration may be calculated using readily accessible rainfall and temperature data. It is the potential evaporation from soils plus plant transpiration. The evaporation rate is affected by climatic circumstances, notably the sun's radiative radiation, wind, the air's vapour deficit, and temperature. Evapo-transpiration is significantly impacted by the available soil moisture.

New-LoClim 1.10 estimates the amount potential of evapo-transpiration in the study area with three option of estimation high estimation, average estimation and low estimation respectively. The average estimation of evapo-transpiration is considered for this study in estimation discharge from catchments. According to analysis evaporation and transpiration rate is high between 2nd and 5th months (February-May) and 10th -11th (October and November). The lowest evaporation rate occurs between 6th -9th (June up to September). In average the highest and lowest amount of evapotranspiration rate is occur at March and August which is 120.9 mm and 77.5 mm respectively.

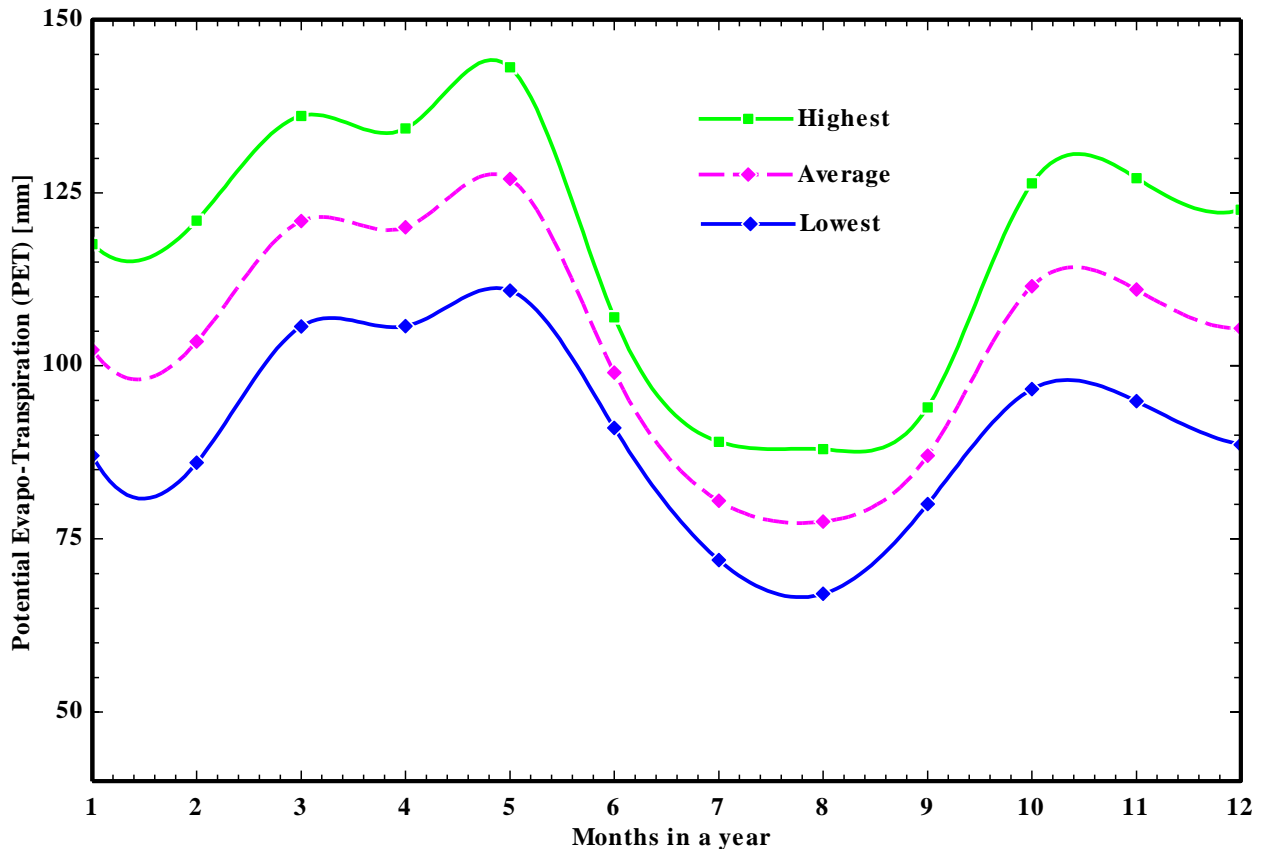


Figure 4.3: Potential Evapo-Transpiration amount in mm

4.2. Discharge estimation of Girar River

The discharge of the selected catchment in study area can be estimated from a rainfall amount in area with NRSCS curve number method by using ASRTM DEM delineation in ArcGIS considering parameters such as, flow direction, flow accumulation, flow length, stream ordering, stream networking, contour, slope as well as land use and land cover (LULC) of the catchment.

4.2.1. Stream order and stream networking

Stream order is concerned with the hierarchy of streams from the source (or head waters) to downstream. It's calculated in ArcGIS using Strahler method. The head waters are the first order, while downstream parts are designated at confluences (two stream running into each other).

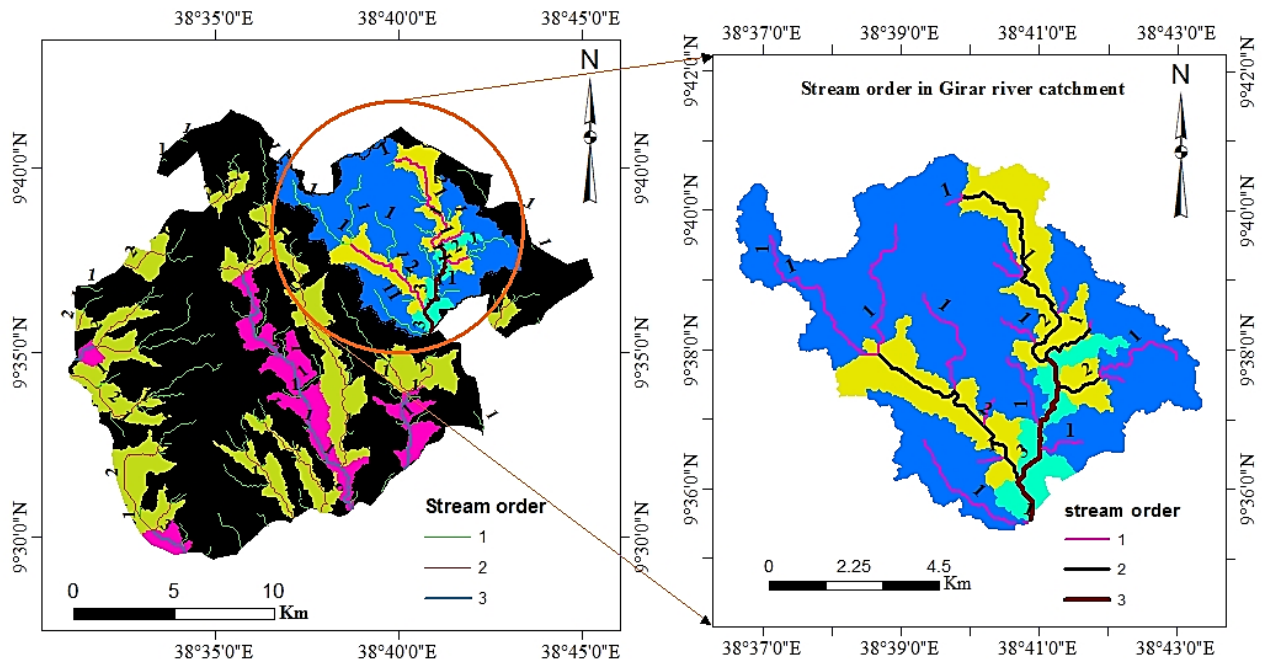


Figure 4.4: Stream ordering and flow direction of rivers and streams in study area.

The classification of the flow accumulation is determined with two classes and the stream order is arranged with three orders where the first is headwater, the second order arrangement is tributaries the highest order (3rd order) is the main river. The highest order indicate there is high water accumulation in stream when compared to the upper stream flow.

4.2.2. Analysis of Catchment area (Drainage area)

It is an important parameter for calculating discharge of ungauged river based on rainfall intensity on the drainage area. To determine the catchment of the Girar river parameters such as, stream order, flow accumulation and flow directions are considered as input parameters. The Girar river catchment is the second largest catchment in Yaya Gulele district, which has 62.69 km² of shape area, in Figure 4.5b. Due to the topographical infeasibility, the first catchment (Aleltu River) with 76.15 Km² of shape area is not suitable for micro-hydro power generation system.

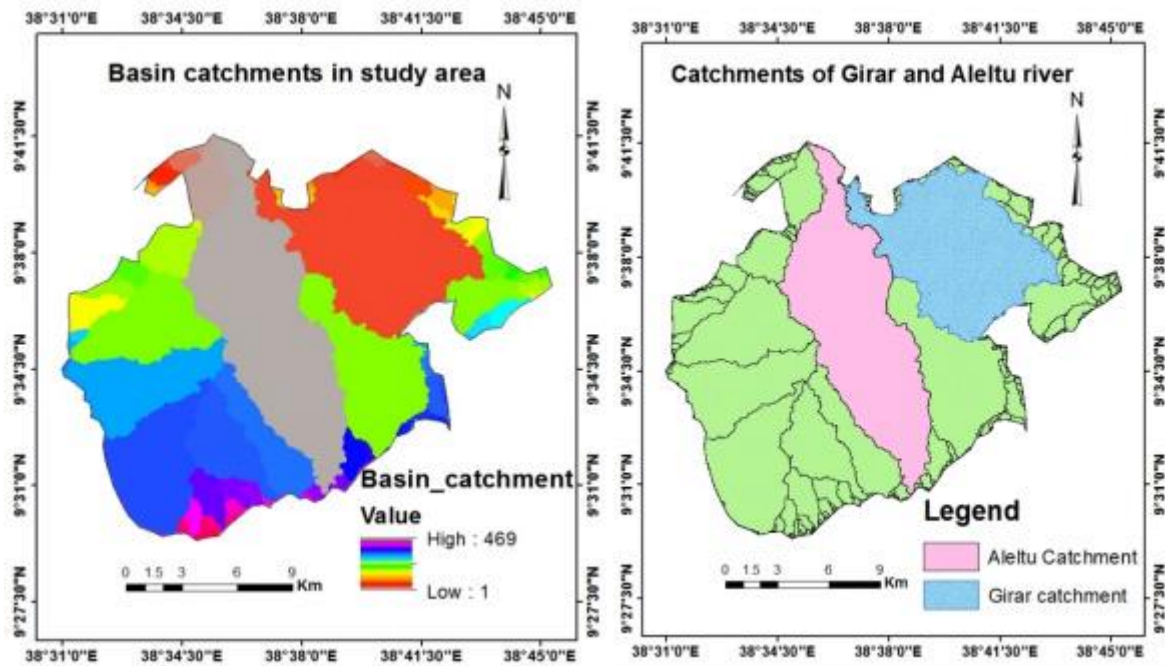


Figure 4.5: a) Degree of basin catchments in study area b) catchment area of Girar and Aleltu River

Changes in land use and land cover, as well as rainfall, have a substantial impact on the hydrological response of river basins. The Natural Resource and Soil Conservation Service-curve number (NRSCS-CN) approach was used in combination with a geographic information system (GIS) and remote sensing (RS) to predict surface runoff in the Girar watershed in the Yaya Gulele region. Significant runoff-associated watershed variables such as land use/land cover (LULC), hydrologic soil group (HSG), slope, and climatic conditions have the most effect. LULC analysis show that six main land use and cover classification such as Good covered forest, thin stand cover forest, cultivated land with treatment, cultivated land without treatment, Settlement area and River flow basins are considered in detail [Figure 4.6](#).

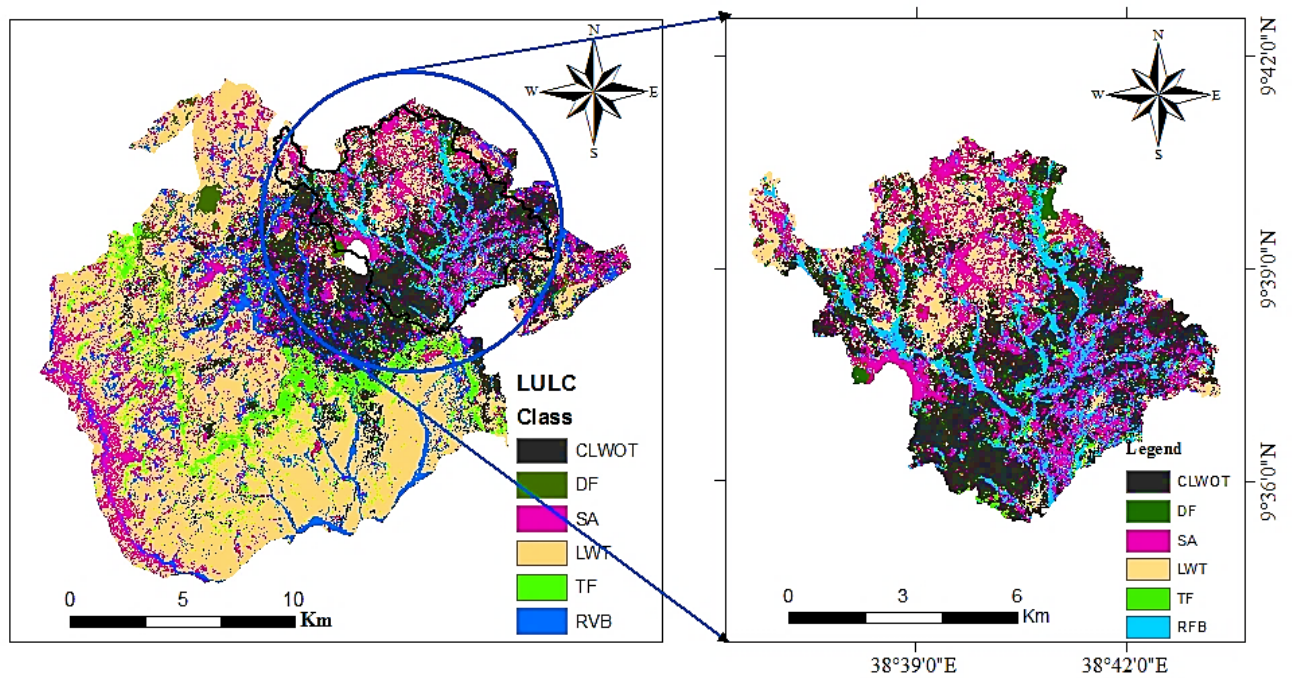


Figure 4.6: Land Use Land Cover classification of Girar River Catchment

In this study the LULC analysis was done for Girar river catchments to determine the monthly flow rate of the river based on soil type of catchments and rainfall intensity falling in area for each month. The (x, y) co-ordinates of ground truth points are collected by integration of Google-earth pro with ERDAS Imagine software. An overall accuracy and Kappa co-efficient (K) of 89.58 % and 0.877 were achieved respectively. Since runoff in catchments depends on infiltration, potential retention, slope percentage and abstraction, it's necessary to classify LULC of study area through satellite remote sensing image classification method to determine curve number (CN) and potential retentions of the catchments in estimation of discharge. Therefore, according to software analysis of LULC, from total area of Girar River Catchments the portion of each classification in percentage is the area of each class divided by total area of catchments as shown in [Table 4.1](#).

Table 4.1: Percentage of Land use and land cover classification of catchment area

LULC classification	Sum of Area (Km ²)	Percentage (%)
Cultivated land without treatment (CLWOT)	41.23	65.5153044
Cultivated land with treatment (CLWT)	9.65	15.3279448
Dense forest (DF)	0.31	0.4960461
Settlement area (SA)	6.08	9.6604878
River flow basins (RFB)	0.04	0.0646744
Thin forest (TF)	5.62	8.9355425
Total	62.93	100

4.2.3. Hydrologic soil Group (HSG) of the catchments

Based on obtained percentage of area, the hydrologic properties such as soil types has identified to determine the Curve number of the catchment. The covered area of each soil type is calculated using ArcGIS software by raster to polygon conversion tools. Figure 4.7 illustrates the ArcGIS output of soil types with their corresponding HSG. Then the polygon areas corresponding to each soil type is converted as excel file to calculate the total area of each soil types as shown in Table 4.2. The corresponding HSG of soil type is based on data given in Appendix-A Table-A10.

Table 4.2: Percentage of Soil type and HSG classification of catchment area

Soil Type	Sum of Area [km ²]	Group	Percentage	HSG %
Pellic vertisols	0.88	B	1.41	B=6.98 %
Eutric nitsols	3.51	B	5.57	
Eutric cambisols	58.57	D	93.02	D=93.02 %
Total	62.96		100	

In this work, HSG, B & D are considered for Girar River catchment based on ArcGIS HSG analysis method using conversion tool from raster to polygon. The analysis in Figure 4.7 shows that the covering areal percentage of soil types in the catchments are 1.4 % Pellic vertisols, 5.58 % Eutric nitsols and 93.02 % Eutric cambisols respectively. All soil type in this catchment area, corresponds its HSG according to world HSG classification standards as shown in a Table 4.2.

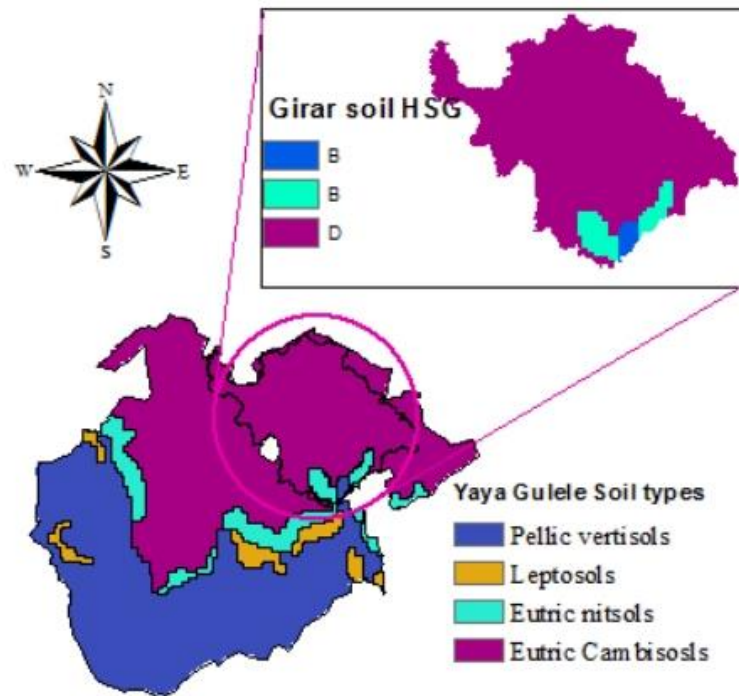


Figure 4.7: Hydrologic soil group in Girar catchments

The weighted curve number of the study area depends on LULC of the catchment. Considering Table-A 13 in Appendix-A, as a reference and Table 4.2, the calculated portion of soil type is 6.98 percent for type B and 93.02 percent for type D.

Table 4.3: LULC percentage of Girar River Catchment and corresponding HSG with curve number.

Land Uses	Hydrologic soil Group						
	%	B		D		Product	
		CN	Product	%	CN		
Settlement area	0.675	68	45.9	8.99	79	710.21	
Cultivated land	Without conservation treatment	4.57	71	324.47	60.94	81	4936.14
	With conservation Treatment	1.07	81	86.67	14.26	91	1297.66
Wood or forest land	Thin stand and poor cover	0.625	66	41.25	8.31	83	689.73
	Good cover	0.035	55	1.925	0.46	77	35.42
River flow basin	0.005	100	0.5	0.06	100	6	
Total	6.98 %	-	500.715	93.02 %	-	7675.16	

Therefore, Weighted curve number

$$CN = \frac{500.715 + 7675.16}{100} = 81.76$$

$$S = \frac{1000}{CN} - 10 = \frac{1000}{81.76} - 10 = 2.23 \text{ inch} = 56.66 \text{ mm}$$

A high CN indicates low infiltration and high runoff, while a low CN implies high infiltration and low runoff.

4.2.4. Analysis of Slopes and contours

Natural catchments are defined by distinct drainage patterns and topographies that indicate the boundaries of a catchment area. Because the slopes and topographies of the Girar catchments are acquired from ArcGIS, catchment size is not a reliable predictor of discharge effects such as land use, soil type, and slope are more relevant, but catchment size is extremely important in terms of absolute values. Contour lines passing through the catchment and slope percentages are presented by Figure 4.8.

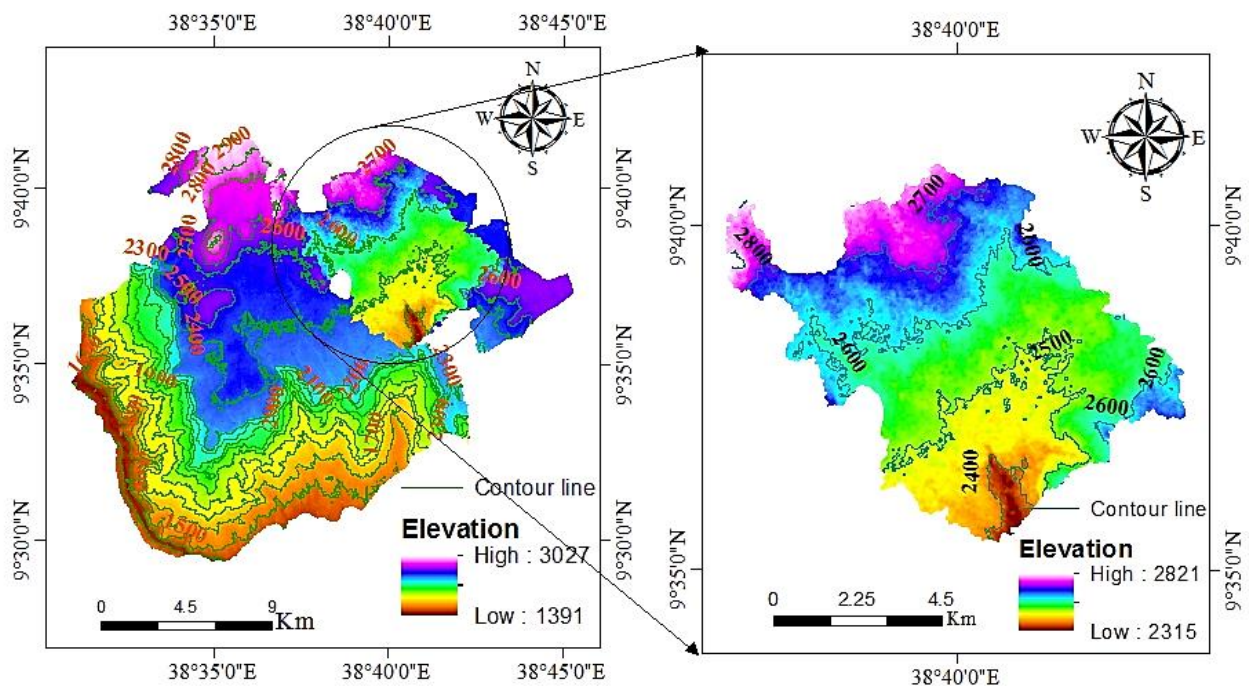


Figure 4.8: Elevation and Contours passing through the catchment

As shown in [Figure 4.8](#), the contours passing in the catchments are in meters with contours interval of 100 m. The slope of the basin is determined as percentage of slope and it can also be obtained from multiplying the sum of the length of contours passing through the catchment with the contour interval and dividing for catchment area in meter square. From the [Figure 4.8](#) length of contours passed through the catchments are 2400 m, 2500m, 2600 m, 2700 m and 2800 m.

$$\begin{aligned} \text{slope}(Y) &= \frac{100 \times CI}{A} = \frac{100 \times (2400 + 2500 + 2600 + 2700 + 2800)m \times 100m}{62941348.4 m^2} \\ &= 2.065 \end{aligned}$$

4.2.5. Monthly Stream flow rate estimation

The parameters analysed above, such as rainfall amount, infiltration and potential retention are used to calculate monthly stream flow of Girar River. Infiltration and potential retention are parameters that depends on LULC and soil type in the catchment of the ungauged Girar River.

Based on the precipitation amount, losses due to properties losses of the soil type, slopes and drainage area of the catchments monthly discharge of Girar River is calculated by substituting the analysed value of listed parameters into equation (2.17) . The results are tabulated in [Appendix-A Table-A 12](#). The obtained result is based on meteorological rainfall data from NMA. The Monthly discharge of New-LoClim, and NASA precipitation data are also analysed for comparison as illustrated by [Figure 4.9](#). According to NMA, the maximum, minimum and average flow rate of Girar river is 4.22 m³/s (July), 0.01 m³/s (January) and 0.975 m³/s respectively.

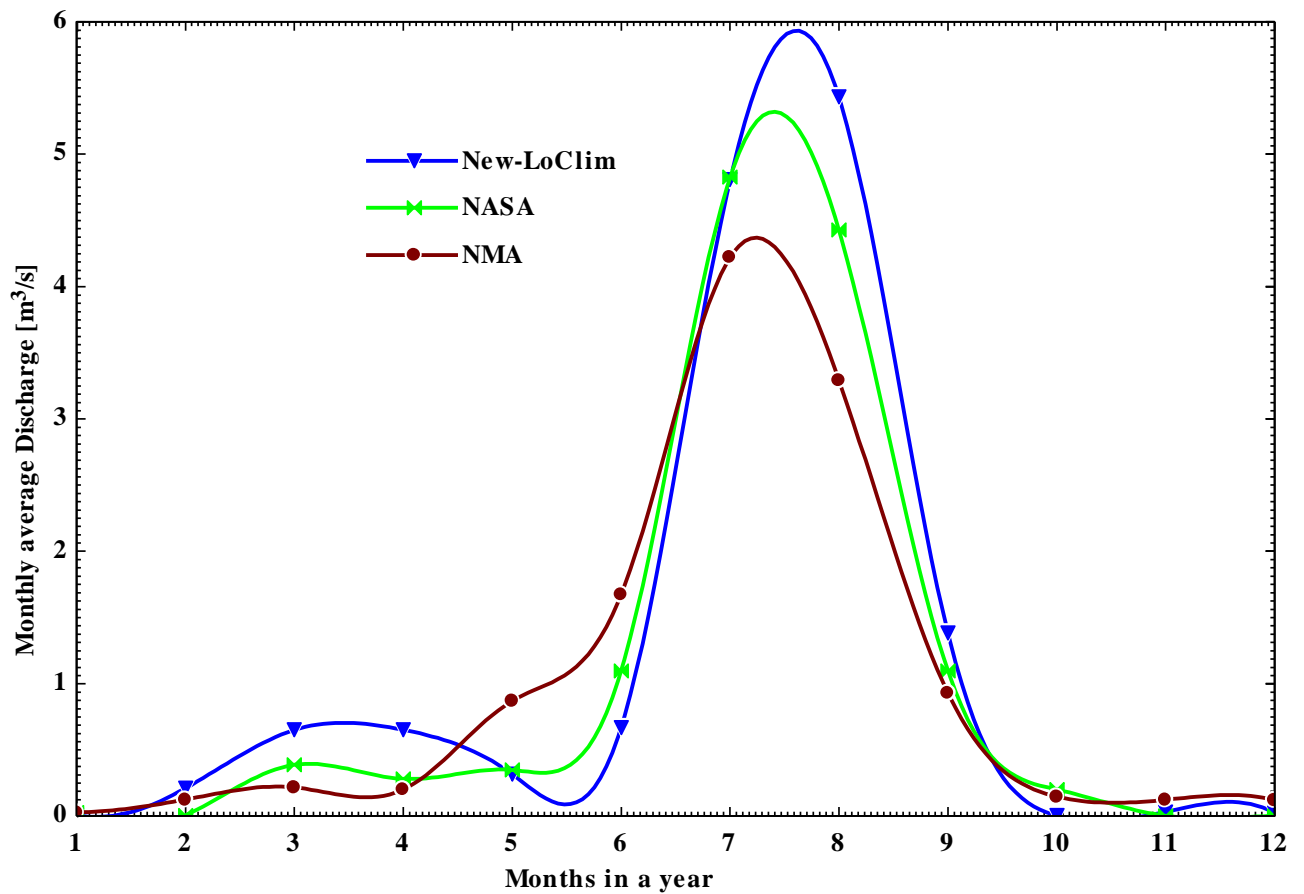


Figure 4.9: Estimated discharge of Girar catchments.

Table 4.4: Flow rate arrangement in ascending order and ranking

Months in a year	NMA flow [m³/s]	NASA flow [m³/s]	New-LoClim flow [m³/s]	Rank	Excedence(%)
1	0.01	0.00086	0.00784	12	100
2	0.0118	0.0015	0.02416	11	91.67
3	0.0122	0.00427	0.03058	10	83.33
4	0.124	0.02707	0.03192	9	75
5	0.146	0.2003	0.2097	8	66.67
6	0.201	0.2801	0.3154	7	58.33
7	0.216	0.348	0.6507	6	50
8	0.869	0.387	0.6506	5	41.67
9	0.929	1.094	0.6658	4	33.33
10	1.671	1.095	1.381	3	25
11	3.291	4.426	4.807	2	16.67
12	4.222	4.828	5.432	1	8.33

FDC considers a total time series of flows that represent equal increments of time for each measurement value, such as mean daily, weekly, or monthly flows, and ranks the flows according to magnitude. According to a figure above a full year flow is at 0.01 m³/s which is at 100% of exceedance.

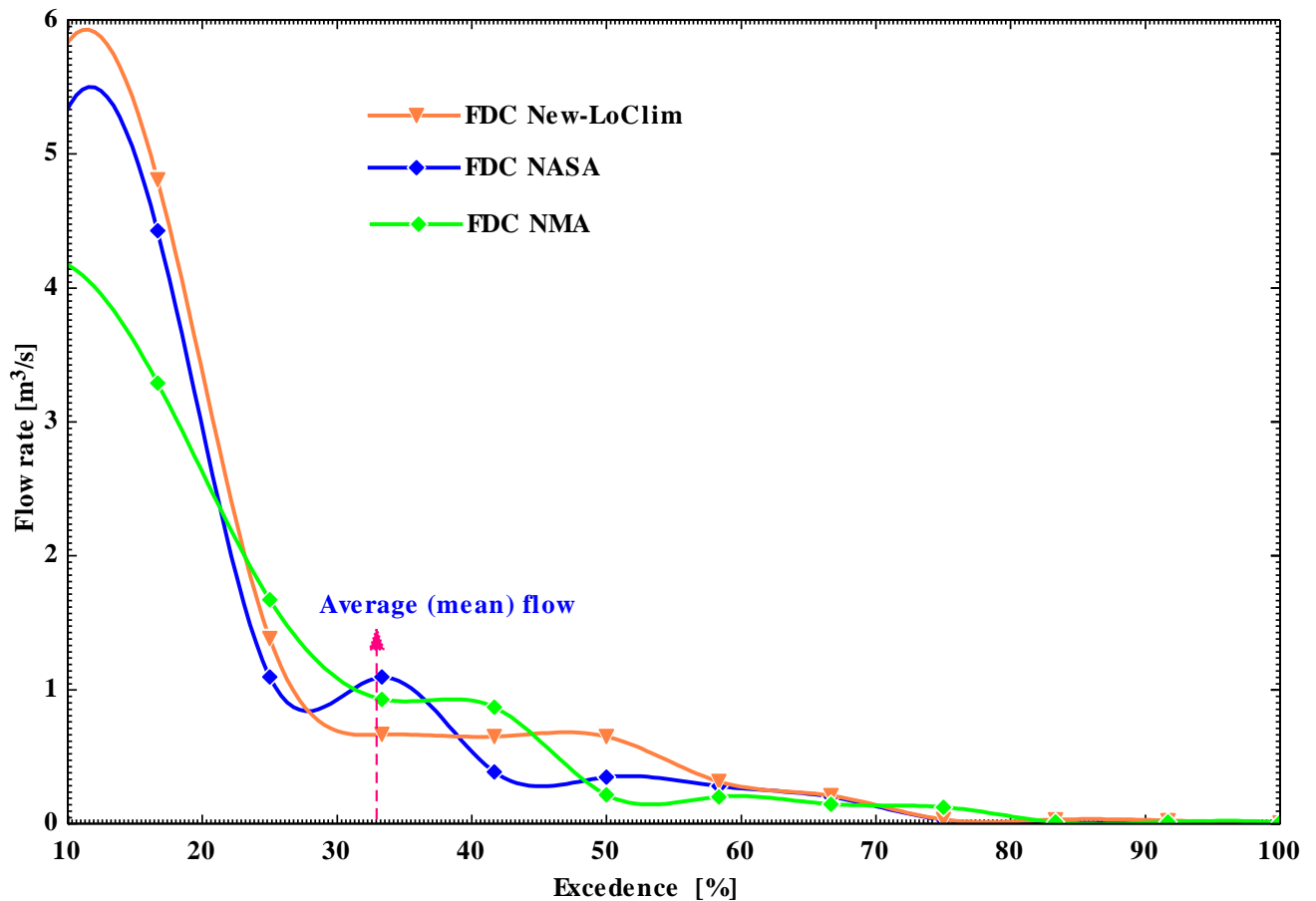


Figure 4.10: Flow duration curve based on rank order technique

The Average (mean) flow rate are 0.975 m³/s, 1.057 m³/s and 1.184 m³/s from NMA, NASA and New-LoClim respectively. Since the micro hydropower system is integrated with photovoltaic, the Mean flow rate at 33.85% of flow time (exceedance) is considered as the design flow of the system. The design flow of the system is 0.975 m³/s according to estimated discharge from NMA data. Considering the average of NMA, NASA and New-LoClim data the average design flow becomes 1.05 m³/s.

4.3. Micro-Hydropower Potential of study area

4.3.1. Estimation Gross Head

Gross head is the vertical height between the downstream at the hydropower house and upstream at the intake point along the river. It is sometimes called an elevation difference. The gross head for micro-hydro power generation system for Girar River is estimated by Contour lines generated on DEM of the Yaya Gulele district using ArcGIS. Contour lines are generated with 50 m interval from DEM using spatial analyst tool in ArcGIS.

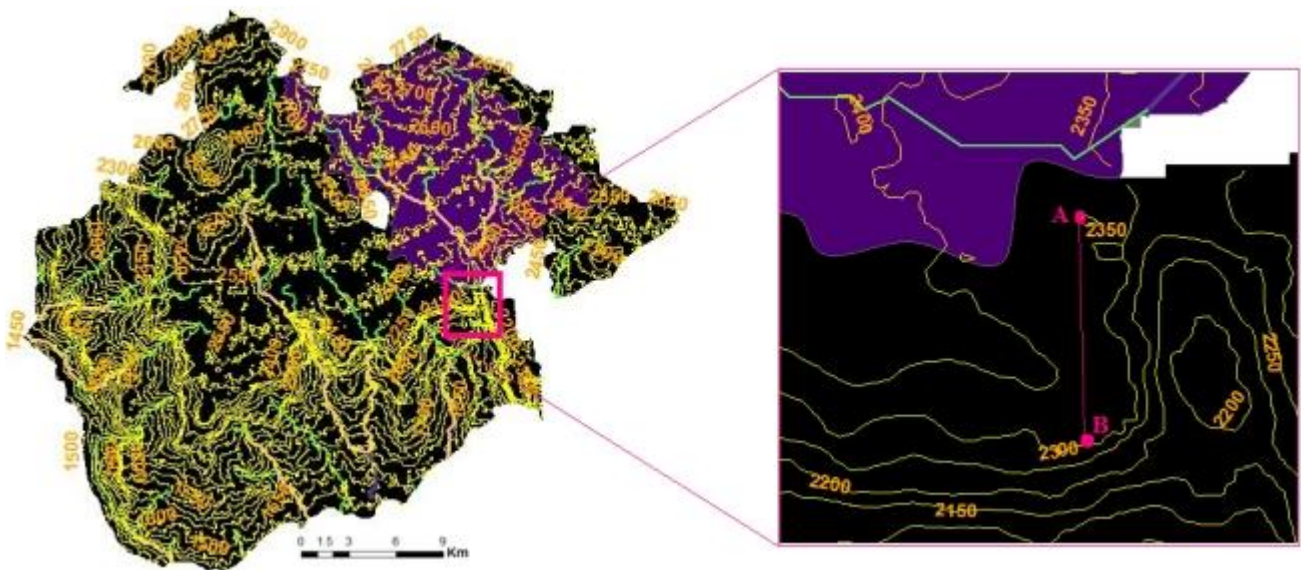


Figure 4.11: Gross head measurement using contour lines based on DEM.

The gross head is measured based on the difference between contour value at point A and point B as presented in Figure 4.11. Point A is considered as intake point of the diversion weir and point B as a power house. The designation of Point A is targeted at the outlet of the catchment at which there is high flow accumulation. The value of contour at Point A and B is 2350 m and 2300 m respectively. Therefore, the possible value of gross head that can be developed from the elevation is assumed to be between the range of the difference between point A and point B for this study. The difference between the two points is 50 m. The Gross head value between 50 and 60 m is considered for sensitivity analysis of this work.

According to Hydropower classification of Ethiopia in Table 1.2, Micro-Hydropower ranges from 11-500 KW. Therefore, the power generation Potential of Girar River in study area is calculated by using equation (2.3) and (2.4) The rate is taken as average mean flow of the year-round flow of the river based on the flow duration curve.

The mean average flow rate of $0.918 \text{ m}^3/\text{s}$ at 34.12% of flow time (exceedance) is considered as the year-round design flow of the system. The hydro turbine efficiency was estimated to be 75.2 % from hydro turbine manufacturer's specification with net head of 50 m.

$$P = \rho \times Q \times g \times H \times \eta$$

$$P = 1000 \text{ Kg}/\text{m}^3 \times 0.918 \text{ m}^3/\text{s} \times 9.18 \text{ m}^2/\text{s} \times 50 \text{ m} \times 0.752$$

$$P = 338.61 \text{ KW}$$

4.4.Solar energy Potential assessment

4.4.1. Estimation of solar radiation

To estimate available solar energy resource of the area, the relevant data collected from the National Meteorological Agency (NMA) of Yaya Gulele district based on the sunshine hours. Sunshine hour is an important parameter that helps to estimate the solar radiation at a given location. As shown in figure, the study area's sunshine duration is increasing from October to May and slightly decrease in the summer season. The result shows that the maximum of 8.59 sunshine hours is in November and a minimum of 5.26 hours in July.

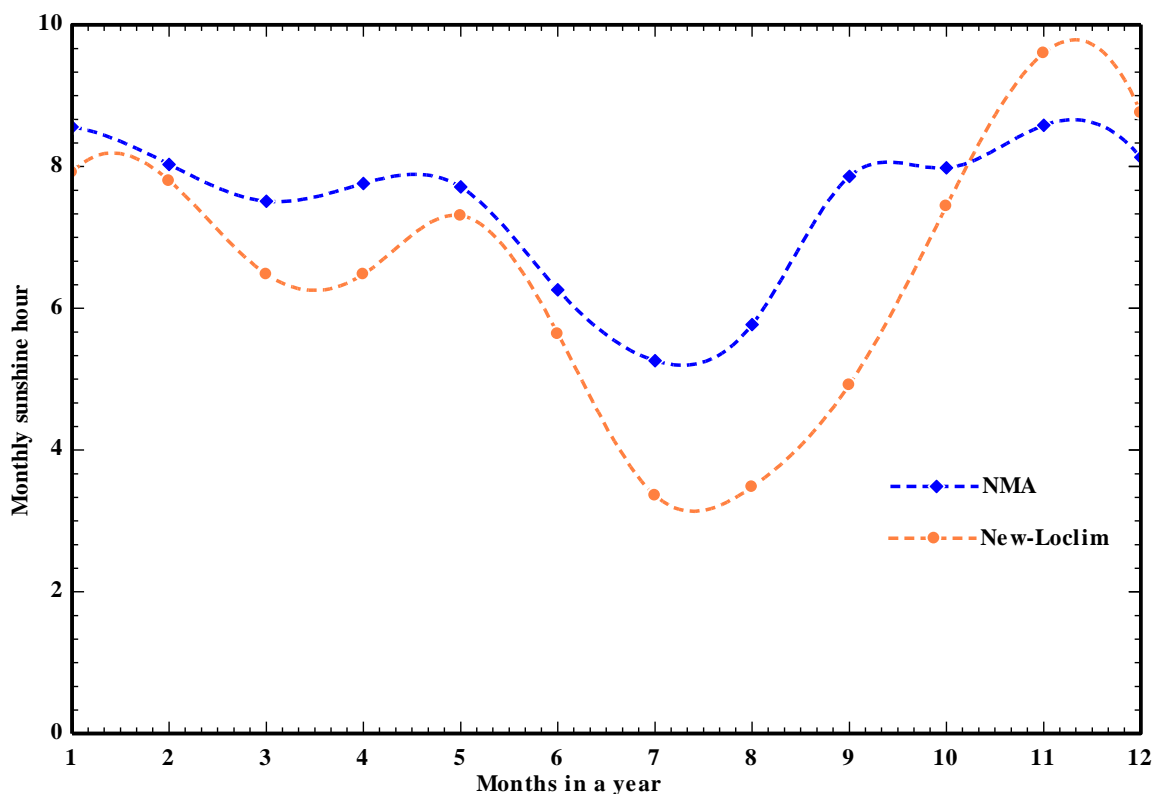


Figure 4.12: Variation of Sunshine hour in months of the year

Monthly average Beam radiation, diffuse radiation and diffuse reflected radiation are calculated from National Meteorological Agency data of the study area. The results obtained from solar radiation calculations, by using sunshine hours of the locations $9^{\circ}3'N$ and $38^{\circ}6'N$ longitudes Variation of solar radiation of each day gives the different energy potential in the year. According to estimated value using the NMA data, the peak value of the beam radiation for Goda Warke Village is 24.3 MJ/m^2 in December. In addition, the minimum beam radiation is 14 MJ/m^2 occurs in July. The annual average beam solar radiation is 19.84 MJ/m^2 .

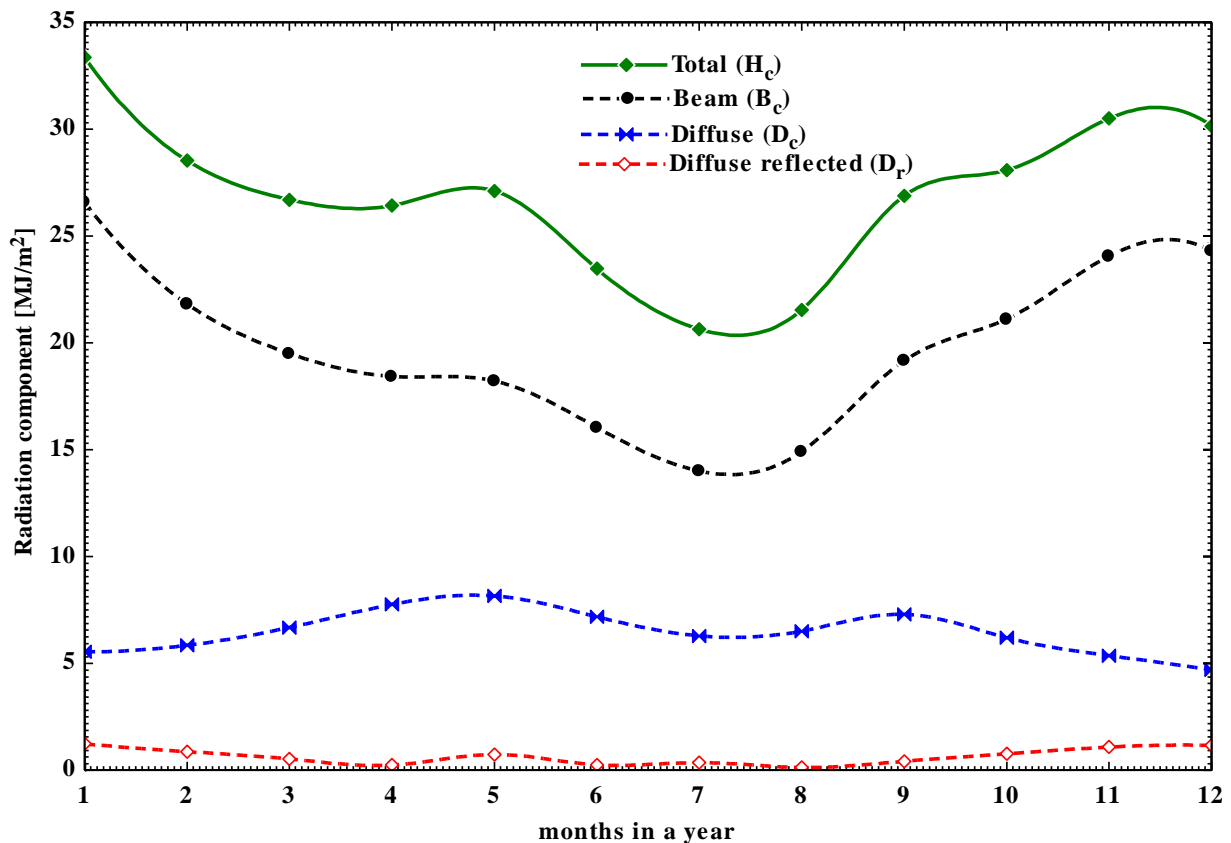


Figure 4.13: Solar radiation components of tilted surface.

The Monthly average global solar radiation is also determined from beam, diffuse and diffuse reflected solar radiation based on meteorology data. The obtained value of monthly average global radiation was compared with NASA and New-LoClim radiation [Figure 4.14](#). The result shows that the maximum radiation was received in January, which is $5.9 \text{ KWh/m}^2/\text{day}$, and minimum of $4.29 \text{ KWh/m}^2/\text{day}$ was received in August. However as indicated by NASA and NewLo-Clim, the maximum global solar radiation is $6.59 \text{ KWh/m}^2/\text{day}$ and $5.93 \text{ KWh/m}^2/\text{day}$ in February and November respectively.

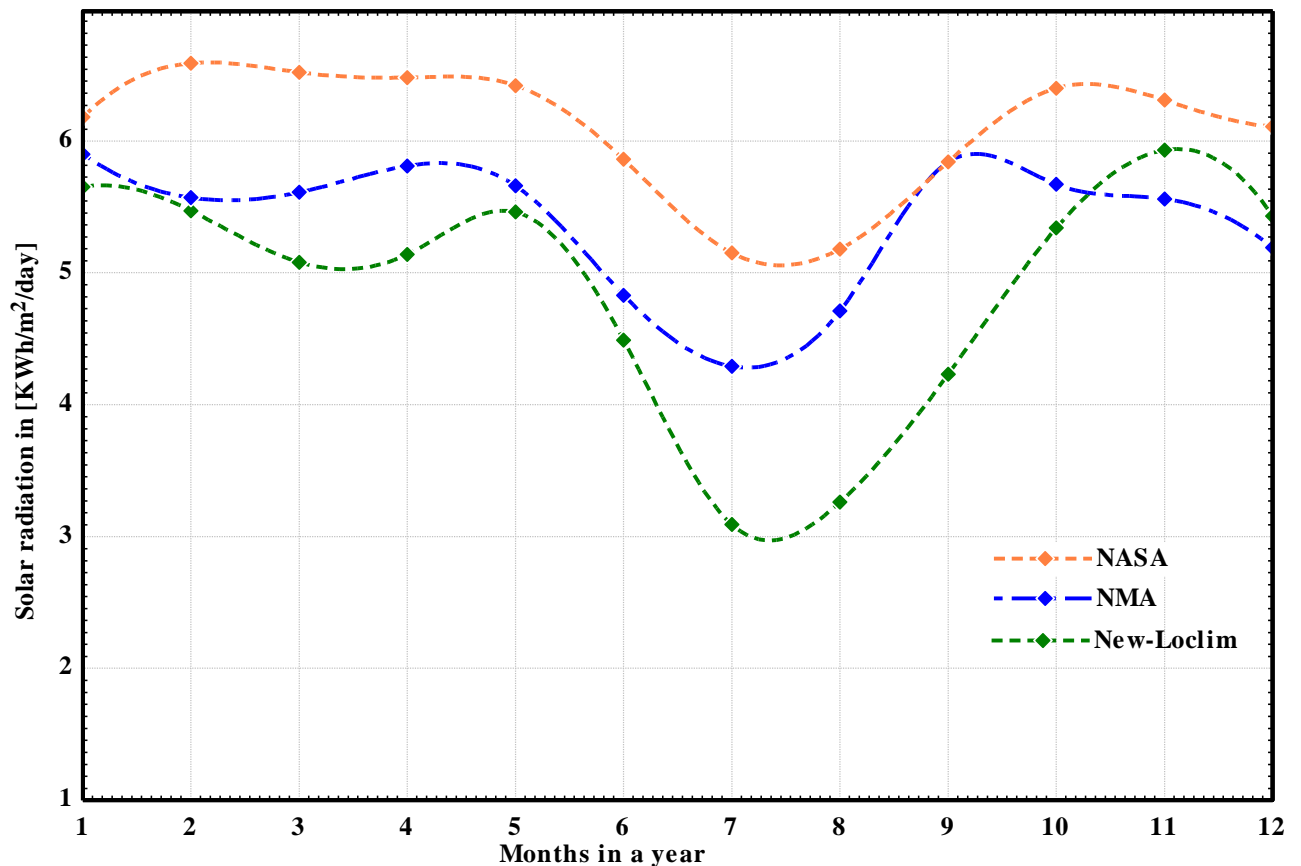


Figure 4.14: Monthly average Global solar radiation of study area.

4.4.2. Mapping of solar radiation in study area

Solar radiation distribution in study area is mapped by using ArcGIS software for determining the assessment of solar radiation intensity of the area. The solar radiation distribution was extracted based on DEM delineation in ArcGIS. According to the assessment analysis result the areas located in lower elevation has low intensity of solar radiation due to shading of terrain and low altitude. Solar radiation mapping is necessary for identify possible area for PV array installation based on distance location of study village from installed PV array.

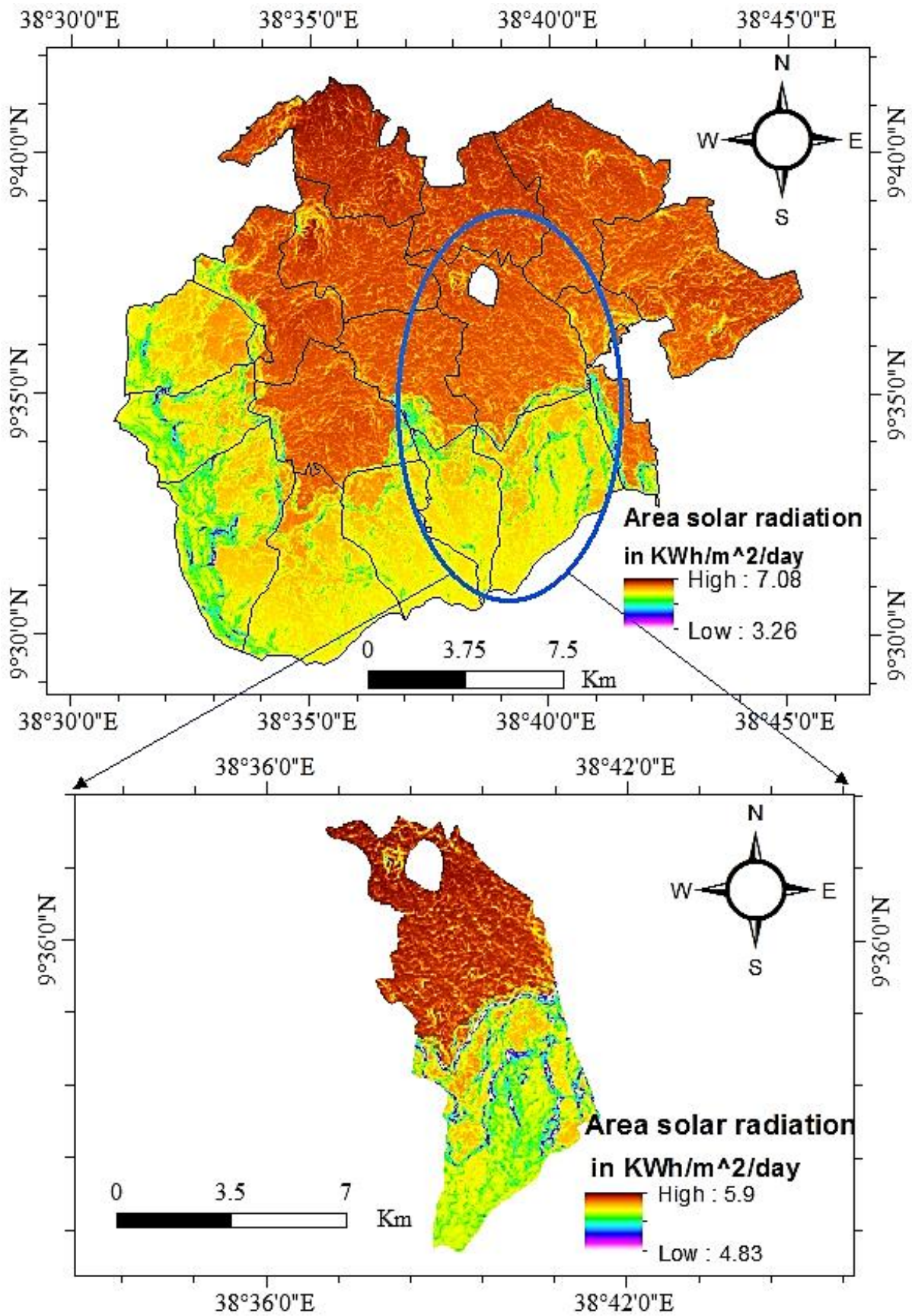


Figure 4.15: Areal solar radiation distribution of Yaya Gulele district in 2021.

4.4.3. Estimation of optimum operating tilt angle and effects of ambient temperature on Photovoltaic performance

4.4.3.1. Tilt Angle

The tilt angle of photovoltaic module has positive and negative effects on the power output and efficiency of the photovoltaic array. The increase in tilt angle has advantage in reducing soiling or dust accumulation as well as rain drop shading. However, the value of tilt angle of the PV module to collect required potential of solar irradiance is different through months in the year. In this study the tilt angle of the array is estimated based on the declination angle of the study area. This is due to variation in declination angle and the day number (N) of months in the year. In October, November, December, January, February and March the optimum value of tilt angle is obtained as it varies from 0° to 80° . The absorbed solar irradiance raises and reaches its optimum value at optimum tilt angle and start decreasing after peak point. The peak point is the point at which the optimum tilt angle located for installation of the solar array.

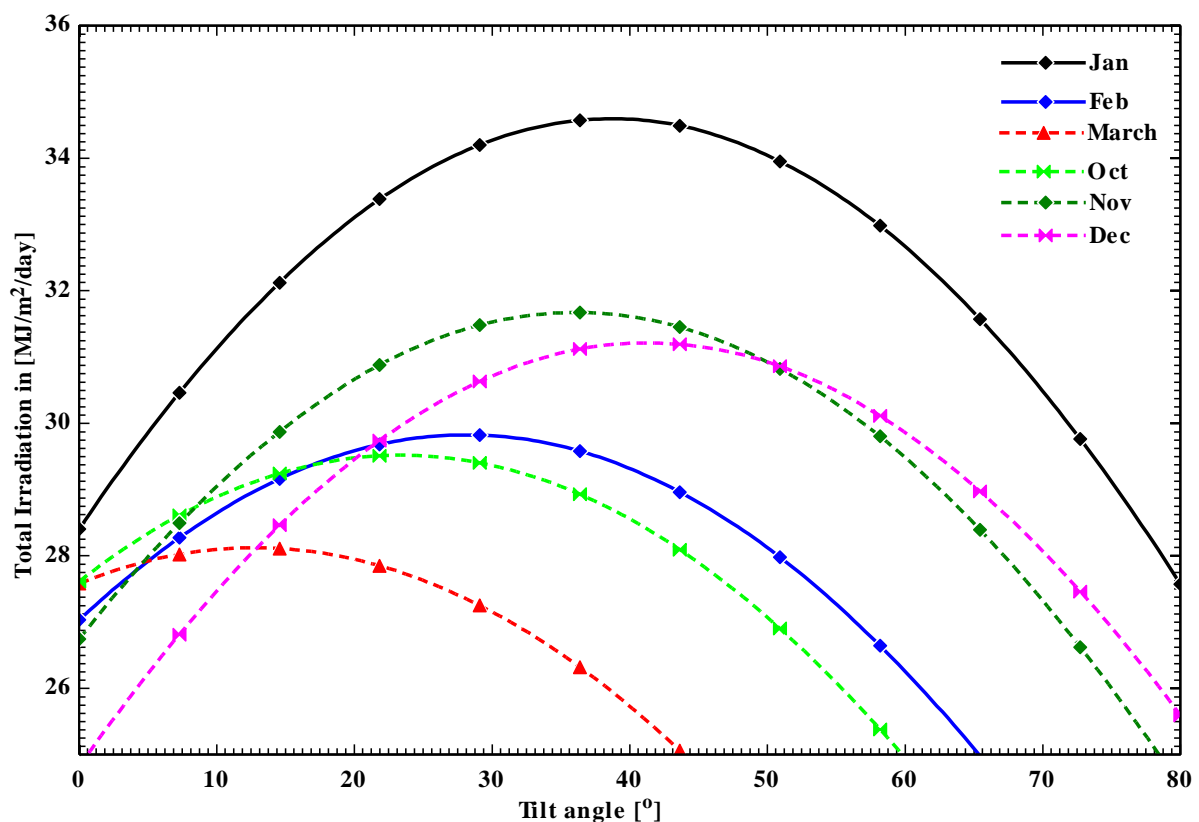


Figure 4.16: The optimum tilt angle in shiny season of the year

In April, May, June, July, August and September the maximum amount of irradiance can be absorbed when tilt angle is at 0° . However, it is less when compared to the remaining months.

The figure shows that the amount of solar radiation absorbed start decreasing as tilt angles increases from 0° to 25°.

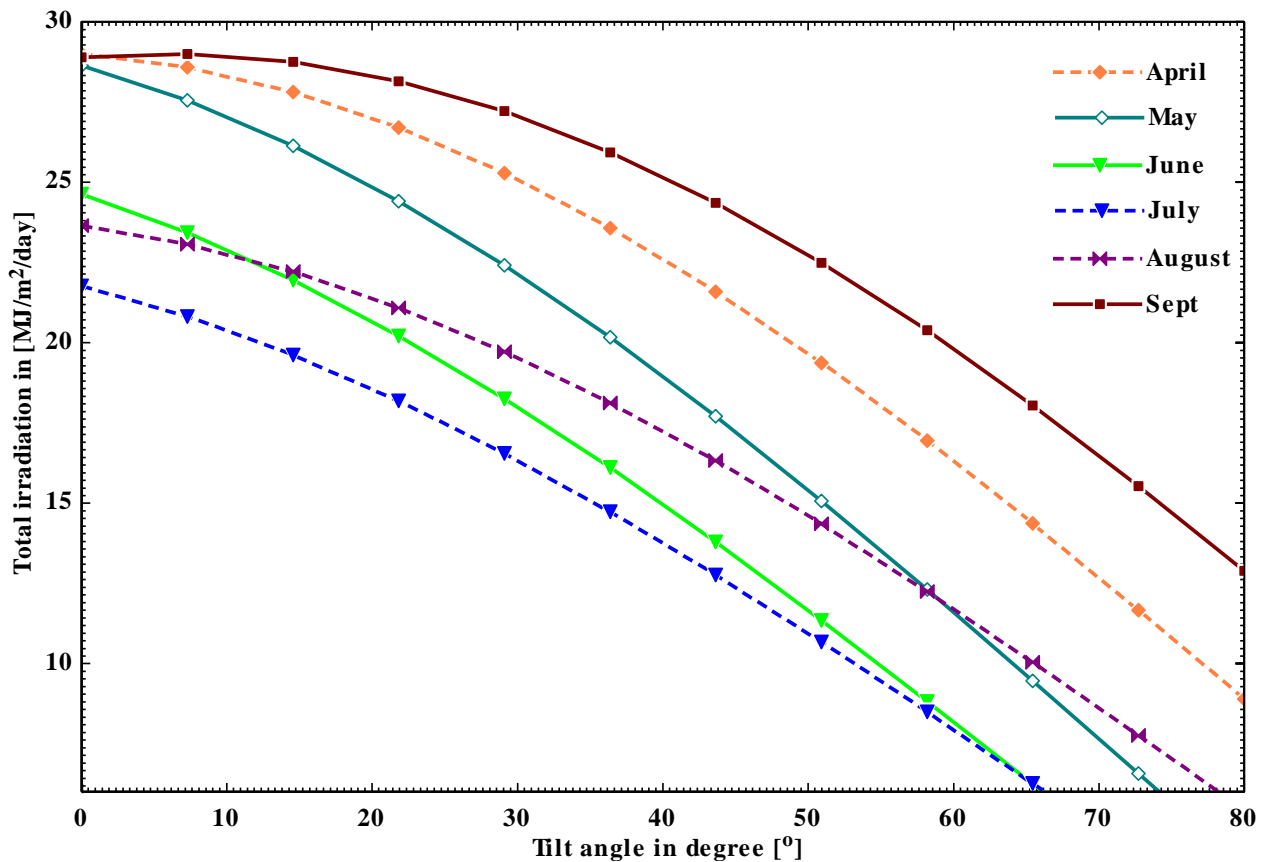


Figure 4.17: The Optimum tilt angle in rainy and partially cloudy seasons of the year.

The summary of the above graph is shown in Table 4.5, which is the optimum tilt angle of each month of the year with their corresponding solar irradiance absorbed.

Table 4.5: Optimum tilt angle of months with the maximum irradiance that can be absorbed.

Shiny season			Partially cloudy or Rainy season		
Months of the year	Tilt angle (β)	Solar irradiation MJ/m ² /day	Months of the year	Tilt angle (β)	Solar irradiation MJ/m ² /day
October	21.82	29.51	April	0	29
November	36.36	31.67	May	0	28.63
December	43.64	31.19	June	0	24.62
January	36.36	34.57	July	0	21.77
February	29.09	29.82	August	0	23.65
March	14.55	28.11	September	7.27	29

The variation of tilt angle results in power loss of photovoltaic arrays. Since the optimum operating tilt angle of months is varying, the power loss also varies through months in a year. The loss increases as tilt angle of the module increases from 0° to 80° . The negative sign of loss indicates that the PV cell temperature T_{NOCT} is below the operating temperature of the PV cell. The value of Nominal operating cell temperature is obtained from solar cell manufacturer specification. Therefore, the loss is negative in summer autumn season of the study area, since the cell temperature (T_C) is less than the nominal operating cell temperature (T_{NOCT}).

In March and April, the cell, temperature T_C exceeds nominal operating cell temperature T_{NOCT} . Therefore, the loss is positive and it results from the increase in the cell temperature of the PV. The nominal operating cell temperature of Longi-Solar cell with model type LR-4-60HPB 345-365M is selected for this study as 25°C . Since the value of T_C increases in March and April, the loss increases at small tilt angle and decreases as the tilt angle increases.

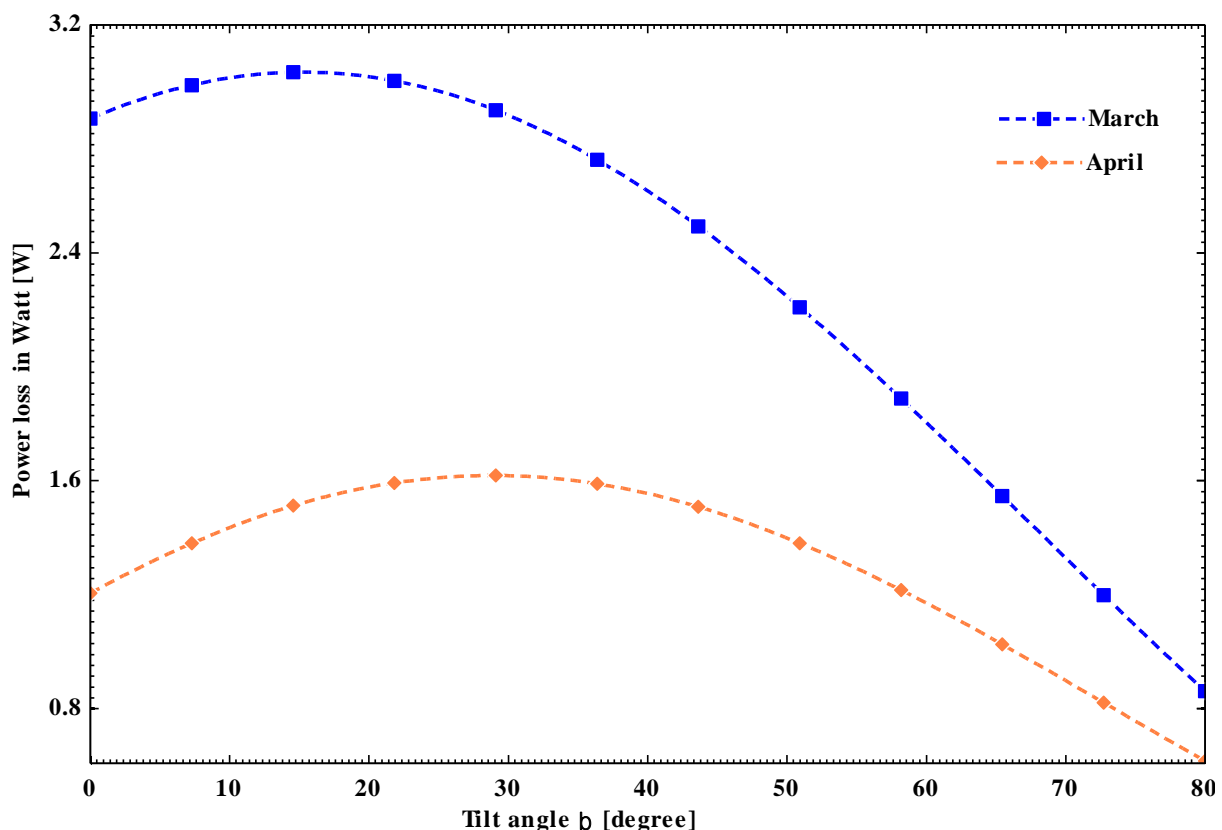


Figure 4.18: Power loss due to increase in cell temperature.

The power output of photovoltaic cell depends on the variation of tilt angle and cell temperature. If the optimum tilt angle is not selected properly in specified site for PV installation, some losses in output power of PV was occurred. The following result shows the

relation between the tilt angle and the cell temperature estimated from the meteorological data of the study area. The PV module cell temperature varies from 25.5 °C to 26.56 °C in March and April.

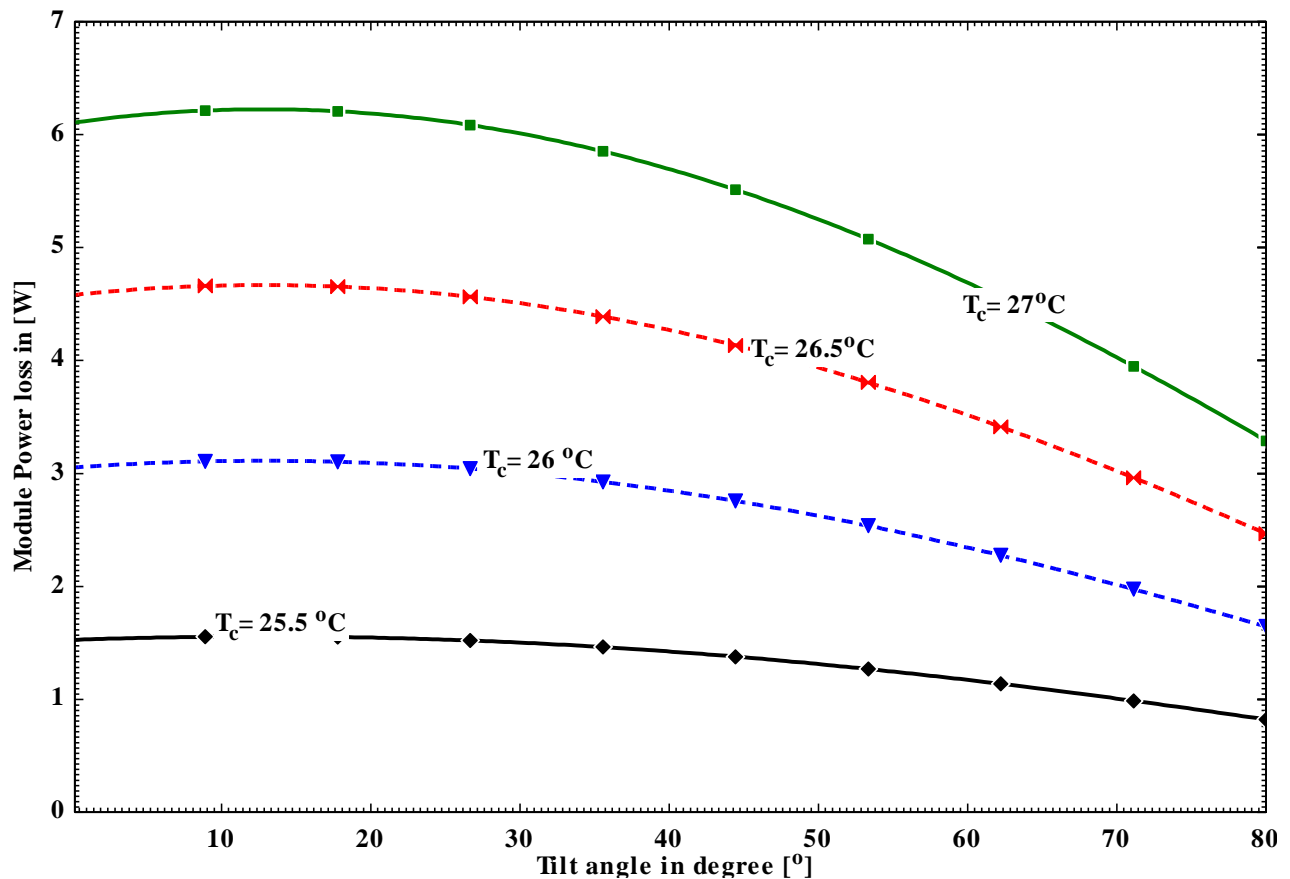


Figure 4.19: Power loss variation with cell temperature and tilt angle.

The results show that the loss increases as the temperature of the cell increases. However, the increase in tilt angle of the PV cell results in decreases in losses for overheated PV arrays. The loss is zero at 25 °C when cell temperature and nominal operating cell temperature is equal. Nevertheless, it increases as the cell temperature passes 25°C and decrease as β increase. In March and April, the power loss decreases as the tilt angle of the module increases with wind speed.

When the wind speed in the area is 0.5 m/s the loss is 2.178 W per module that is the maximum loss. However, the increase in the wind speed can reduce the loss since it helps as cooling media for the PV module during overheating time in March and April. The Figure 4.20 shows that when the wind speed reaches 2 m/s the loss become 1.49 W per module which is a minimum loss.

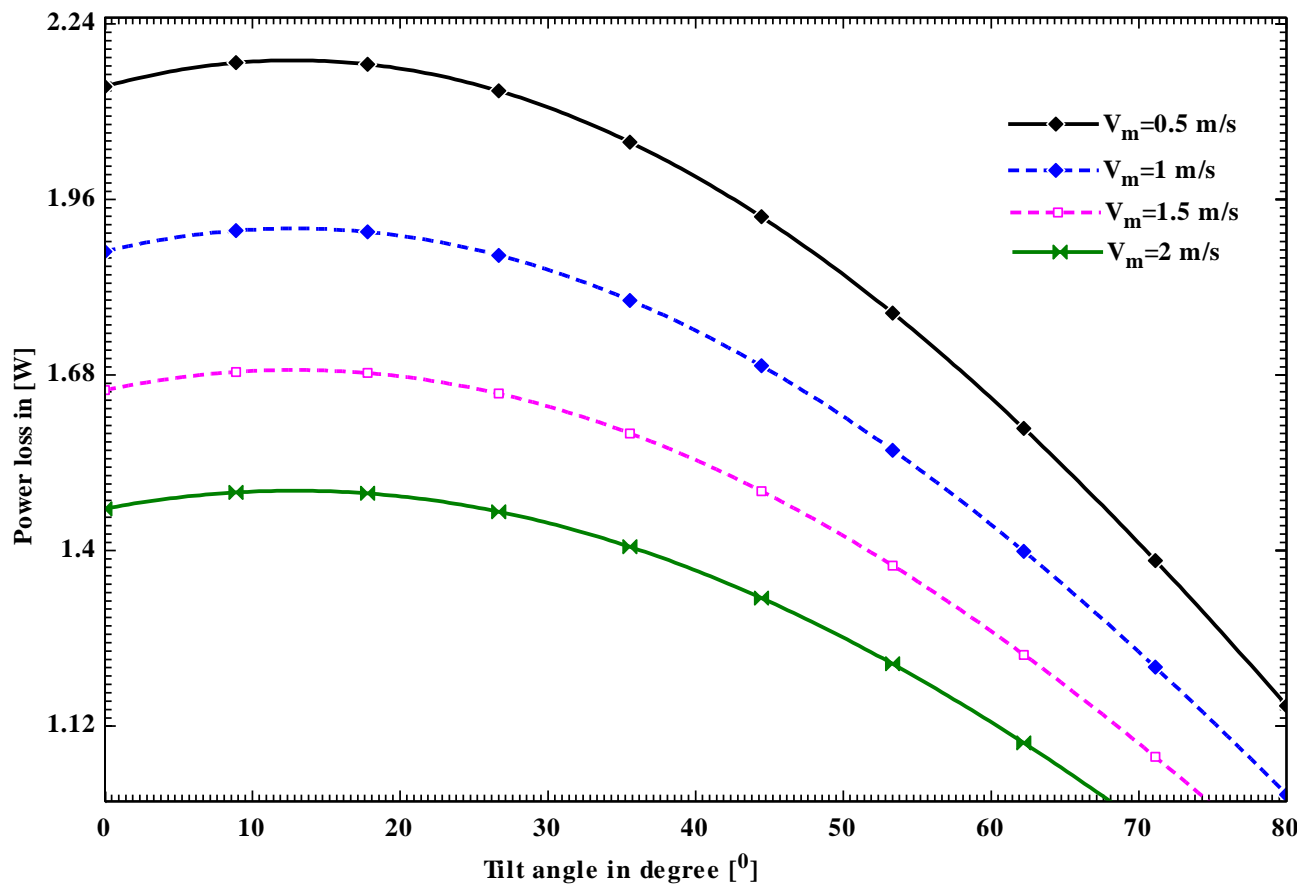


Figure 4.20: Power loss of PV module with variation of tilt angle at constant wind speed.

The maximum wind speed in March and April is not more than 2 m/s in study area. Therefore, the wind speed has positive effect on PV arrays, which helps as the cooling medium when the PV array is overheated. As a result, the increase in wind speed helps to decrease power loss due to increase in the cell temperature of the cell.

According to [Awashti et al., \[47\]](#) the best optimum tilt angle of PV module ranges from 15°-35°. Therefore, the analysis result shows that, the optimum operating tilt angle of 29.09° reduces the PV module loss by 0.067 W and helps to receive enough solar radiation in March and April for study area.

4.5. Economic assessment, Optimization and sensitivity analysis

4.5.1. Optimized Simulation Results

The optimized output of simulation is categorized as a list of feasible combination of PV/Diesel/Micro-hydro/generator convertor/battery and PV/Micro-hydro/generator convertor/battery hybrid system set up. The results are generated with the ranked system configuration, according to least NPC, least COE and high renewable fraction. Based on simulation parameters, Micro-hydro/PV/Diesel/ battery is the least cost system with \$USD 1.22 million (64.66 million ETB) NPC. The system is a combination of 150 KW PV, 50 KW Diesel Generator, 338 KW micro-hydro and 100 KWh Li-Ion battery. The initial capital, COE, operation and maintenance (O&M) costs are \$910069 (46413519 ETB), \$0.204 (10.81 ETB) and \$1078 (54978 ETB) respectively.

Table 4.6: Optimized output category of simulation

PV (KW)	Hydro (KW)	DG (KW)	Battery (Strings)	Convertor KW	Dispatch Strategy	COE USD	Total NPC in USD	Operating cost USD/yr	Initial cost (USD)	Diesel in (L)	Production KWh/yr
150	338	50	11	100	CC	0.204 10.81 ETB	1.22 M 64.66M ETB	31,527 1607877 ETB	889,129	14513	274037
250	338	-	22	150	CC	0.214 11.34 ETB	1.28 M 67.84 M ETB	25064 1278264 ETB	99,3914	-	456,728

The Hydro/PV/DG/Battery system is the most optimal and economical system with lowest net present cost (NPC) followed by Hydro/PV/Battery system when compared to grid extension and other alternatives. However, as diesel fuel price increases and rises above 0.7 \$USD/KWh, which shows the Hydro/PV/Battery system is more economical with the lowest NPC and average cost of energy (COE) of 0.215 \$USD/KWh equivalent to 10.96 ETB.

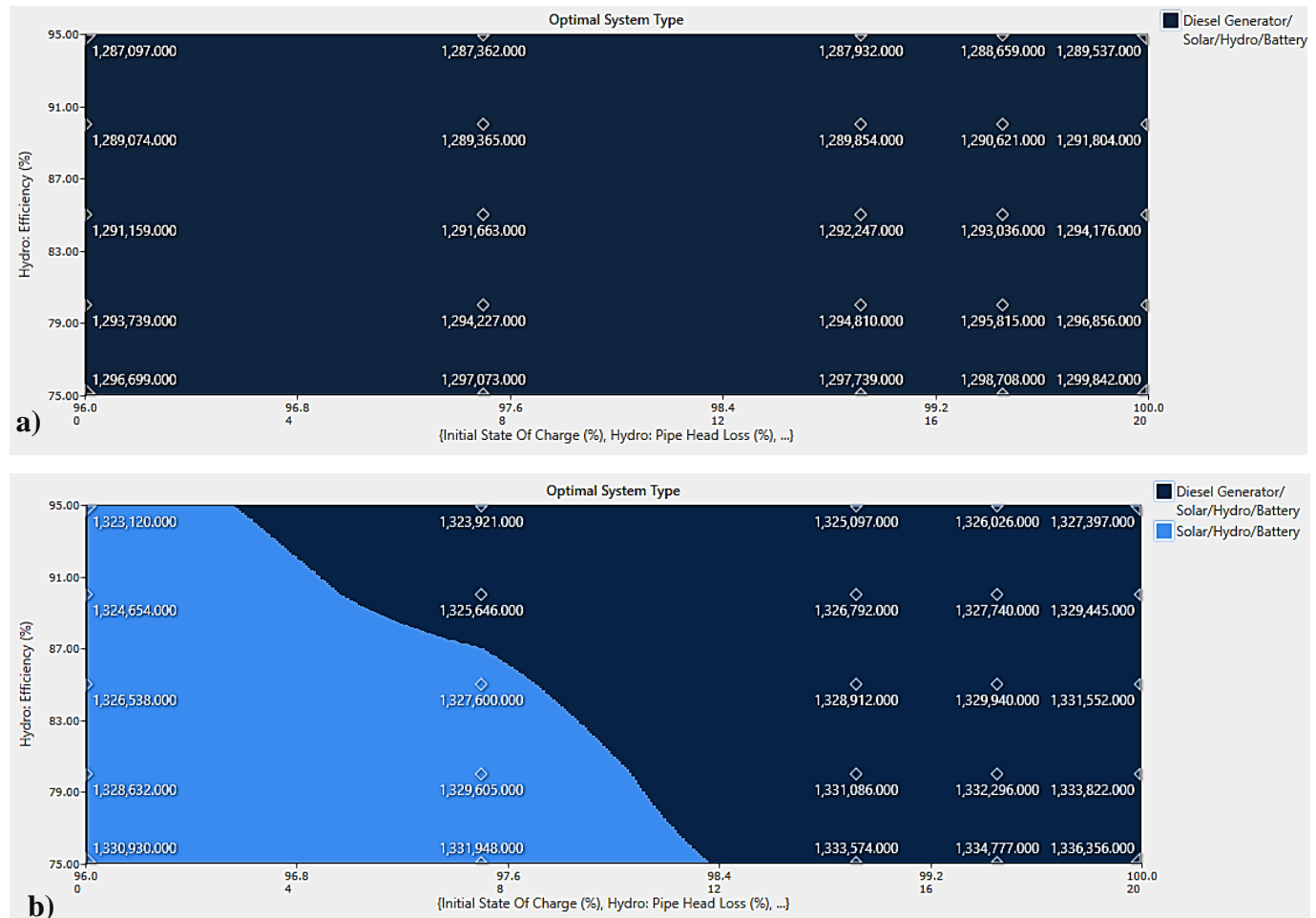


Figure 4.21: a) Optimal system type at DFP=0.5 \$/KWh and b) at DFP = 0.07\$/KWh

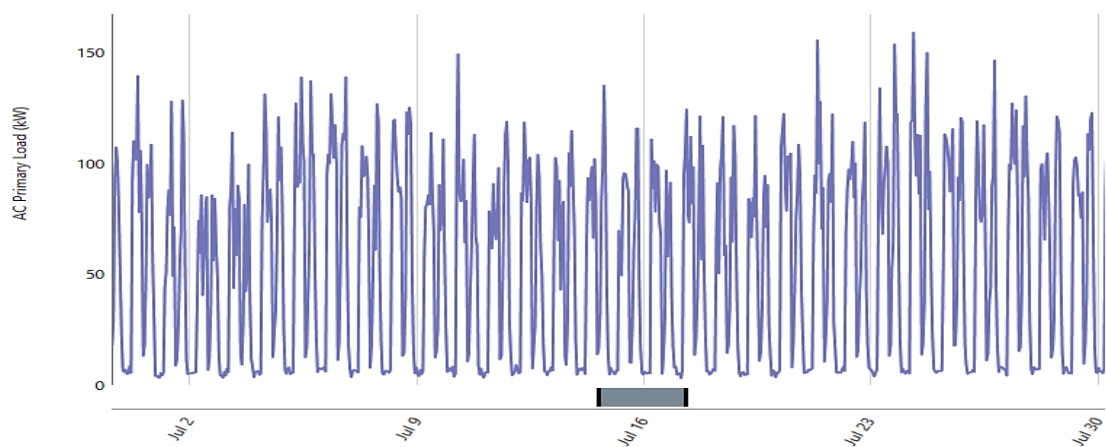


Figure 4.22: AC primary load in peak month (July)

The architecture of the proposed system, in Table 4.6 has 338KW Hydro, 150 KW PV, and 50 KW DG with 11 strings of Li-ion Battery. Most of the electricity production is dominated by hydro power which is 84.1 % of power production per year whereas PV and DG accounts for 15.9% and 2.7 % respectively. Power Generated from DG is widely utilized during winter season when there is low amount of hydro power flow rate potential. During this season the PV, DG and battery system power output are serves together to cover the load. The DG operates as backup system during low flow season (less hydro potential). The battery was fully charged when there is high potential of river flow between March up to October. The energy stored is used with DG and PV system to cover residential load in months between October up to February.

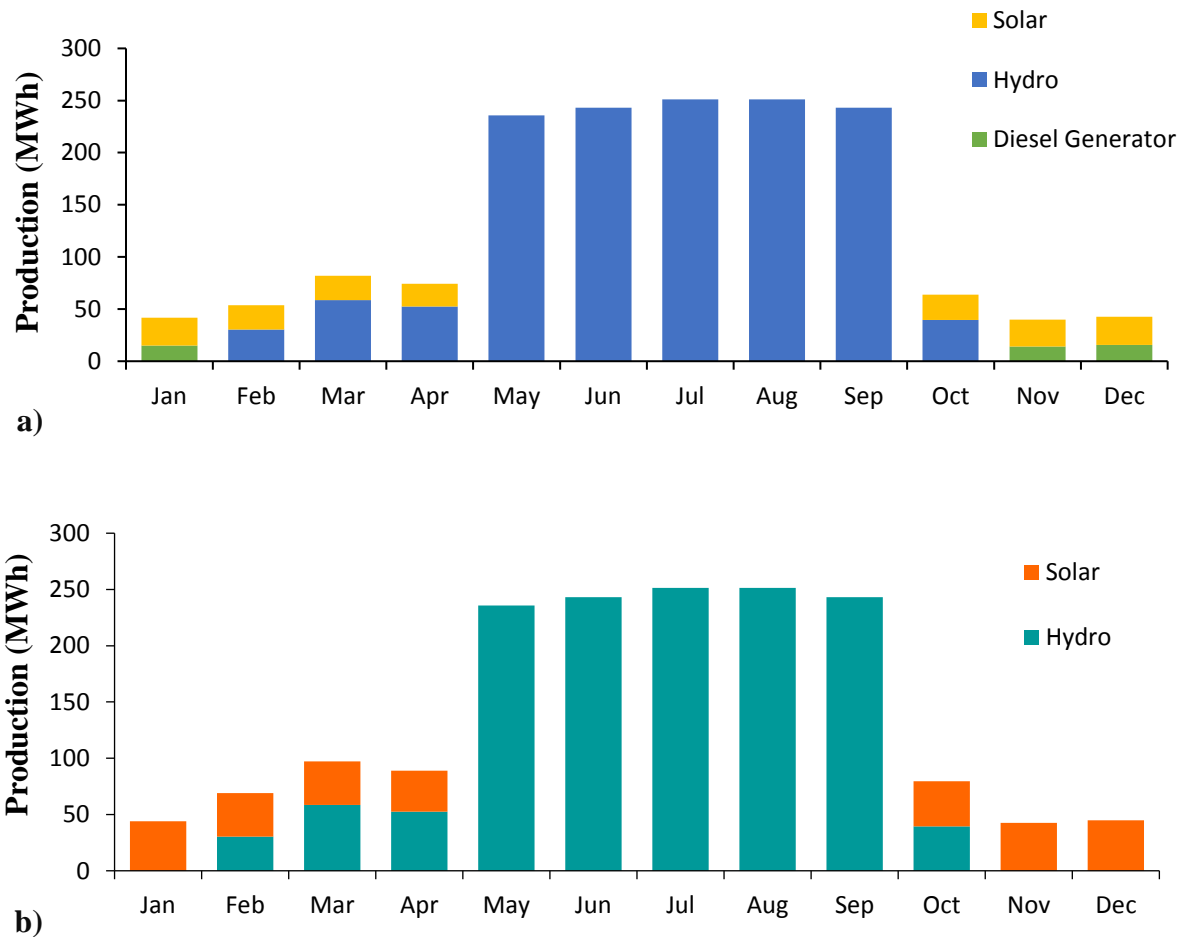


Figure 4.23: Electricity production of a) Micro-Hydro/PV/DG and b) Micro-Hydro/PV System through months in a year

4.5.1.1. Hydropower Output

The hydro resource in study area has the potential of producing 338 KW of power which is a nominal capacity of the hydro output. The Levelized cost of energy (LCOE), capacity factor, operating time and total production of are 0.0057 \$/KWh, 47.5 %, 6552 hrs/yr and 1,405,375 KWh/yr respectively. The hydro power penetration of the optimized system is 299 %. The power output is increased at high discharge season of the year which is in summer season as shown in Figure 4.24.

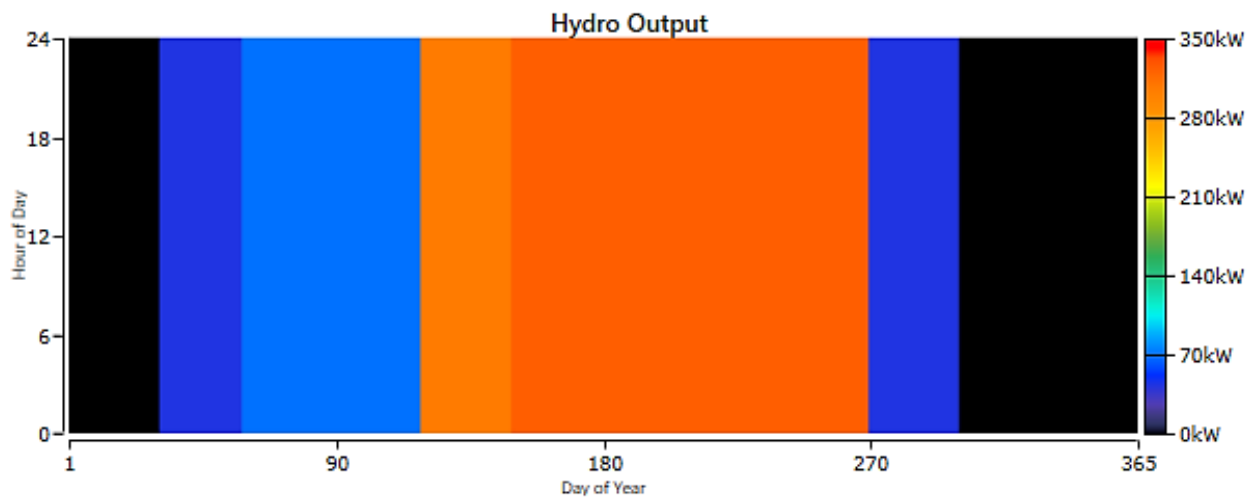


Figure 4.24: Hydropower production capacity in days of the year

4.5.1.2. Photovoltaic power Output

The output power obtained power from photovoltaic higher at the time of the days when high solar radiation falls on the PV arrays. The amount of solar radiation falling on PV arrays varies from hours in a days and months in the year. The maximum radiation can be obtained during noon time during the day and during January and in study area as shown in Figure 4.25. The lowest radiation is received in July. The rated power output is 50 kW when sky clearness index $\bar{K}_T = 1$, the maximum power output considering losses is 46.1 KW and the mean power output is 751 KWh/day. The Levelized cost of energy (LCOE), PV penetration, capacity factor and hours of operations are 0.049 \$/KWh, 58.2%, 20.9% and 4464 hrs/yr respectively. Hence there is excess energy from hydropower between May up to September, Solar PV array were considered to be disconnected for these months.

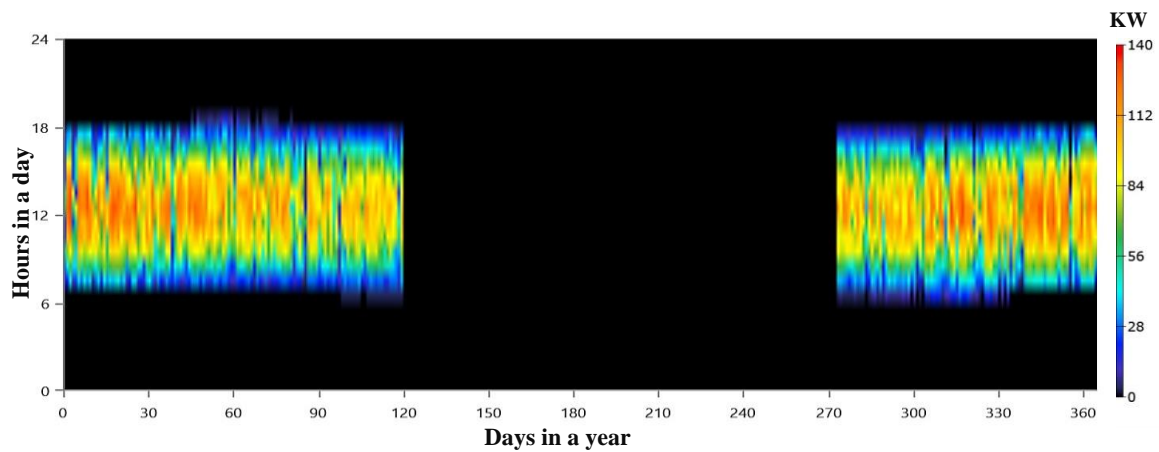


Figure 4.25: Electric energy production by PV system through days in a year.

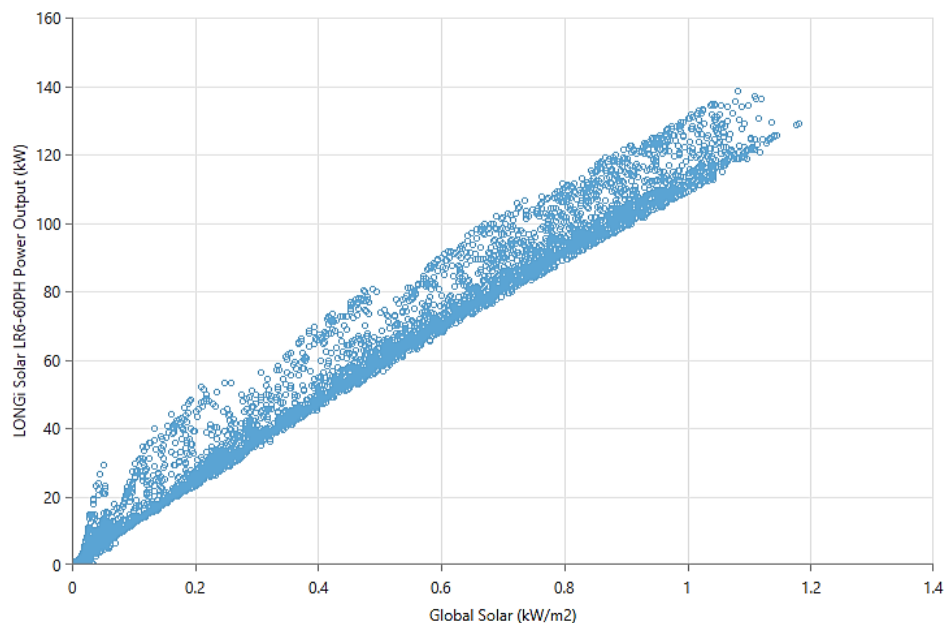


Figure 4.26: Scatter plot of relation between PV power output with Global irradiance

4.5.1.3. Diesel Generator output

Diesel generator is considered in the hybrid system in order to compensate low flow rate of the hydropower and to stabilize the load consumption rate during low energy production season. As the result shows the diesel generator produce high output during November up to January and it is almost decreased to zero between March-October. In these months the energy production from Hydro and PV system is good enough to support the load consumption. After October the capacity of hydropower decreases due to decreasing of hydropower flow rate and the power generation from diesel generator starts raising. As shown by simulation result on figure below, the DG is used as backup system during Morning and evening session when the load consumption is high.

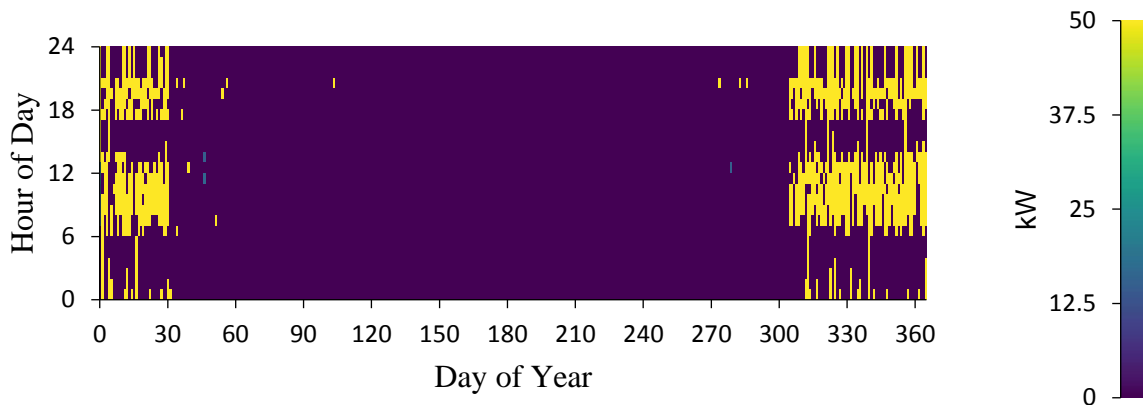


Figure 4.27: Diesel generator Power output throughout the year.

The Diesel generator in this hybrid system generates mean power output of 49.7 KW and minimum electrical output of 15 KW. The generator operates for 954 hrs/yr with operational life of 15.7 yr and total fuel consumption of 14,513 liter.

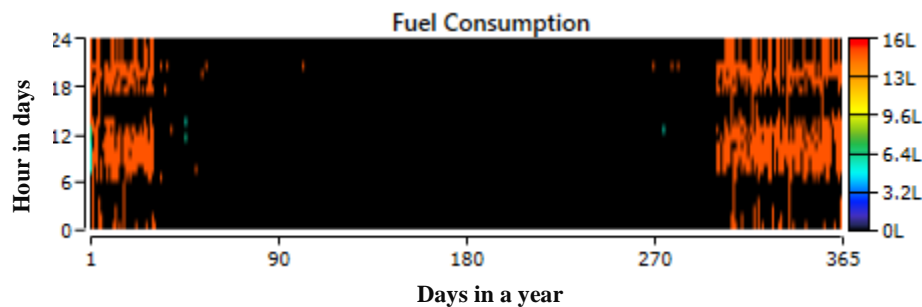


Figure 4.28: Diesel fuel consumption in L/hr

The DG operate with its full capacity in January, November and December. The DG power generation in April and May is not that much appreciable when compared to months with full capacity of time of operation. In the other remaining months of the year the load consumption can be covered by only Hydro/PV/Battery system with renewable fraction of 100%.

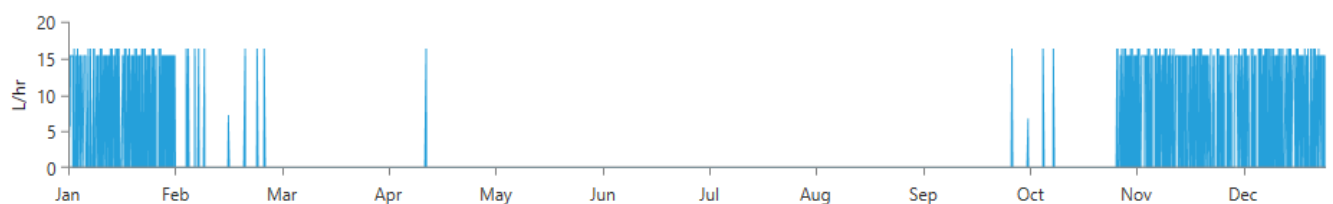


Figure 4.29: Operating time of Diesel Generator

4.5.1.4.Storage system output

The Li-ion battery is considered in a hybrid system as the storage component during excess electricity production. The battery system has annual throughput autonomy of 61820 KWh/yr. The amount of energy into the battery (E_{in}) 64844 KWh/yr. The energy used to serve the load (E_{out}) is 58647 KWh/yr while the remaining is 304 KWh/yr storage depletion and 6500 KWh/yr

is losses. The Discharge of the battery occurs during low hydro potential season in January, November and December. It's recharged in between months of March and December as shown in Figure 4.30.

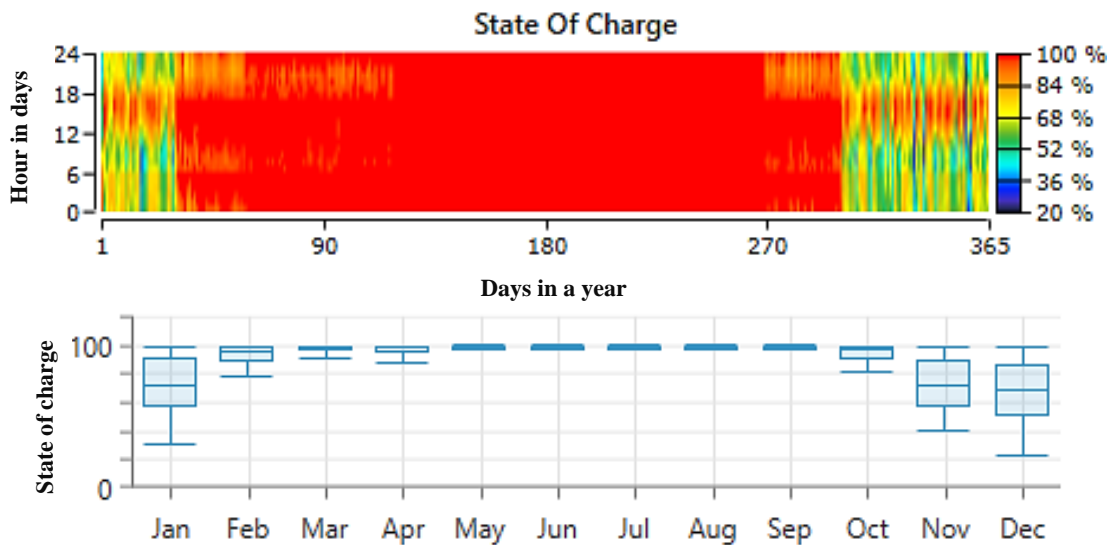


Figure 4.30: Charging and discharging time of the battery system

4.5.1.5. Converter power Output

The DC power source in hybrid system connection schemes are Battery system and Solar PV system. PV system generates the maximum power output during the day while the battery system discharge is during evening time. Hence the AC power is required for serving the load, the converter system converts DC to AC power. In addition, power output from battery and PV system are widely exploited during low potential season of hydro power and when solar resource is available as shown in figure below. An Inverter and rectifier perform opposite function. An inverter transforms a low voltage DC current to a high voltage AC current during Discharging of battery and power conversion of PV system. While a rectifier takes power from an AC source and converts it to DC, usually of a lower voltage during recharging of the battery system.

Table 4.7: summary of converter system

Parameters	Inverter	Rectifier
Hours of operation (hr/yr)	3340	699
Energy Out (KWh/yr)	121700	22884
Energy in (KWh/yr)	126770	23837
Losses (KWh/yr)	5071	953

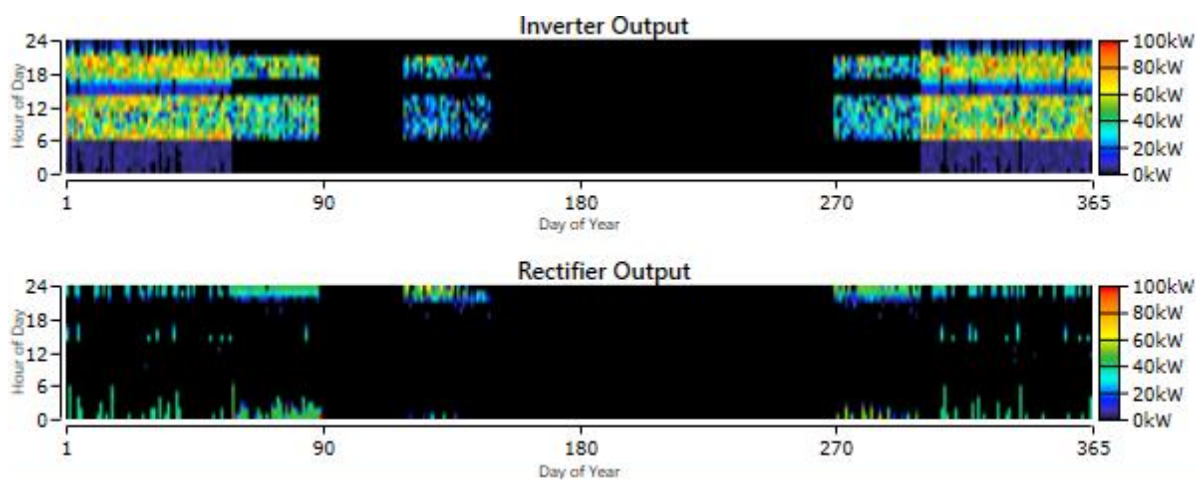


Figure 4.31: Bi-directional convertor system operating profile

4.5.2. Sensitivity Analysis

Sensitivity variables are used to determine the effect of different variables on techno-economic analysis of the optimized system. The variables considered in simulation are stated in [Table 3.6](#). According to report on Power Africa Project [\[7\]](#) electrification scenario, the study village (Goda Warke) will be connected to national grid in 2030. The scenario is classified based on the location distance of the area from the national grid. The report states, the area is categorized under a mid-term electrification plan of Ethiopia. The projected energy demand of the area over project lifetime is considered in this work, as a sensitivity variable to compare with grid extension upto 2030.

The increase in diesel fuel price increases the total NPC of the overall system with rapid change. When the DFP is 0.5\$USD/KWh an average total NPC of the system is 1293469.5 USD. As shown in [Figure 4.21b](#), as DFP rises to 0.7 \$USD/KWh the average total NPC increased to 1329738 US dollar. In addition, as the diesel fuel price kept constant on 0.7 \$/KWh, The Hydro/PV/Battery system is more economical with renewable fraction of (RF) 100 %. The pipe head loss, hydropower efficiency and initial state of charge of the battery (SOC) system are 8%, 87% and 97.6 % respectively.

Even though, Hydro/PV/DG/Battery system is still optimum type with the maximum renewable fraction of 97.18 %, when pipe head loss and battery initial SOC are greater than 98.4 % and 12 % respectively as depicted by [Figure 4.32](#). However, as DFP rise above 0.7 \$USD/Ltr Hydro/PV/Battery system is the only best optimum option. In General, cost of diesel fuel and Pipe head loss are the most sensitive variable compared to other sensitivity variables.

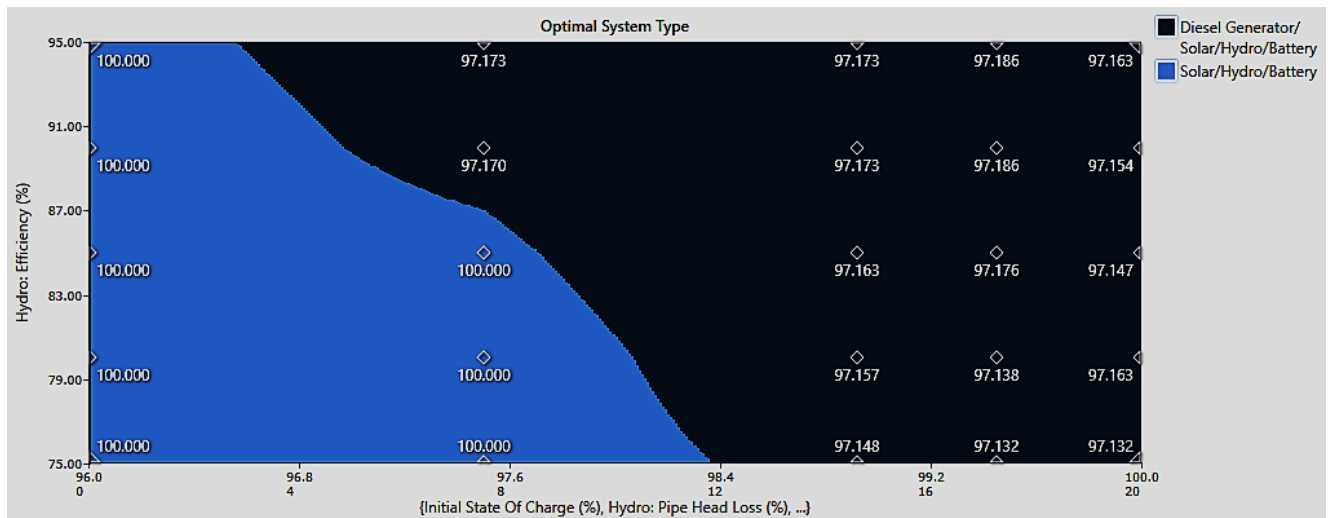


Figure 4.32: Optimal system plot superimposed with RF at a diesel fuel price of 0.7 \$USD/L. Another most sensitive variable are COE, NPC and electric load consumption. As diesel fuel price increases the COE and NPC of the system increases. When electric load consumption is constant at 1269.79KWh/day and diesel fuel price varies from 0.5 \$/KWh to 0.8 \$/ KWh, the COE increases from an average value of 0.204 \$/KWh to 0.214 \$/KWh. After rise in diesel fuel price above 0.8 \$/KWh, there is no anymore appreciable change in COE. In contrast as electric load consumption increases from 1269.79 KWh/day to 1300 KWh/day, COE decreases from average value of 0.204 \$/KWh to 0.2025 \$/KWh. It's observed that the increase in both diesel fuel price and electric load consumption keeps increasing the NPC of the optimized system.

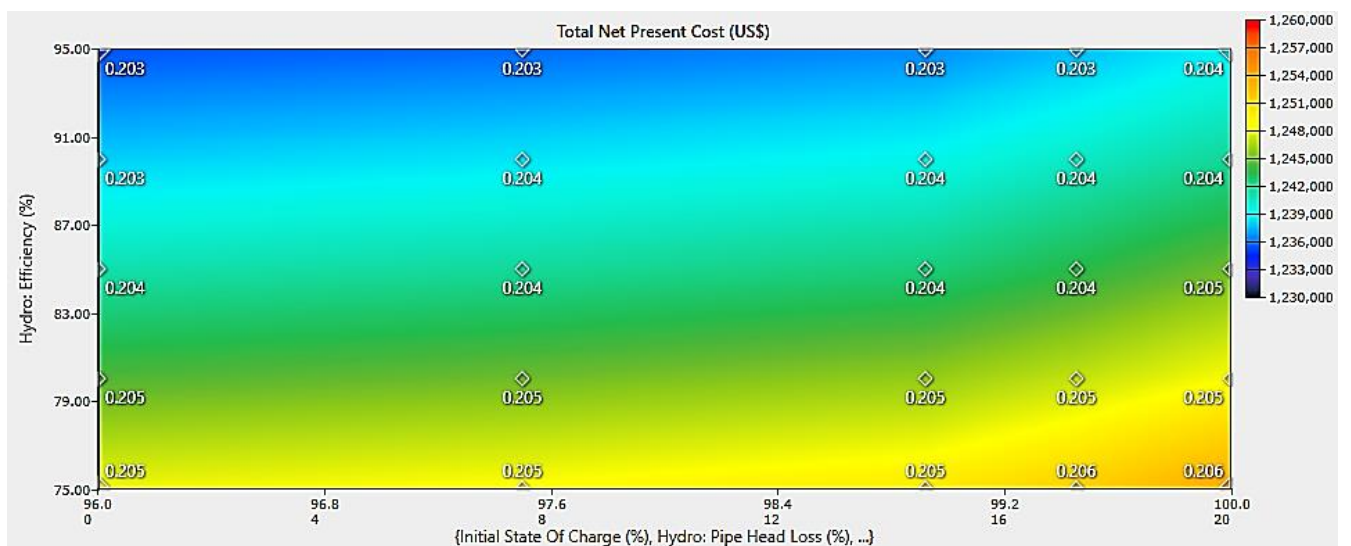


Figure 4.33: Surface plot of hydro efficiency versus other sensitivity parameters, superimposed with COE, at DFP of 0.5 \$/KWh.

Tilahun et al.,(2017) [10], obtained a load consumption of 1466 KWh/day for 505 households with COE of 0.133 \$/KWh. In addition Odou et al., (2020) [61] obtained 850 load consumption KWh/day for 383 households with COE of 0.264 \$/KWh. This work obtained 128 9.78 KWh/day of load consumption which has electrification capacity of 411 households with COE of 0.205 \$/KWh. Therefore, this work is better when compared to these two works in a case of considering the number of households and COE of the system together.

The Convertor system and solar PV has the highest initial costs as shown in figure below. The battery system has highest replacement cost the replacement of battery occurs after 15 years during the project lifetime. Solar PV and Hydropower engine has the large operating cost as depicted by Figure 4.34 a. The fuel price of diesel generator is the highest costing input resource in configuration schemes.

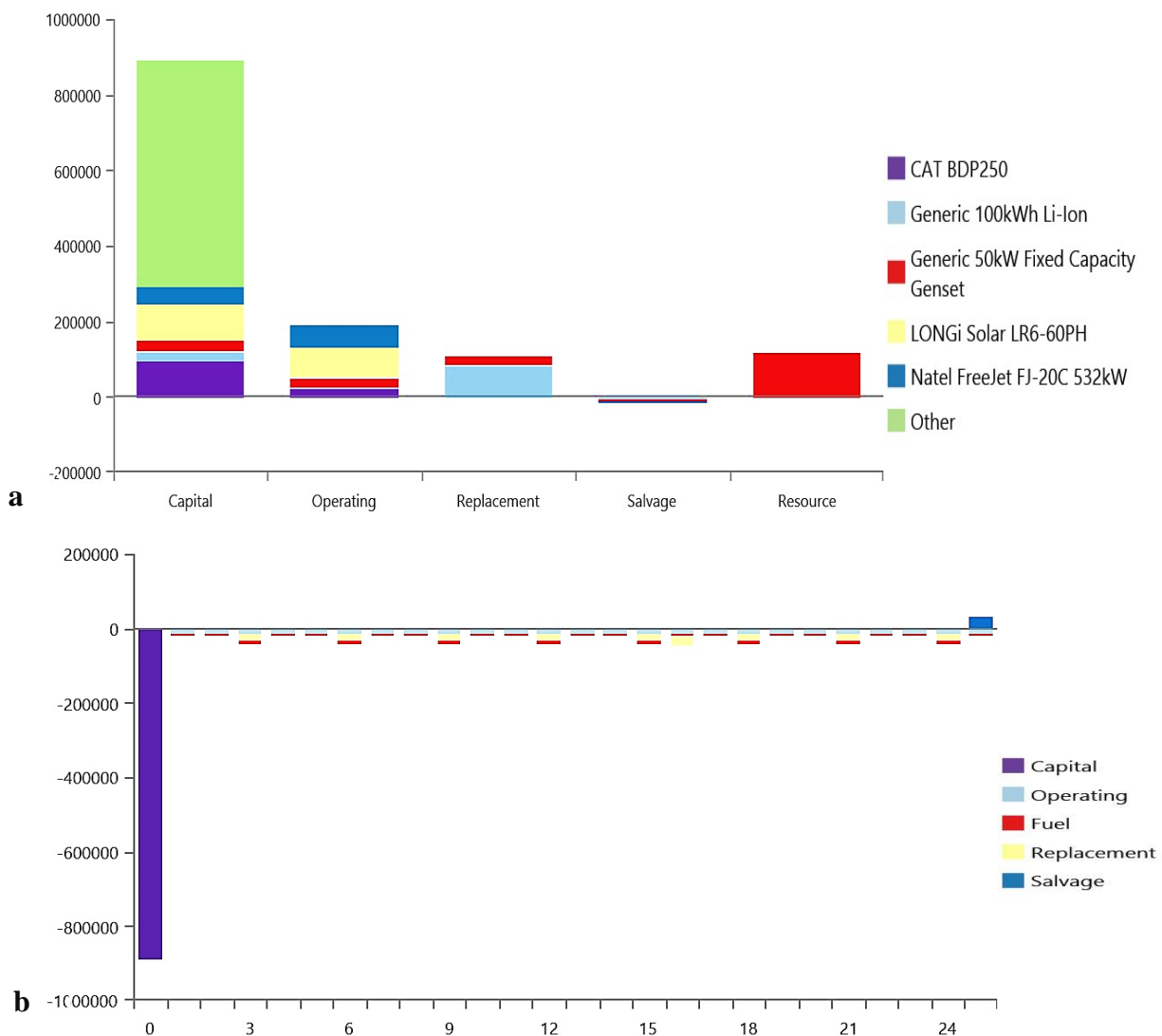


Figure 4.34: a) Hydro/PV/DG/Battery cost summary by components b) Cash flow

The national grid electric price in Ethiopia is 0.1 USD/KWh [10]. However, compared to National Grid extension distance the Hydro/PV/DG/battery system is system that is more economical appeared to be fit the load of Goda Warki village. HOMER selects this system than the grid extension cost.

The total cost of Grid extension becomes similar with total NPC of Hydro/PV/DG/battery system at BGED of 14.46 Km. When Grid extension distance rises above BGED value, the Grid extension cost is more than the total NPC of the optimum system. The distance location of study area from national grid is more than 15 Km. Therefore, the optimum system becomes feasible electrification option than that of national grid at BGED of less than 14.46 Km.

The optimum system is cost competitive with COE of 0.205 USD/KWh which is more than the current national grid price in the country because of the majority of electricity supply is from Hydropower. Generally, considering the current high energy demand in rural area and small COE gap with the national Grid, the optimum system in this work is a possible solution to achieve the National electrification programme (NEP.2) launched by MoWIE.

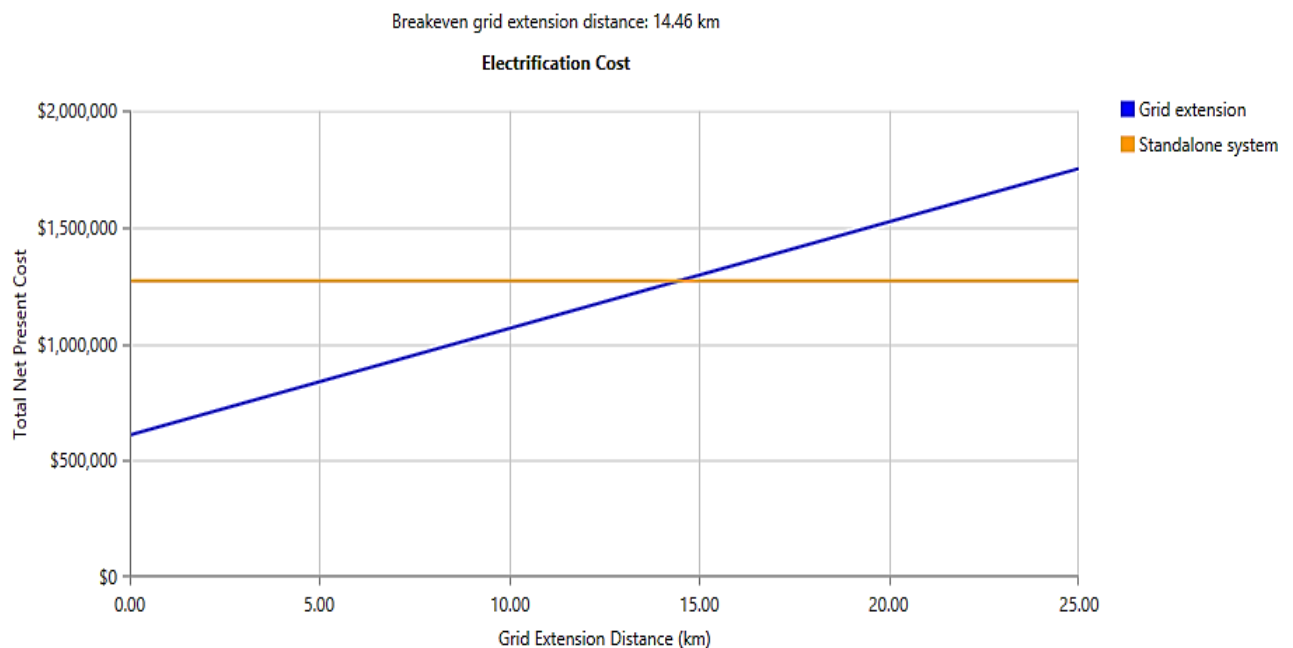


Figure 4.35: Comparison of Grid extension with the Optimum system

CHAPTER 5

5. CONCLUSION AND RECOMMENDATION

5.1. Conclusion

Ethiopia is the 2nd country, abundant with hydropower resource in Africa. Of 45000 MW, less than 10% is exploited. Most of the Local Rivers are ungauged and there is no adequate data of potential assessment for the purpose of power generation. This work presents about energy potential assessment and techno economic analysis of micro-hydropower with solar PV system for rural electrification. Based on NRSCS-CN method analysis, Girar River in study area has an average monthly flow rate of 0.975 m³/s. In analysis of LULC of the River catchment an overall accuracy and Kappa co-efficient (K) of 89.58 % and 0.877 were achieved respectively. HOMER simulation analysis shows that, from the optimum system, the hydropower potential of the study area is 338 KW with penetration of 279 % and an average solar radiation is 5.39 KWh/m²/day. The optimum system is the combination of Hydro/PV/DG/Battery system. From total Production, the portion of hydropower is 81.4 %. The remaining 15.9 % is solar PV and 2.7 % is a power produced by DG.

It's observed that DG in a hybrid system can reduce land area and cost required for PV installation by 163.5 m² (64286 USD equivalent to 3,278,586 ETB) as well as reduce a number of Battery storage strings by 11 which is (11000 USD equivalent to 583000 ETB). The Total NPC of the optimum system is \$USD 1.22 million with COE of \$USD 0.204. The DFP is a sensitive parameter due to rapid increasing throughout the year. When DFP rises above \$ USD 0.9/Ltr, Hydro/PV/Battery system is the optimum system with NPC of \$USD 1.28 million. The production capacity of the system is 25.8 % solar PV and 74.2 % hydropower. Generally, the configuration of proposed hybrid renewable power generation system has the capacity of electrifying 411 households with load consumption of 1269.79 KWh/day.

5.2. Recommendation

The following recommendation are addressed for the future works

- ✓ Estimation of flow rate for ungauged river requires daily flow measurement of the river using flow-measuring instruments such as current meter, water flow meter altimeter, GPS and topographic maps. To obtain the accurate value of stream flow data of Girar River, field survey using the mentioned instrument is recommended for future works. In addition, this paper considered only the catchments in Yaya Gulale districts, but also few catchments are located in other neighbouring districts, which could be results in better stream flow of the river when added to this work analysis.
- ✓ The effect of environmental temperature on the performance of battery storage system was not studied in this work. Therefore, future works can consider the Performance evaluation of Energy Storage System by varying self-discharge parameter with ambient temperature.
- ✓ The investment cost of photovoltaic system higher when compared to that of micro hydropower in this study. Therefore, reducing the number of PV panel results in decreases NPC of the system. However, it needs increasing power output from the hydropower system that operates with the PV system to cover the load consumption of the study area. Using GPS and Theodolite during field survey Could be, result in the best net head value which is used to increases hydro power output and decrease the investment cost of photovoltaic system and area covered by PV array.
- ✓ An Excess electricity of 1148627 KWh/yr is obtained from the optimum system of this work. The future researcher can perform thermal load and Deferrable load assessment in addition to electrical load assessment of study area, to minimize excess electricity production.
- ✓ This study can be considered as possible reference solution for MoWIE, NGOs and other Volunteer organization to achieve national electrification plan 2 (NEP 2) in Ethiopia, by utilization of solar and hydro energy resources available in a remote area community.

Reference

- [1] Getnet Zewde Somano and Getachew Shunki Tibba, “Energy Resource Potential Assessment for Solar Photovoltaic-Micro Hydro Hybrid Power Generation System. (A case study for Jimma, Toli Kerse, Minko Village),” *Int. J. Eng. Res. Technol.*, vol. 5, no. 1, pp. 333–340, 2016.
- [2] S. Hoseinzadeh, M. H. Ghasemi, and S. Heyns, “Application of hybrid systems in solution of low power generation at hot seasons for micro hydro systems,” *Renew. Energy*, vol. 160, pp. 323–332, 2020, doi: 10.1016/j.renene.2020.06.149.
- [3] F. F. Li, J. Qiu, and J. H. Wei, “Multiobjective optimization for hydro-photovoltaic hybrid power system considering both energy generation and energy consumption,” *Energy Sci. Eng.*, vol. 6, no. 5, pp. 362–370, 2018, doi: 10.1002/ese3.202.
- [4] W. Yuan, Z. Liu, C. Su, and X. Wang, “Photovoltaic capacity optimization of small and medium-sized hydro-photovoltaic hybrid energy systems considering multiple uncertainties,” *J. Clean. Prod.*, vol. 276, p. 124170, 2020, doi: 10.1016/j.jclepro.2020.124170.
- [5] E. Bryan, A. H. Mondal, E. Bryan, C. Ringler, D. Mekonnen, and M. Rosegrant, “Ethiopian energy status and demand scenarios : Prospects to improve energy efficiency and mitigate GHG emissions,” *Energy*, vol. 149, no. February, pp. 161–172, 2018, doi: 10.1016/j.energy.2018.02.067.
- [6] B. Gouthami Padam, Dana Rysankova, Elisa Portale, Bryan Bonsuk Koo, Sandra Keller and Gina FleurantinConnections, “Beyond Connections.”
- [7] P. A. O. Project, “Off-Grid Solar Market Assessment Ethiopia,” no. October, 2019.
- [8] C. Ratnayake, “Low Cost Grid Electrification Technologies a handbook for electrification practitioners,” Eschborn, 2015. doi: <http://euei-pdf-org/downloads/flagship-publication>.
- [9] K. River and Z. Girma, “Techno-Economic Feasibility of Small Scale Hydropower in Ethiopia : The Case Techno-Economic Feasibility of Small Scale Hydropower in Ethiopia : The Case of the Kulfo River , in Southern Ethiopia,” no. March, 2016, doi: 10.1155/2016/8037892.

- [10] T. Nigussie, W. Bogale, F. Bekele, and E. Dribssa, "Feasibility study for power generation using off- grid energy system from micro hydro-PV-diesel generator-battery for rural area of Ethiopia: The case of Melkey Hera village, Western Ethiopia," *AIMS Energy*, vol. 5, no. 4, pp. 667–690, 2017, doi: 10.3934/energy.2017.4.667.
- [11] F. D. Republic, I. Planning, and U. Access, "National Electrification Program 2 . 0 National Electrification," 2019.
- [12] S. Bekele, "Building the Market for Rural Electrification in Ethiopia A mini-grid productive use assessment," 2020.
- [13] A. B. Kassa, "Iranian (Iranica) Journal of Energy & Environment Current Status , Future Potential and Barriers for Renewable Energy Development in Ethiopia," *Iran. J. Energy Environ.*, vol. 10, no. 4, pp. 269–274, 2019.
- [14] B. Sosi, J. Barongo, A. Getabu, and S. Maobe, "Electrical-hydraulic conductivity model for a weatheredfractured aquifer system of Olbanita, Lower Baringo Basin, Kenya Rift," *J. Groundw. Sci. Eng.*, vol. 7, no. 4, pp. 360–372, 2019, doi: 10.19637/j.cnki.2305-7068.2019.04.007.
- [15] M. Gagugna, "Climate-Resilient Green Economy Implementation and Best Practices on Climate Action in Ethiopia," 2020.
- [16] I. C. Dhingra, "Ethiopias Climate-Resilient Green Economy: Economy Strategies," Addis Ababa, 2011. doi: 10.4324/9781003206729-4.
- [17] S. Roy and B. Mistri, "Estimation of Peak Flood Discharge for an Ungauged River: A Case Study of the Kunur River, West Bengal," *Geogr. J.*, vol. 2013, no. February, pp. 1–11, 2013, doi: 10.1155/2013/214140.
- [18] U. G. Wali, "Estimating Hydropower Potential of an Ungauged Stream," *Int. J. Emerg. Technol. Adv. Eng.*, vol. 3, no. January 2013, p. 11, 2014, [Online]. Available: www.ijetae.com.
- [19] H. Oubanas, I. Gejadze, P. Malaterre, and M. Durand, "Discharge Estimation in Ungauged Basins Through Variational Data Assimilation : The Potential of the SWOT Mission Water Resources Research," pp. 2405–2423, 2018, doi: 10.1002/2017WR021735.

- [20] D. E. Fantina, *A Comparison of Runoff Estimation Techniques*. 2012.
- [21] U. B. and S. karki Keshav Basnet, “Comparative Study of Design Discharge Calculation Approaches: A case study on Padhu Khola, Kaski, Nepal,” *A J. TUTA, Pashchimanchal Campus*, vol. 5, no. 1, pp. 41–49, 2018.
- [22] D. Girma, “Ethiopian Field Epidemiology Training Program (EFETP) Compiled Body of Works in Field Epidemiology :Addis Ababa University , Collage of Health Science , School of Public Health,” 2019.
- [23] Gutu Tesso Bezabih Emanu and Mengistu Ketema, “A TIME SERIES ANALYSIS OF CLIMATE VARIABILITY AND ITS IMPACTS ON FOOD PRODUCTION IN NORTH SHEWA ZONE IN ETHIOPIA,” *African Crop Sci. J.*, vol. 20, no. Supplement s2, pp. 261–274, 2012.
- [24] A. T. Ayalew, “Assessment of Power Compeers Prospective of Gobecho Micro Hydropower Plant on Ganga River , Genale Dawa River Basin , Ethiopia,” *Am. J. Electr. Power Energy Syst.*, vol. 10, no. 2, pp. 25–31, 2021, doi: 10.11648/j.epes.20211002.12.
- [25] C. Bousquet, I. Samora, P. Manso, L. Rossi, P. Heller, and J. Anton, “Assessment of hydropower potential in wastewater systems and application to Switzerland,” 2017.
- [26] A. Biak, H. Dim, M. Rutten, W. W. Zin, and O. A. Hoes, “Estimation of Hydropower Potential in Myanmar Global Journal of Engineering and Technology Review Estimation of Hydropower Potential in Myanmar,” *Glob. J. Eng. Technol. Rev.*, vol. 4, no. January, pp. 78–85, 2019, doi: www.gjetr.org.
- [27] L. W. M. Ven Te Chow, David R. Maidment, “Applied Hydrology.” pp. 1–294, 1998.
- [28] V. Te Chow, D. R. Maidment, and L. W. Mays, *Development of Hydrology*. 1988.
- [29] Wikipedia, “Moody chart,” 2021. .
- [30] Mdm.Nur Irwany Bint Ahmad, “Small hydro power system.” doi: irwany@unimap.edu.my.
- [31] P. K. Nag, *power plant engineering*. .

- [32] A. C. and V. D. : Aline Choulot, Gema San Bruno, “Energy recovery in existing infrastructures with small hydropower plants.”
- [33] B. A. Nasir, “Suitable Selection Of Components For The Micro-Hydro-Electric Power Plant,” no. June, 2018, doi: 10.13189/aep.2014.020102.
- [34] W. S. E. I. D. P. (SEIDP) Bank, “Micro hydropower system design guide lines,” 2020.
- [35] S. O. Otuagoma, “Turbine Selection Criteria for Small Hydropower Development – The River Ethiop Experience . S O Otuagoma,” *Int. J. Latest Res. Eng. Technol. (IJLRET)*, vol. 02, no. 05, pp. 34–40, 2016.
- [36] S. Sangal, A. Garg, and D. Kumar, “Review of Optimal Selection of Turbines for Hydroelectric Projects,” *Rev. Optim. Sel. Turbines Hydroelectr. Proj.*, vol. 3, no. 3, pp. 424–430, 2013.
- [37] B. A. Nasir, “Suitable Selection of Components for the Micro-Hydro-Electric Power Plant,” *Adv. Energy Power DOI 10.13189/aep.2014.020102*, vol. 2, no. 1, pp. 7–12, 2014, doi: 10.13189/aep.2014.020102.
- [38] Abera Tadele and Ferew Dereje, “ASSESSMENT OF DABENA MINI HYDRO POWER PLANT AT,” *Int. J. Eng. Technol. Manag. Res.*, vol. 7, no. 11, pp. 30–38, 2020.
- [39] N. U. R. Azirah and B. Abdul, “SIMULATION OF MICRO HYDRO POWER BASED ON RIVER CONFIGURATION AT RIVER UPSTREAM,” UNIVERSITI MALAYSIA PAHANG, 2013.
- [40] R. Prophet, “An Investigation into the Feasibility of a Micro-hydro Installation for the Guardbridge Energy Centre as Part of a Brownfield Redevelopment,” University of Strathclyde Engineering, 2015.
- [41] S. Sishah, “Rainfall runoff estimation using GIS and SCS-CN method for awash river basin, Ethiopia,” *Int. J. Hydrol.*, vol. 5, no. 1, pp. 33–37, 2021, doi: 10.15406/ijh.2021.05.00263.

- [42] A. B. Woldesenbet, "Hydrologic soil group based curve number matrix modeling for Enset-Based land use system in Meki River Watershed , Western Lake Ziway Sub-Basin , Central Rift Valley of Ethiopia," 2021.
- [43] Donald E. Woodward, Kenneth M. Kent, Claudia C. Hoefl, Annette Humpal and Geoffrey Cerrelli, "Hydrology National Engineering Handbook Chapter 15, Time of Concentration," in *Part 630-Hydrology National Engineering Handbook-United states department of agriculture and Natural Resource Conservation Service (NRCS)*, 2010, pp. 1–15.
- [44] Ethio Resource Group, "Opportunities for creatin photovoltaic industry in Ethiopia:Solar energy vision for Ethiopia:International solar energy institute/ Solar Energy Development association of ethiopia, Freiburg (Germany) / Addis Ababa (Ethiopia)," 2012.
- [45] S.Kalogirou, *Solar energy engineering process and system*, London: *ELSIVIER*(www.elsevier.com), *BOOK AID international* (www.bookaid.org) and *Sabre foundation* (www.sabre.org). 2009.
- [46] J. A. D. Deceased and W. A. Beckman, *Solar Engineering of Thermal Processes:New Jersey, Canada, University of Wisconsin-Madison:(www.wiley.com.)*. 2013.
- [47] A. Awasthi, R. Chauhan, A. Sharma, and M. Ali, "Case Studies in Thermal Engineering Correlation formulation for optimum tilt angle for maximizing the solar radiation on solar collector in the Western Himalayan region," vol. 26, no. June, 2021, doi: 10.1016/j.csite.2021.101185.
- [48] M. Koehl, M. Heck, S. Wiesmeier, and J. Wirth, "Solar Energy Materials & Solar Cells Modeling of the nominal operating cell temperature based on outdoor weathering," *Sol. Energy Mater. Sol. Cells*, vol. 95, no. 7, pp. 1638–1646, 2011, doi: 10.1016/j.solmat.2011.01.020.
- [49] B. Hashemi, S. Taheri, A. Cretu, and E. Pouresmaeil, "Systematic photovoltaic system power losses calculation and modeling using computational intelligence techniques Number of Hidden Units," *Appl. Energy*, vol. 284, no. September 2020, p. 116396, 2021, doi: 10.1016/j.apenergy.2020.116396.

- [50] A. M. Tanaka, “Investigation of Efficiency Loss of Distributed Solar Power Due to Soiling and Efficiency Recovery by Rainfall,” University of Nevada Las Vegas (UNLV), 2019.
- [51] B. Karasu, Z. E. Oytaç, E. S. Ergani, and A. F. Buluç, “Solar Glass Panels : A Review Cam Güneş Panelleri : Bir Derleme,” no. 20, pp. 548–565, 2020, doi: 10.31590/ejosat.746056.
- [52] M. Rudnicka and E. Klugmann-Radziemska, “The Issue of Shading Photovoltaic Installation Caused by Dust Accumulation on the Glass Surface,” *Ecol. Chem. Eng. S*, vol. 28, no. 2, pp. 173–182, 2021, doi: 10.2478/eces-2021-0013.
- [53] K. Chiteka, R. Arora, and V. Jain, “CFD Prediction of dust deposition and installation parametric optimisation for soiling mitigation in non-tracking solar PV modules,” *Int. J. Ambient Energy*, vol. 42, no. 11, pp. 1307–1320, 2021, doi: 10.1080/01430750.2019.1594373.
- [54] H. A. and R. G. Hassan Qasem, Thomas R. Betts, Harald Müllejans, “Dust-induced shading on photovoltaic modules,” *Prog. PHOTOVOLTAICS*, vol. 22, no. 6, pp. 218–226, 2014, doi: 10.1002/pip.2230.
- [55] M. A. Afridi *et al.*, “Determining the Effect of Soiling and Dirt Particles at Various Tilt Angles of Photovoltaic Modules,” *Int. J. Eng. Work.*, vol. 4, no. 8, pp. 143–146, 2017.
- [56] A. K. Tripathi, S. Ray, M. Aruna, and S. Prasad, “Evaluation of solar PV panel performance under humid atmosphere,” *Mater. Today Proc.*, vol. 45, pp. 5916–5920, 2020, doi: 10.1016/j.matpr.2020.08.775.
- [57] A. Saleh, M. Faridun, N. Tajuddin, M. Ra, A. Azmi, and M. A. M. Ramli, “Optimization and sensitivity analysis of standalone hybrid energy systems for rural electrification : A case study of Iraq,” vol. 138, pp. 775–792, 2019, doi: 10.1016/j.renene.2019.02.004.
- [58] A. Bhatt, M. P. Sharma, and R. P. Saini, “Feasibility and sensitivity analysis of an off-grid micro hydro – photovoltaic – biomass and biogas – diesel – battery hybrid energy system for a remote area in Uttarakhand state , India,” *Renew. Sustain. Energy Rev.*, vol. 61, pp. 53–69, 2016, doi: 10.1016/j.rser.2016.03.030.

- [59] R. Syahputra and I. Soesanti, "Renewable energy systems based on micro-hydro and solar photovoltaic for rural areas: A case study in Yogyakarta, Indonesia," *Energy Reports*, vol. 7, pp. 472–490, 2021, doi: 10.1016/j.egy.2021.01.015.
- [60] T. Kaur and R. Segal, "Designing rural electrification solutions considering hybrid energy systems for Papua New Guinea," *Energy Procedia*, vol. 110, no. December 2016, pp. 1–7, 2017, doi: 10.1016/j.egypro.2017.03.092.
- [61] O. D. T. Odou, R. Bhandari, and R. Adamou, "Hybrid off-grid renewable power system for sustainable rural electrification in Benin," *Renew. Energy*, vol. 145, pp. 1266–1279, 2020, doi: 10.1016/j.renene.2019.06.032.
- [62] T. Lambert, P. Gilman, and P. Lilienthal, "Micropower System Modeling with Homer," *Integr. Altern. Sources Energy*, pp. 379–418, 2006, doi: 10.1002/0471755621.ch15.
- [63] S. Kumar, T. Kaur, M. K. Arora, and S. Upadhyay, "Resource estimation and sizing optimization of PV/micro hydro-based hybrid energy system in rural area of Western Himalayan Himachal Pradesh in India," *Energy Sources, Part A Recover. Util. Environ. Eff.*, vol. 41, no. 22, pp. 2795–2807, 2019, doi: 10.1080/15567036.2019.1576075.
- [64] M. Shahzad *et al.*, "Economic analysis and optimization of a renewable energy based power supply system with different energy storages for a remote island," *Renew. Energy*, vol. 164, pp. 1376–1394, 2021, doi: 10.1016/j.renene.2020.10.063.
- [65] X. Yin *et al.*, "ScienceDirect t Optimization for Hydro-Photovoltaic-Wind Power Generation Optimization for Power Generation system based on modified version of multi-objective whale optimization algorithm," *Energy Procedia*, vol. 158, pp. 6208–6216, 2019, doi: 10.1016/j.egypro.2019.01.480.
- [66] C. S. Lai and G. Locatelli, "Economic and financial appraisal of novel large-scale energy storage technologies," *Energy*, vol. 214, p. 118954, 2021, doi: 10.1016/j.energy.2020.118954.
- [67] Florida Solar Energy Center Creating energy independence, "Solar cell, Module and arrays," 2022. .
- [68] K. Neumeister, "Cheap Solar Panels: 2021 Guide to Affordable Solar Panels," *EcoWatch*, 2021. .

- [69] M. SADIQI, “Basic Design and Cost Optimization of a Hybrid power system in rural communities in Afghanistan,” 2012.
- [70] S. Market, “Battery sizes and pricing.” .
- [71] S. k. S. and A. Y. Anuradha, “Modelling of DC Linked PV/Hydro Hybrid System for Rural Electrification journal of Recent development in control Automation power engineering(RDCAPE),” vol. 3, pp. 3–7, 2017.
- [72] A. Ali *et al.*, “Design and implementation of an electromechanical control system for micro - hydropower plants,” *Electr. Eng.*, no. January, 2020, doi: 10.1007/s00202-020-00921-y.
- [73] M. M. A. Seedahmed, M. A. M. Ramli, H. R. E. H. Bouchekara, M. S. Shahriar, A. H. Milyani, and M. Rawa, “A techno-economic analysis of a hybrid energy system for the electrification of a remote cluster in western Saudi Arabia,” *Alexandria Eng. J.*, vol. 61, no. 7, pp. 5183–5202, 2022, doi: 10.1016/j.aej.2021.10.041.
- [74] R. A. Gupta, R. Kumar, and A. K. Bansal, “BBO-based small autonomous hybrid power system optimization incorporating wind speed and solar radiation forecasting,” *Renew. Sustain. Energy Rev.*, vol. 41, pp. 1366–1375, Jan. 2015, doi: 10.1016/J.RSER.2014.09.017.
- [75] G. Liu, M. G. Rasul, M. T. O. Amanullah, and M. M. K. Khan, “Techno-economic simulation and optimization of residential grid-connected PV system for the Queensland climate,” *Renew. Energy*, vol. 45, pp. 146–155, Sep. 2012, doi: 10.1016/J.RENENE.2012.02.029.
- [76] O. Access, “Ethiopia electricity prices september 2021,” 2021. .
- [77] S. S. Shaita, “Socio-Economic Benefits and Challenges of Energy Efficient Cook Stoves Utilization for Women and Children in Yaya Gulele District , North Western Ethiopia,” 2014.
- [78] “Yaya Gulele - WikiVisually.pdf.” .
- [79] singapore world vision, “Yaya Gulele Area Development Programme, Ethiopia:www.worldvision.org.sg,” 2021.

- [80] M. Alam, “Decentralized renewable hybrid mini-grid based electrification of rural and remote off- grid areas of Bangladesh,” 2017.
- [81] Y. Muñoz, J. Guerrero, and A. Ospino, “Evaluation of a hybrid system of renewable electricity generation for a remote area of colombia using homer software,” *Tecciencia*, vol. 9, no. 17, pp. 57–67, 2014, doi: 10.18180/tecciencia.2014.17.6.
- [82] M. Alam and S. Bhattacharyya, “Decentralized renewable hybrid mini-grids for sustainable electrification of the off-grid coastal areas of Bangladesh,” *Energies*, vol. 9, no. 4, 2016, doi: 10.3390/en9040268.
- [83] Deutsche Gesellschaft für internationale (GIZ), “What size shall it be ? A guide to mini-grid sizing and demand forecasting, How to assess the electricity demand of a community and determine the appropriate size of a new solar mini-grid.,” 2016.
- [84] “<http://www.daftlogic.com/information.htm>, ‘Draft logic,’ Amazon.Co.UK, [Online]. Available: <http://www.daftlogic.com/information-appliance-power-consumption.htm>,” 2021. .
- [85] Y. Kebede, F. Baudron, F. J. J. A. Bianchi, and P. Tittone, “Drivers, farmers’ responses and landscape consequences of smallholder farming systems changes in southern Ethiopia,” *Int. J. Agric. Sustain.*, vol. 17, no. 6, pp. 383–400, 2019, doi: 10.1080/14735903.2019.1679000.
- [86] J. Mugisha, M. A. Ratemo, B. C. Bunani Keza, and H. Kahveci, “Assessing the opportunities and challenges facing the development of off-grid solar systems in Eastern Africa: The cases of Kenya, Ethiopia, and Rwanda,” *Energy Policy*, vol. 150, no. May 2020, p. 112131, 2021, doi: 10.1016/j.enpol.2020.112131.
- [87] “customer penetration.pdf.” .
- [88] A. R. and B. D. M. Awal Nopriyanto Bahasoan, Andini Nurhajra, Taufik Hidayat B Tahawa, “THE POPULATION GROWTH FORECASTING TOWARDS NEED FOR WASTE,” <http://ejurnal.binawakya.or.id/index.php/MBI>, vol. 15, no. 8, pp. 5003–5010, 2021.

- [89] D. Guta and J. Börner, “Energy security, uncertainty and energy resource use options in Ethiopia: A sector modelling approach,” *Int. J. Energy Sect. Manag.*, vol. 11, no. 1, pp. 91–117, 2017, doi: 10.1108/IJESM-04-2015-0005.
- [90] C.-H. W. and C.-C. K. * Teketay Mulu Beza, “applied sciences Optimal Sizing and Techno-Economic Analysis of Minigrid Hybrid Renewable Energy System for Tourist Destination,” *Appl. Sci.*, vol. 11, no. 1, pp. 1–22, 2021, doi: <https://doi.org/10.3390/app11157085>.
- [91] M. A. H. Mondal, E. Bryan, C. Ringler, and M. Rosegrant, “Ethiopian power sector development: Renewable based universal electricity access and export strategies,” *Renew. Sustain. Energy Rev.*, vol. 75, no. October, pp. 11–20, 2017, doi: 10.1016/j.rser.2016.10.041.
- [92] D. Yogi Goswami, *Principles of SOLAR ENGINEERING*, Third edit. Boca Raton, London, New York CRC: CRC Press Taylor & Francis Group, 2015.

Appendix-A: Load Assessment and calculated Meteorological data

Table-A 1: Electric load demand of High class household

Household category	Appliances	Radio	TV	DVD	charger	stove	Fridge	Light	Total	
High class household (72)	Rated power	10 W	120W	24W	5 W	1200 W	100 W	11W		
	No. of appliance per household	1	1	1	1	1	1	4		
	Probability of Using	100	100	100	100	100	75	100		
	7:00	0.72	8.64			0.36	24	5.4	39.12	
	8:00	0.72	8.64			0.36		5.4	15.12	
	9:00	0.72		1.72				5.4	7.84	
	10:00	0.72		1.72			24	5.4	31.84	
	11:00	0.72		1.72			24	5.4	31.84	
	12:00	0.72		1.72		0.36		5.4	8.2	
	13:00	0.72	8.64			0.36		5.4	15.12	
	14:00	0.72	8.64			0.36		5.4	15.12	
	15:00			1.72				5.4	7.12	
	16:00			1.72				5.4	7.12	
	17:00			1.72				5.4	7.12	
	18:00	0.72		1.72				5.4	3.168	11.008
	19:00	0.72	8.64				24	5.4	3.168	41.928
	20:00	0.72	8.64				24	5.4	3.168	41.928
	21:00	0.72	8.64	1.72				5.4	3.168	19.648
	22:00			1.72		0.36		5.4	3.168	10.648
	23:00					0.36		5.4		5.76
24:00					0.36		5.4		5.76	
1:00							5.4		5.4	

2:00						5.4	5.4
3:00						5.4	5.4
4:00						5.4	5.4
5:00						5.4	5.4
6:00	0.72				24	5.4	30.12
Total Kwh/day	9.36	60.48	17.2	2.88	144	129.6	15.84
%							379.36

Table-A 2: Electric load demand of Medium class house hold

Household category	Appliances	Radio	TV	DVD	charger	Stove	Light	Total
Medium class household (178)	Rated power	10 W	120W	24W	5 W	1200 W	11W	
	No. of appliance per household	1	1	1	1	1	3	
	Probability of Using %	100	75	100	100	100	100	
	7:00	0.14	2.29			0.11	59.3	61.84
	8:00	0.14	2.29			0.11		2.54
	9:00	0.14						0.14
	10:00	0.14					59.3	59.44
	11:00	0.14			0.53		59.3	59.97
	12:00	0.14			0.53	0.11		0.78
	13:00	0.14	2.29			0.11		2.54
	14:00	0.14	2.29			0.11		2.54
	15:00				0.53			0.53
	16:00				0.53			0.53
	17:00							0
	18:00	0.14						5.87

19:00	0.14	2.29			59.3	5.87	67.6
20:00	0.14	2.29			59.3	5.87	67.6
21:00	0.14	2.29	0.53			5.87	8.83
22:00			0.53	0.11		5.87	6.51
23:00				0.11			0.11
24:00				0.11			0.11
1:00							0
2:00							0
3:00							0
4:00							0
5:00							0
6:00	0.14				59.3		59.44
Total Kwh/day	1.82	16.03	3.18	0.88	355.8	29.35	407.06
%							

Table-A 3: Electric load demand of Low Class house holds

Household category	Appliances	Radio	TV	DVD	charger	stove	Light	Total
Low class household (161)	Rated power	10 W	120W	24W	5 W	1200 W	11W	
	No. of appliance per household	1	1	1	1	1	2	
	Probability of Using %	100	25	25	100	100	100	
	7:00	1.61	4.83		0.8	26.83		34.07
	8:00	1.61	4.83		0.8			7.24
	9:00	1.61						1.61
	10:00	1.61						1.61
	11:00	1.61		0.96				2.57
	12:00	1.61		0.96	0.8	53.66		57.03

13:00	1.61	4.83		0.8	53.66		60.9
14:00	1.61	4.83		0.8	53.66		60.9
15:00			0.96		53.66		54.62
16:00			0.96		53.66		54.62
17:00							0
18:00	1.61					3.54	5.15
19:00	1.61	4.83				3.54	9.98
20:00	1.61	4.83				3.54	9.98
21:00	1.61	4.83	0.96			3.54	10.94
22:00			0.96	0.8		3.54	5.3
23:00				0.8			0.8
24:00				0.8			0.8
1:00							0
2:00							0
3:00							0
4:00							0
5:00							0
6:00	1.61				26.83		28.44
Total KWh/day	20.93	33.81	5.76	6.4	321.96	17.7	406.56
%							

Table-A 4: Total electric load demand of households

Appliances	Radio	TV	DVD	charger	stove	Fridge	Light	
Rated power	10 W	120 W	24 W	5 W	1200 W	100 W	11 W	Total
7:00	3.462	13.47		0.26	77.6	0.23		95.022
8:00	3.462	29.49		0.26	59.3	0.23		92.742
9:00	3.462	24.66	0.29		59.3	0.23		87.942
10:00	3.462		0.29		77.6	0.23		81.582
11:00	3.462		0.98		77.6	0.23		82.272
12:00	3.462	20.85	0.98	0.26	59.3	0.23		85.082
13:00	3.462	20.85		0.26	59.3	0.23		84.102
14:00	3.462	4.83		0.26		0.23		8.782
15:00		4.83	0.98			0.23		6.04
16:00		24.66	0.98			0.23		25.87
17:00		24.66	0.29		59.3	0.23		84.48
18:00	3.462	8.64	0.29		59.3	0.23	12.58	84.502
19:00	3.462				77.66	0.23	12.58	93.932
20:00	3.462				77.66	0.23	12.58	93.932
21:00	3.462	29.49	0.98			0.23	12.58	46.742
22:00			0.98	0.26		0.23	12.58	14.05
23:00				0.26		0.23		0.49
24:00				0.26		0.23		0.49
1:00						0.23		0.23
2:00						0.23		0.23
3:00						0.23		0.23
4:00						0.23		0.23
5:00						0.23		0.23

Variation of Time within a days

6:00	3.462	0.26				77.66	0.23		81.612
Total Kwh/day	45.006	206.69	7.04	2.08		821.58	5.52	62.9	1150.816
%									

Table-A 5: estimated community load demand

Community sectors																			
Clients	church			School							Small Clinic				Street Light	Kebele admn.	FTC		Total
Appliances	Light indoor	Lighting outdoor	Sound amplifier	TV	Light indoor	Light Outdoor	bell	Photocopier	Desktop	printer	TV	Light indoor	Light Outdoor	Fridge	Light	Light	Lighting indoor	Lighting Outdoor	
Power (W)	11	11	82	120	11	11	30	30	120	30	120	11	11	100	100	11	11	11	
Number	8	6	1	1	20	20	2	3	3	3	1	6	6	2	50	2	4	3	
No. of hrs	7	11	6	5	4	11	8	8	8	8	8	12	10	24	11		2	11	
7:00	0.088		0.082	0.12										0.12		0.022	0.044	0.48	
8:00				0.12			0.06	0.09	0.36	0.09	0.12			0.12				0.96	
9:00							0.06	0.09	0.36	0.09	0.12			0.12				0.84	
10:00				0.12			0.06			0.09				0.12				0.39	
11:00							0.06	0.09	0.36	0.09	0.12			0.12				0.84	
12:00							0.06	0.09	0.36		0.12			0.12				0.75	
13:00							0.06			0.09	0.12			0.12				0.39	
14:00				0.12			0.06	0.09	0.36	0.09				0.12				0.84	
15:00				0.12			0.06	0.09	0.36		0.12			0.12				0.87	
16:00								0.09	0.36	0.09				0.12				0.66	
17:00								0.09	0.36	0.09	0.12			0.12				0.78	
18:00					0.22						0.12			0.12				0.46	
19:00		0.066			0.22							0.066	0.066	0.12	5	0.022		0.033	
20:00		0.066			0.22	0.22					0.12	0.066	0.066	0.12	5	0.022		0.033	

21:00		0.066		0.22	0.22		0.066	0.066	0.12	5		0.033	5.79
22:00		0.066			0.22		0.066	0.066	0.12	5		0.033	5.57
23:00		0.066			0.22		0.066	0.066	0.12	5		0.033	5.57
24:00:00		0.066			0.22		0.066	0.066	0.12	5		0.033	5.57
1:00	0.088	0.066	0.082		0.22		0.066	0.066	0.12	5		0.033	5.74
2:00	0.088	0.066	0.082		0.22		0.066	0.066	0.12	5		0.033	5.74
3:00	0.088	0.066	0.082		0.22		0.066	0.066	0.12	5		0.033	5.74
4:00	0.088	0.066	0.082		0.22		0.066	0.066	0.12	5		0.033	5.741
5:00	0.088	0.066	0.082		0.22		0.066	0.066	0.12	5		0.033	5.741
6:00	0.088	0.066	0.082		0.22				0.12		0.044		0.62
Total		1.982			8.7		5.412			55	0.066	0.451	
%													100%

Table-A 6: Estimated commercial load

Small business center (Barber + Beauty Salon +Tailor)							Flour Mill	Total
Appliances	Light	hair clipper	Hair roller	hair straighter	Sewing	Motor		
Rated power	11 W	15 W	400 W	300 W	100 W	7500 W		
No. appliance	10	6	2	2	6	1		
Operating hr	4	12	12	12	12	6		
7:00							0	
8:00	0.11						0.11	
9:00		0.09	0.8	0.6	0.6		2.09	
10:00		0.09	0.8	0.6	0.6	7.5	9.59	
11:00		0.09	0.8	0.6	0.6	7.5	9.59	

12:00		0.09	0.8	0.6	0.6	7.5	9.59
13:00		0.09	0.8	0.6	0.6		2.09
14:00		0.09	0.8	0.6	0.6		2.09
15:00		0.09	0.8	0.6	0.6	7.5	9.59
16:00		0.09	0.8	0.6	0.6	7.5	9.59
17:00		0.09	0.8	0.6	0.6		2.09
18:00	0.11	0.09	0.8	0.6	0.6	7.5	9.7
19:00	0.11	0.09	0.8	0.6	0.6		2.2
20:00	0.11	0.09	0.8	0.6	0.6		2.2
21:00							0
22:00							0
23:00							0
24:00							0
1:00							0
2:00							0
3:00							0
4:00							0
5:00							0
6:00							0
Total			25.52			45	
%							

Table-A 7: forecasted population growth of Goda warki village

Year	Growth rate %	No population in base year	n	P_n
2021	2.6	1644	0	1644
2022	2.6	1644	1	1686.74
2023	2.6	1644	2	1730.59
2024	2.6	1644	3	1775.59
2025	2.6	1644	4	1821.76
2026	2.6	1644	5	1869.13
2027	2.6	1644	6	1917.72
2028	2.6	1644	7	1967.58
2029	2.6	1644	8	2018.74
2030	2.6	1644	9	2071.23
2031	2.6	1644	10	2125.08
2032	2.6	1644	11	2180.33
2033	2.6	1644	12	2237.02
2034	2.6	1644	13	2295.18
2035	2.6	1644	14	2354.86
2036	2.6	1644	15	2416.08
2037	2.6	1644	16	2478.90
2038	2.6	1644	17	2543.35
2039	2.6	1644	18	2609.48
2040	2.6	1644	19	2677.33
2041	2.6	1644	20	2746.94
2042	2.6	1644	21	2818.36
2043	2.6	1644	22	2891.64
2044	2.6	1644	23	2966.82
2045	2.6	1644	24	3043.95

Table-A 8: Energy demand forecasting for projected number of households in project lifetime

Year	electric demand E_o	customer penetration %	No. of HH in i^{th} year h_i	No. HH in base year h_o	annual average/HH E	i^{th} year ann. avg energy demand E_i
2021	1269.8	0.54	411	411	2.64	1269.8
2022	1269.8	0.54	421.68	411	2.56	1287.18
2023	1269.8	0.54	432.65	411	2.49	1304.11
2024	1269.8	0.54	483.29	411	2.23	1372.37
2025	1269.8	0.54	495.85	411	2.17	1387.14
2026	1269.8	0.54	508.75	411	2.12	1401.55
2027	1269.8	0.54	521.97	411	2.06	1415.58
2028	1269.8	0.54	535.55	411	2.01	1429.26
2029	1269.8	0.54	549.47	411	1.96	1442.60
2030	1269.8	0.54	563.76	411	1.91	1455.59
2031	1269.8	0.54	578.42	411	1.86	1468.26
2032	1269.8	0.54	593.45	411	1.82	1480.61
2033	1269.8	0.54	608.88	411	1.77	1492.65
2034	1269.8	0.54	624.72	411	1.73	1504.37
2035	1269.8	0.54	640.96	411	1.68	1515.81
2036	1269.8	0.54	657.62	411	1.64	1526.95
2037	1269.8	0.54	674.72	411	1.59	1537.81
2038	1269.8	0.54	692.26	411	1.56	1548.39
2039	1269.8	0.54	710.26	411	1.52	1558.71
2040	1269.8	0.54	728.73	411	1.48	1568.76
2041	1269.8	0.54	747.68	411	1.44	1578.56
2042	1269.8	0.54	767.12	411	1.40	1588.15
2043	1269.8	0.54	787.06	411	1.37	1597.43
2044	1269.8	0.54	807.52	411	1.34	1606.50
2045	1269.8	0.54	828.52	411	1.30	1615.34

Table-A 9: Average rainfall data of study area from NMA

Month	Years							average
	2012	2013	2014	2015	2016	2017	2018	
1	5.2	17.9	17.4	0	15.1	9.1	0	9.24
2	1	19.4	7.9	11.3	40	11.1	31.9	17.51
3	49.6	36.5	72.1	24.9	43.1	20.8	10.4	36.77
4	22.5	41.9	22.1	20.7	94	34.9	53.9	41.43
5	22.5	39.7	92	78.7	154.6	165.5	35.4	84.06
6	127.5	119.5	74.6	163.4	202.3	157.1	271.6	159.4
7	294.1	199.6	185.6	264.5	258.5	230.4	249.5	207
8	240.9	217.9	242.8	167	217.4	192.6	228.3	215.3
9	91.8	133.5	79.2	72.1	84.5	69.7	81.2	87.43
10	0.5	51	70.7	0	34.1	43.1	32.3	39.26
11	5.7	10.6	20	9.4	10.6	6.8	12.4	10.78
12	16.3	0	0.9	17.3	8.2	5.3	3.7	7.38
Average	73.13	73.96	73.78	69.11	96.87	78.87	84.22	76.29

Table-A 10: Hydrologic soil group of different soil types [42]

Soil Types	Hydrologic soil Group (HSG)	Soil Types	Hydrologic soil Group (HSG)	Soil Types	Hydrologic soil Group (HSG)
Orthic Acrisols	B	Calcaric Fluvisols	B	Eutric Nitosols	B
Chromic Cambisols	B	Eutric Fluvisols	B	Dystric Histosols	D
Dystric Cambisols	B	Chromic Luvisols	B	Eutric Histosols	D
Eutric Cambisols	B	Orthic Luvisols	B	Cambric Arenosols	A
Humic Cambisols	C	Vertic Luvisols	C	Calcaric Regosols	A
Calcic Cambisols	B	Dystric Nitosols	B	Eutric Regosols	A
Vertic cambisols	B	Caloic xerosols	B	Humic Andosols	B
Calcic chernozems	B	Luvic Xerosols	C	Mollic Andosols	B
Rendzinas	D	Gypsic Yermosols	B	Vitric Andosols	B
Haplic Pheozems	C	Gleyic Solonchaks	D	Chromic Vertisols	D
Luvic Pheozems	C	Orthic Solonchaks	B	Haplic xerosols	B
Lithosols	D	Pellic Vertisols	D		

Table-A 11: Monthly sunshine hour data of NMA for study area

Months	Year					Average
	2016	2017	2018	2019	2020	
January	9.94	7.92	7.32	9	8.62	8.56
February	9.77	6.57	9.3	6.19	8.34	8.034
March	8.63	7.57	7.36	7.09	6.91	7.512
April	8.66	7.35	5.37	8.08	9.33	7.758
May	7.96	8	7.51	6.98	8.08	7.706
June	6.82	6.81	6.59	5.7	5.4	6.264
July	7.53	4.82	4.41	4.64	4.88	5.256
Aug	5.63	4.73	4.64	8.32	5.51	5.766
September	7.68	5.79	6.95	9.09	9.8	7.862
October	9.95	7.58	8.84	4.88	8.63	7.976
November	9.35	8.12	6.87	10.36	8.19	8.578
December	7.33	9.23	7.56	9.62	6.92	8.132

Table-A 12: Estimated monthly discharge of Girar River

Months in a year	New-LoClim discharge [m ³ /s]	NMA discharge [m ³ /s]	NASA discharge [m ³ /s]
1	0.00784	0.01	0.02707
2	0.2097	0.1237	0.004276
3	0.6506	0.2156	0.3866
4	0.6506	0.2001	0.2801
5	0.3154	0.8696	0.348
6	0.6658	1.671	1.094
7	4.807	4.222	4.828
8	5.432	3.291	4.426
9	1.381	0.929	1.095
10	0.03192	0.1459	0.2003
11	0.03058	0.01223	0.001509
12	0.02416	0.01182	0.0008599

Table-A 13: Runoff curve number for various land uses [27], [28]

Land Use Description		Hydrologic soil Group			
		A	B	C	D
Cultivated land	Without conservation treatment	72	81	88	91
	With conservation treatment	62	71	78	81
Pasture or range land	Poor condition	68	79	86	89
	Good condition	39	61	74	80
Meadow good condition		30	58	71	78
Wood or forest land	Thin stand poor cover no mulch	45	66	77	83
	Good cover	25	55	70	77
Open space, lawns, parks, golf courses, cemeteries etc.	Good condition: grass cover on 75% more of the area	39	61	74	80
	Fair condition grass cover on 50% to 75% of the area	49	69	79	84
Commercial and business area (85% impervious)		89	92	94	95
Industrial Districts (72% impervious)		81	88	91	93
Residential					
Average lot size	Average % impervious				
1/8 acre or less	65	77	85	90	92
1/4 acre	38	61	75	83	87
1/3 acre	30	57	72	81	86
1/2 acre	25	54	70	80	85
1 acre	20	51	68	79	84

Table-A 14: Reflectivity Values for Characteristic Surfaces (Integrated over Solar Spectrum and Angle of incidence)[92]

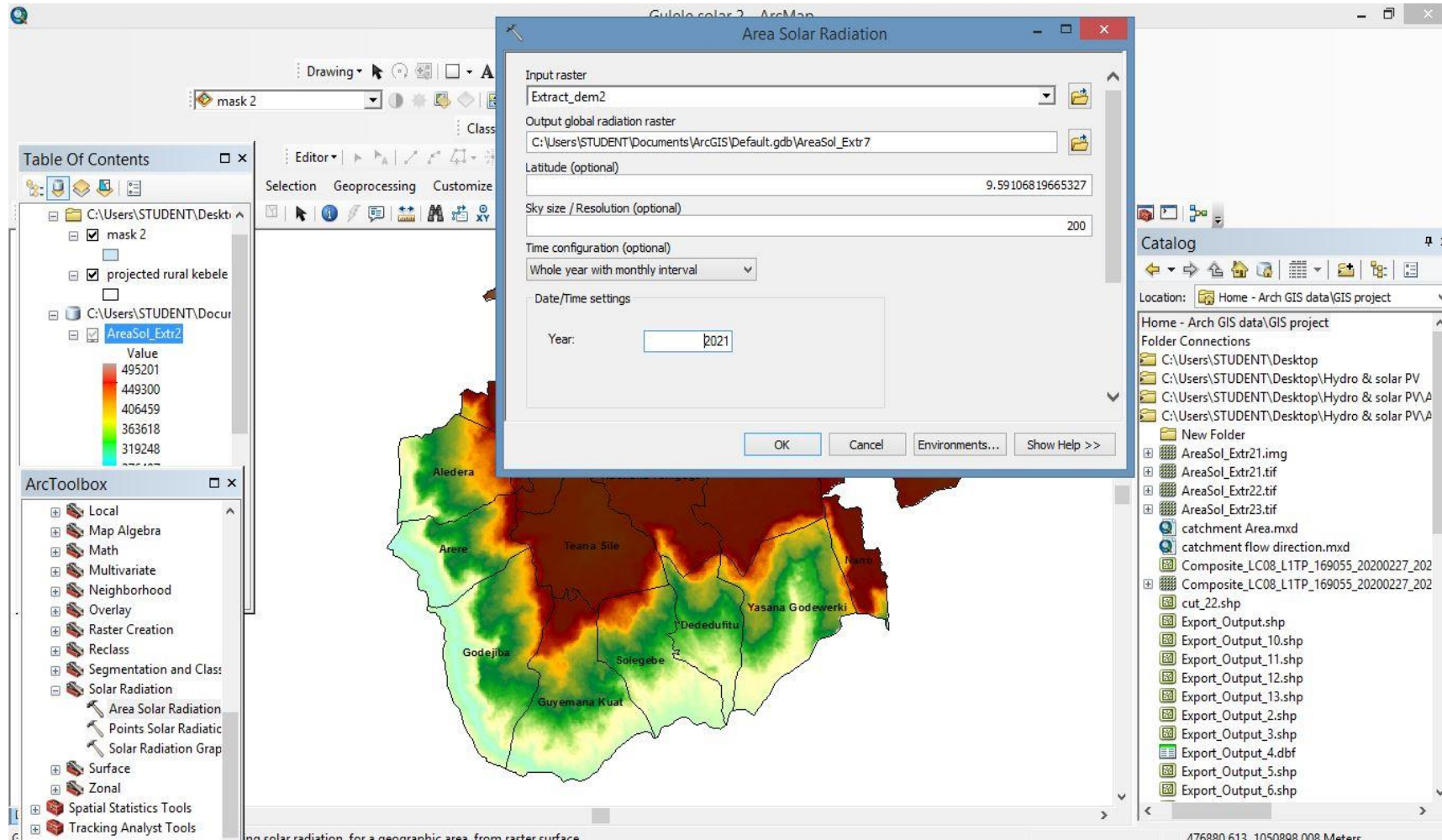
Surface	Average Reflectivity
Snow (freshly fallen or with ice film)	0.75
Water surfaces (relatively large incidence angles)	0.07
Soils (clay, loam, etc.)	0.14
Earth roads	0.04
Coniferous forest (winter)	0.07
Forests in autumn, ripe field crops, plants	0.26
Weathered blacktop	0.10
Weathered concrete	0.22
Dry grass	0.2
Green grass	0.26
Bituminous and gravel roof	0.13
Crushed rock surface	0.2
Building surfaces, dark (red brick, dark paints, etc.)	0.27
Building surfaces, light (light brick, light paints, etc.)	0.60
Dead leaves	0.30

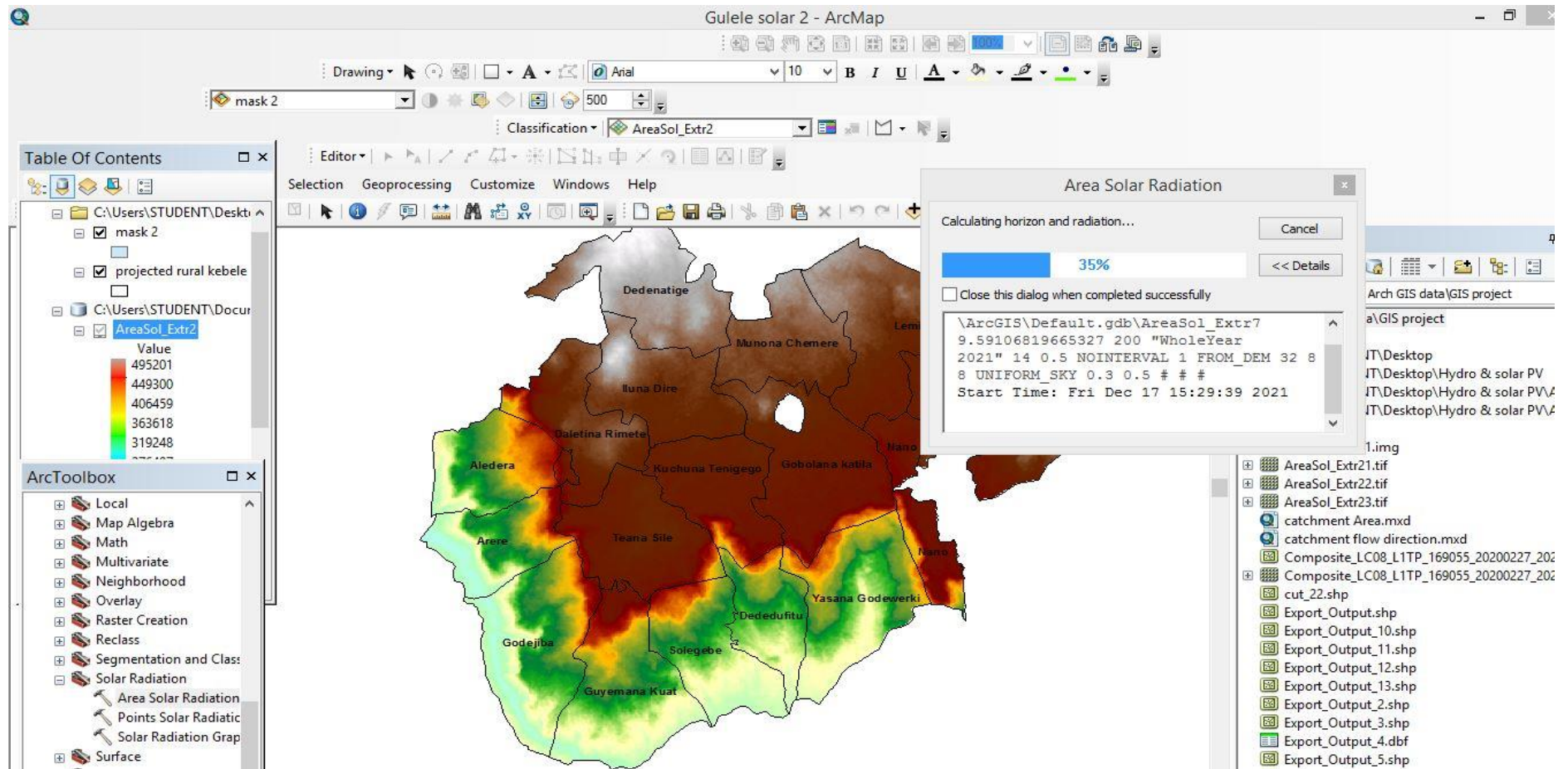
Table-A 15 Solar radiation in KWh/m²/day of the study area from three different source.

Months	Solar radiation in KWh/m ² /day		
	New-LoClim	NMA	NASA
January	5.65	5.9	6.18
February	5.47	5.57	6.59
March	5.08	5.61	6.52
April	5.14	5.81	6.48
May	5.46	5.66	6.42
June	4.49	4.83	5.86
July	3.09	4.29	5.15
August	3.26	4.71	5.18
September	4.23	5.84	5.84
October	5.34	5.67	6.40
November	5.93	5.56	6.31
December	5.43	5.19	6.11
Average	4.88	5.39	6.08

Appendix-B: Software simulation inputs and analysis flow process

Appendix-B 1: ArcGIS analysis of solar Areal solar radiation calculation





The screenshot shows the ArcGIS Desktop interface. A 'Table' window is open, displaying a table with 5 rows of data. A 'Calculate Geometry' dialog box is overlaid on the table, with 'Area' selected as the property to calculate. The dialog box is configured to use the coordinate system of the data source (PCS: WGS 1984 UTM Zone 37N) and the units are set to Square Kilometers [sq km].

OBJECTID *	Shape *	Id	gridcode	Shape_Length	Shape_Area	Soil_type	Area
1	Polygon	1	2	6890.929379	1368683.9109		
2	Polygon	2	3	55790.024557	58426196.05180		
3	Polygon	3	1	4422.816549	883231.2276		
4	Polygon	4	2	7215.508189	2144555.88736		
5	Polygon	5	3	2049.953359	141199.43651		

Appendix-B 2: Accuracy assessment and Kappa co-efficient value evidence of LULC analysis by ERDAS Imagine software

CLASSIFICATION ACCURACY ASSESSMENT REPORT

Image File : g:/efi/ephrem and ashe final recode.img
 User Name : Afu
 Date : Fri May 06 06:46:55 2022

ERROR MATRIX

Classified Data	Background	Reference Data		
		Class 1	Class 2	Class 3
Background	17	12	0	0
Class 1	0	45	0	0
Class 2	0	0	41	0
Class 3	0	0	0	48
Class 4	0	0	0	0
Class 5	0	0	0	0
Class 6	0	0	0	0
Column Total	17	57	41	48

Classified Data	Class 4	Reference Data		Row Total
		Class 5	Class 6	
Background	0	0	0	29
Class 1	8	0	0	53
Class 2	0	1	0	42
Class 3	0	2	7	57
Class 4	42	2	1	45
Class 5	0	38	2	40
Class 6	0	0	70	70
Column Total	50	43	80	336

----- End of Error Matrix -----

----- End of Error Matrix -----

ACCURACY TOTALS

Class Name	Reference Totals	Classified Totals	Number Correct	Producers Accuracy	Users Accuracy
Class 0	17	29	17	---	---
Class 1	57	53	45	78.95%	84.91%
Class 2	41	42	41	100.00%	97.62%
Class 3	48	57	48	100.00%	84.21%
Class 4	50	45	42	84.00%	93.33%
Class 5	43	40	38	88.37%	95.00%
Class 6	80	70	70	87.50%	100.00%
Totals	336	336	301		

Overall Classification Accuracy = 89.58%

----- End of Accuracy Totals -----

KAPPA (K[^]) STATISTICS

Overall Kappa Statistics = 0.8767

Conditional Kappa for each Category.

Class Name	Kappa
Class 0	0.5642
Class 1	0.8182
Class 2	0.9729
Class 3	0.8158
Class 4	0.9217
Class 5	0.9427
Class 6	1.0000

----- End of Kappa Statistics -----

Appendix-B 3: Base Case System and Optimum System by HOMER software

		Architecture							Cost	
									NPC (US\$)	Initial capital (US\$)
Base system									\$1.29M	\$818,843
Current system									\$1.25M	\$889,129

Metric	Value
Present worth (\$)	\$37,689
Annual worth (\$/yr)	\$2,915
Return on investment (%)	7.9
Internal rate of return (%)	10.5
Simple payback (yr)	7.68
Discounted payback (yr)	10.51

[Charts...](#)

Appendix-B 4: EES Software Analysis of Total radiation of the study area and loss analysis due to tilt angle

```

L=9.62                {Latitude in degree}
h=2.581              {elevation in Km}
LST_1=12             {at noon time}
LST_2=18             {afternoon}
W_1=(LST_1-12)*15    {hour angle at noon time =0}
W_2=(LST_2-12)*15    {hour angle at afternoon time}
{ days of the year in each months of the year}
N_1=17
N_2=47
N_3=75
N_4=105
N_5=135
N_6=162
N_7=198
N_8=228
N_9=258
N_10=288
N_11=318
N_12=344
{Declination angle based number of days}
delta_1=23.45*sin((360/365)*(284+N_1))
delta_2=23.45*sin((360/365)*(284+N_2))
delta_3=23.45*sin((360/365)*(284+N_3))
delta_4=23.45*sin((360/365)*(284+N_4))
delta_5=23.45*sin((360/365)*(284+N_5))
delta_6=23.45*sin((360/365)*(284+N_6))
delta_7=23.45*sin((360/365)*(284+N_7))
delta_8=23.45*sin((360/365)*(284+N_8))
delta_9=23.45*sin((360/365)*(284+N_9))
delta_10=23.45*sin((360/365)*(284+N_10))
delta_11=23.45*sin((360/365)*(284+N_11))
delta_12=23.45*sin((360/365)*(284+N_12))
{Average sunshine hour in each month of the year from National meteorological agency NMA}
sn_1=8.56
sn_2=8.03
sn_3=7.51
sn_4=7.76
sn_5=7.71
sn_6=6.26
sn_7=5.26
sn_8=5.77
sn_9=7.86
sn_10=7.98
sn_11=8.58
sn_12=8.13
{Value of n for ith day of the months}
nd_1=17
nd_2=16
nd_3=16
nd_4=15
nd_5=15
nd_6=11
nd_7=17
nd_8=16
nd_9=15
nd_10=15
nd_11=14
nd_12=10
{day length in each months}
NL_1=(2/15)*arccos((-tan(L))*tan(delta_1))
NL_2=(2/15)*arccos((-tan(L))*tan(delta_2))
NL_3=(2/15)*arccos((-tan(L))*tan(delta_3))
NL_4=(2/15)*arccos((-tan(L))*tan(delta_4))
NL_5=(2/15)*arccos((-tan(L))*tan(delta_5))
NL_6=(2/15)*arccos((-tan(L))*tan(delta_6))
NL_7=(2/15)*arccos((-tan(L))*tan(delta_7))
NL_8=(2/15)*arccos((-tan(L))*tan(delta_8))
NL_9=(2/15)*arccos((-tan(L))*tan(delta_9))
NL_10=(2/15)*arccos((-tan(L))*tan(delta_10))
NL_11=(2/15)*arccos((-tan(L))*tan(delta_11))
NL_12=(2/15)*arccos((-tan(L))*tan(delta_12))

```

{Regression constant a & b}

$$\begin{aligned} a_1 &= (-0.309) + (0.539 \cdot \cos(L)) - (0.0639 \cdot h) + (0.29 \cdot (\text{sn}_1 / \text{NL}_1)) \\ a_2 &= (-0.309) + (0.539 \cdot \cos(L)) - (0.0639 \cdot h) + (0.29 \cdot (\text{sn}_2 / \text{NL}_2)) \\ a_3 &= (-0.309) + (0.539 \cdot \cos(L)) - (0.0639 \cdot h) + (0.29 \cdot (\text{sn}_3 / \text{NL}_3)) \\ a_4 &= (-0.309) + (0.539 \cdot \cos(L)) - (0.0639 \cdot h) + (0.29 \cdot (\text{sn}_4 / \text{NL}_4)) \\ a_5 &= (-0.309) + (0.539 \cdot \cos(L)) - (0.0639 \cdot h) + (0.29 \cdot (\text{sn}_5 / \text{NL}_5)) \\ a_6 &= (-0.309) + (0.539 \cdot \cos(L)) - (0.0639 \cdot h) + (0.29 \cdot (\text{sn}_6 / \text{NL}_6)) \\ a_7 &= (-0.309) + (0.539 \cdot \cos(L)) - (0.0639 \cdot h) + (0.29 \cdot (\text{sn}_7 / \text{NL}_7)) \\ a_8 &= (-0.309) + (0.539 \cdot \cos(L)) - (0.0639 \cdot h) + (0.29 \cdot (\text{sn}_8 / \text{NL}_8)) \\ a_9 &= (-0.309) + (0.539 \cdot \cos(L)) - (0.0639 \cdot h) + (0.29 \cdot (\text{sn}_9 / \text{NL}_9)) \\ a_{10} &= (-0.309) + (0.539 \cdot \cos(L)) - (0.0639 \cdot h) + (0.29 \cdot (\text{sn}_{10} / \text{NL}_{10})) \\ a_{11} &= (-0.309) + (0.539 \cdot \cos(L)) - (0.0639 \cdot h) + (0.29 \cdot (\text{sn}_{11} / \text{NL}_{11})) \\ a_{12} &= (-0.309) + (0.539 \cdot \cos(L)) - (0.0639 \cdot h) + (0.29 \cdot (\text{sn}_{12} / \text{NL}_{12})) \end{aligned}$$

$$\begin{aligned} b_1 &= 1.527 - (1.027 \cdot \cos(L)) + (0.0926 \cdot h) - (0.359 \cdot (\text{sn}_1 / \text{NL}_1)) \\ b_2 &= 1.527 - (1.027 \cdot \cos(L)) + (0.0926 \cdot h) - (0.359 \cdot (\text{sn}_2 / \text{NL}_2)) \\ b_3 &= 1.527 - (1.027 \cdot \cos(L)) + (0.0926 \cdot h) - (0.359 \cdot (\text{sn}_3 / \text{NL}_3)) \\ b_4 &= 1.527 - (1.027 \cdot \cos(L)) + (0.0926 \cdot h) - (0.359 \cdot (\text{sn}_4 / \text{NL}_4)) \\ b_5 &= 1.527 - (1.027 \cdot \cos(L)) + (0.0926 \cdot h) - (0.359 \cdot (\text{sn}_5 / \text{NL}_5)) \\ b_6 &= 1.527 - (1.027 \cdot \cos(L)) + (0.0926 \cdot h) - (0.359 \cdot (\text{sn}_6 / \text{NL}_6)) \\ b_7 &= 1.527 - (1.027 \cdot \cos(L)) + (0.0926 \cdot h) - (0.359 \cdot (\text{sn}_7 / \text{NL}_7)) \\ b_8 &= 1.527 - (1.027 \cdot \cos(L)) + (0.0926 \cdot h) - (0.359 \cdot (\text{sn}_8 / \text{NL}_8)) \\ b_9 &= 1.527 - (1.027 \cdot \cos(L)) + (0.0926 \cdot h) - (0.359 \cdot (\text{sn}_9 / \text{NL}_9)) \\ b_{10} &= 1.527 - (1.027 \cdot \cos(L)) + (0.0926 \cdot h) - (0.359 \cdot (\text{sn}_{10} / \text{NL}_{10})) \\ b_{11} &= 1.527 - (1.027 \cdot \cos(L)) + (0.0926 \cdot h) - (0.359 \cdot (\text{sn}_{11} / \text{NL}_{11})) \\ b_{12} &= 1.527 - (1.027 \cdot \cos(L)) + (0.0926 \cdot h) - (0.359 \cdot (\text{sn}_{12} / \text{NL}_{12})) \end{aligned}$$

{Sunset and sun rise hour angle calculation}

$$\begin{aligned} \text{Omega_ss1} &= \arccos((- \tan(L)) \cdot \tan(\text{delta}_1)) \\ \text{Omega_ss2} &= \arccos((- \tan(L)) \cdot \tan(\text{delta}_2)) \\ \text{Omega_ss3} &= \arccos((- \tan(L)) \cdot \tan(\text{delta}_3)) \\ \text{Omega_ss4} &= \arccos((- \tan(L)) \cdot \tan(\text{delta}_4)) \\ \text{Omega_ss5} &= \arccos((- \tan(L)) \cdot \tan(\text{delta}_5)) \\ \text{Omega_ss6} &= \arccos((- \tan(L)) \cdot \tan(\text{delta}_6)) \\ \text{Omega_ss7} &= \arccos((- \tan(L)) \cdot \tan(\text{delta}_7)) \\ \text{Omega_ss8} &= \arccos((- \tan(L)) \cdot \tan(\text{delta}_8)) \\ \text{Omega_ss9} &= \arccos((- \tan(L)) \cdot \tan(\text{delta}_9)) \\ \text{Omega_ss10} &= \arccos((- \tan(L)) \cdot \tan(\text{delta}_{10})) \\ \text{Omega_ss11} &= \arccos((- \tan(L)) \cdot \tan(\text{delta}_{11})) \\ \text{Omega_ss12} &= \arccos((- \tan(L)) \cdot \tan(\text{delta}_{12})) \end{aligned}$$

{when Omega_ss is in radian}

$$\begin{aligned} \text{Omega_ssrad1} &= \pi / 180 \cdot \arccos((- \tan(L)) \cdot \tan(\text{delta}_1)) \\ \text{Omega_ssrad2} &= \pi / 180 \cdot \arccos((- \tan(L)) \cdot \tan(\text{delta}_2)) \\ \text{Omega_ssrad3} &= \pi / 180 \cdot \arccos((- \tan(L)) \cdot \tan(\text{delta}_3)) \\ \text{Omega_ssrad4} &= \pi / 180 \cdot \arccos((- \tan(L)) \cdot \tan(\text{delta}_4)) \\ \text{Omega_ssrad5} &= \pi / 180 \cdot \arccos((- \tan(L)) \cdot \tan(\text{delta}_5)) \\ \text{Omega_ssrad6} &= \pi / 180 \cdot \arccos((- \tan(L)) \cdot \tan(\text{delta}_6)) \\ \text{Omega_ssrad7} &= \pi / 180 \cdot \arccos((- \tan(L)) \cdot \tan(\text{delta}_7)) \\ \text{Omega_ssrad8} &= \pi / 180 \cdot \arccos((- \tan(L)) \cdot \tan(\text{delta}_8)) \\ \text{Omega_ssrad9} &= \pi / 180 \cdot \arccos((- \tan(L)) \cdot \tan(\text{delta}_9)) \\ \text{Omega_ssrad10} &= \pi / 180 \cdot \arccos((- \tan(L)) \cdot \tan(\text{delta}_{10})) \\ \text{Omega_ssrad11} &= \pi / 180 \cdot \arccos((- \tan(L)) \cdot \tan(\text{delta}_{11})) \\ \text{Omega_ssrad12} &= \pi / 180 \cdot \arccos((- \tan(L)) \cdot \tan(\text{delta}_{12})) \end{aligned}$$

{Calculation of the horizontal terrestrial and horizontal extra-terrestrial radiation levels}

$$G_{sc} = 1367 \quad \{\text{solar constant } W/m^2\}$$

{calculation of extra-terrestrial radiation [H_o]}

$$\begin{aligned} H_{o1} &= ((24 \cdot 3600 \cdot G_{sc}) / \pi) \cdot (1 + 0.33 \cdot \cos(360 \cdot \text{nd}_1 / 365)) \cdot ((\cos(L)) \cdot \cos(\text{delta}_1) \cdot \sin(\text{Omega_ss1})) + ((\pi \cdot \text{Omega_ss1} / 180) \cdot \sin(L) \cdot \sin(\text{delta}_1)) \\ H_{o2} &= ((24 \cdot 3600 \cdot G_{sc}) / \pi) \cdot (1 + 0.33 \cdot \cos(360 \cdot \text{nd}_2 / 365)) \cdot ((\cos(L)) \cdot \cos(\text{delta}_2) \cdot \sin(\text{Omega_ss2})) + ((\pi \cdot \text{Omega_ss2} / 180) \cdot \sin(L) \cdot \sin(\text{delta}_2)) \\ H_{o3} &= ((24 \cdot 3600 \cdot G_{sc}) / \pi) \cdot (1 + 0.33 \cdot \cos(360 \cdot \text{nd}_3 / 365)) \cdot ((\cos(L)) \cdot \cos(\text{delta}_3) \cdot \sin(\text{Omega_ss3})) + ((\pi \cdot \text{Omega_ss3} / 180) \cdot \sin(L) \cdot \sin(\text{delta}_3)) \\ H_{o4} &= ((24 \cdot 3600 \cdot G_{sc}) / \pi) \cdot (1 + 0.33 \cdot \cos(360 \cdot \text{nd}_4 / 365)) \cdot ((\cos(L)) \cdot \cos(\text{delta}_4) \cdot \sin(\text{Omega_ss4})) + ((\pi \cdot \text{Omega_ss4} / 180) \cdot \sin(L) \cdot \sin(\text{delta}_4)) \\ H_{o5} &= ((24 \cdot 3600 \cdot G_{sc}) / \pi) \cdot (1 + 0.33 \cdot \cos(360 \cdot \text{nd}_5 / 365)) \cdot ((\cos(L)) \cdot \cos(\text{delta}_5) \cdot \sin(\text{Omega_ss5})) + ((\pi \cdot \text{Omega_ss5} / 180) \cdot \sin(L) \cdot \sin(\text{delta}_5)) \\ H_{o6} &= ((24 \cdot 3600 \cdot G_{sc}) / \pi) \cdot (1 + 0.33 \cdot \cos(360 \cdot \text{nd}_6 / 365)) \cdot ((\cos(L)) \cdot \cos(\text{delta}_6) \cdot \sin(\text{Omega_ss6})) + ((\pi \cdot \text{Omega_ss6} / 180) \cdot \sin(L) \cdot \sin(\text{delta}_6)) \\ H_{o7} &= ((24 \cdot 3600 \cdot G_{sc}) / \pi) \cdot (1 + 0.33 \cdot \cos(360 \cdot \text{nd}_7 / 365)) \cdot ((\cos(L)) \cdot \cos(\text{delta}_7) \cdot \sin(\text{Omega_ss7})) + ((\pi \cdot \text{Omega_ss7} / 180) \cdot \sin(L) \cdot \sin(\text{delta}_7)) \\ H_{o8} &= ((24 \cdot 3600 \cdot G_{sc}) / \pi) \cdot (1 + 0.33 \cdot \cos(360 \cdot \text{nd}_8 / 365)) \cdot ((\cos(L)) \cdot \cos(\text{delta}_8) \cdot \sin(\text{Omega_ss8})) + ((\pi \cdot \text{Omega_ss8} / 180) \cdot \sin(L) \cdot \sin(\text{delta}_8)) \end{aligned}$$

$$H_{o9} = ((24 \times 3600 \times G_{sc}) / \pi) \times (1 + 0.33 \times \cos(360 \times nd_9 / 365)) \times ((\cos(L) \times \cos(\delta_9) \times \sin(\Omega_{ss9})) + ((\pi \times \Omega_{ss9} / 180) \times \sin(L) \times \sin(\delta_9)))$$

$$H_{o10} = ((24 \times 3600 \times G_{sc}) / \pi) \times (1 + 0.33 \times \cos(360 \times nd_{10} / 365)) \times ((\cos(L) \times \cos(\delta_{10}) \times \sin(\Omega_{ss10})) + ((\pi \times \Omega_{ss10} / 180) \times \sin(L) \times \sin(\delta_{10})))$$

$$H_{o11} = ((24 \times 3600 \times G_{sc}) / \pi) \times (1 + 0.33 \times \cos(360 \times nd_{11} / 365)) \times ((\cos(L) \times \cos(\delta_{11}) \times \sin(\Omega_{ss11})) + ((\pi \times \Omega_{ss11} / 180) \times \sin(L) \times \sin(\delta_{11})))$$

$$H_{o12} = ((24 \times 3600 \times G_{sc}) / \pi) \times (1 + 0.33 \times \cos(360 \times nd_{12} / 365)) \times ((\cos(L) \times \cos(\delta_{12}) \times \sin(\Omega_{ss12})) + ((\pi \times \Omega_{ss12} / 180) \times \sin(L) \times \sin(\delta_{12})))$$

{calculation of intra-terrestrial radiation on horizontal surface H_h }

$$H_{h1} = H_{o2} \times (a_1 + b_1 \times (\sin_1 / NL_1))$$

$$H_{h2} = H_{o2} \times (a_2 + b_2 \times (\sin_2 / NL_2))$$

$$H_{h3} = H_{o3} \times (a_3 + b_3 \times (\sin_3 / NL_3))$$

$$H_{h4} = H_{o4} \times (a_4 + b_4 \times (\sin_4 / NL_4))$$

$$H_{h5} = H_{o5} \times (a_5 + b_5 \times (\sin_5 / NL_5))$$

$$H_{h6} = H_{o6} \times (a_6 + b_6 \times (\sin_6 / NL_6))$$

$$H_{h7} = H_{o7} \times (a_7 + b_7 \times (\sin_7 / NL_7))$$

$$H_{h8} = H_{o8} \times (a_8 + b_8 \times (\sin_8 / NL_8))$$

$$H_{h9} = H_{o9} \times (a_9 + b_9 \times (\sin_9 / NL_9))$$

$$H_{h10} = H_{o10} \times (a_{10} + b_{10} \times (\sin_{10} / NL_{10}))$$

$$H_{h11} = H_{o11} \times (a_{11} + b_{11} \times (\sin_{11} / NL_{11}))$$

$$H_{h12} = H_{o12} \times (a_{12} + b_{12} \times (\sin_{12} / NL_{12}))$$

{calculation of monthly clearness index}

$$K_{T1} = H_{h1} / H_{o1}$$

$$K_{T2} = H_{h2} / H_{o2}$$

$$K_{T3} = H_{h3} / H_{o3}$$

$$K_{T4} = H_{h4} / H_{o4}$$

$$K_{T5} = H_{h5} / H_{o5}$$

$$K_{T6} = H_{h6} / H_{o6}$$

$$K_{T7} = H_{h7} / H_{o7}$$

$$K_{T8} = H_{h8} / H_{o8}$$

$$K_{T9} = H_{h9} / H_{o9}$$

$$K_{T10} = H_{h10} / H_{o10}$$

$$K_{T11} = H_{h11} / H_{o11}$$

$$K_{T12} = H_{h12} / H_{o12}$$

{Monthly Diffuse radiation D_h }

$$D_{h1} = H_{h1} \times (0.775 + 0.347 \times (\Omega_{ssrad1} - \pi/2) - (0.505 + 0.0261 \times (\Omega_{ssrad1} - \pi/2)) \times \cos((2 \times K_{T1}) - 1.8))$$

$$D_{h2} = H_{h2} \times (0.775 + 0.347 \times (\Omega_{ssrad2} - \pi/2) - (0.505 + 0.0261 \times (\Omega_{ssrad2} - \pi/2)) \times \cos((2 \times K_{T2}) - 1.8))$$

$$D_{h3} = H_{h3} \times (0.775 + 0.347 \times (\Omega_{ssrad3} - \pi/2) - (0.505 + 0.0261 \times (\Omega_{ssrad3} - \pi/2)) \times \cos((2 \times K_{T3}) - 1.8))$$

$$D_{h4} = H_{h4} \times (0.775 + 0.347 \times (\Omega_{ssrad4} - \pi/2) - (0.505 + 0.0261 \times (\Omega_{ssrad4} - \pi/2)) \times \cos((2 \times K_{T4}) - 1.8))$$

$$D_{h5} = H_{h5} \times (0.775 + 0.347 \times (\Omega_{ssrad5} - \pi/2) - (0.505 + 0.0261 \times (\Omega_{ssrad5} - \pi/2)) \times \cos((2 \times K_{T5}) - 1.8))$$

$$D_{h6} = H_{h6} \times (0.775 + 0.347 \times (\Omega_{ssrad6} - \pi/2) - (0.505 + 0.0261 \times (\Omega_{ssrad6} - \pi/2)) \times \cos((2 \times K_{T6}) - 1.8))$$

$$D_{h7} = H_{h7} \times (0.775 + 0.347 \times (\Omega_{ssrad7} - \pi/2) - (0.505 + 0.0261 \times (\Omega_{ssrad7} - \pi/2)) \times \cos((2 \times K_{T7}) - 1.8))$$

$$D_{h8} = H_{h8} \times (0.775 + 0.347 \times (\Omega_{ssrad8} - \pi/2) - (0.505 + 0.0261 \times (\Omega_{ssrad8} - \pi/2)) \times \cos((2 \times K_{T8}) - 1.8))$$

$$D_{h9} = H_{h9} \times (0.775 + 0.347 \times (\Omega_{ssrad9} - \pi/2) - (0.505 + 0.0261 \times (\Omega_{ssrad9} - \pi/2)) \times \cos((2 \times K_{T9}) - 1.8))$$

$$D_{h10} = H_{h10} \times (0.775 + 0.347 \times (\Omega_{ssrad10} - \pi/2) - (0.505 + 0.0261 \times (\Omega_{ssrad10} - \pi/2)) \times \cos((2 \times K_{T10}) - 1.8))$$

$$D_{h11} = H_{h11} \times (0.775 + 0.347 \times (\Omega_{ssrad11} - \pi/2) - (0.505 + 0.0261 \times (\Omega_{ssrad11} - \pi/2)) \times \cos((2 \times K_{T11}) - 1.8))$$

$$D_{h12} = H_{h12} \times (0.775 + 0.347 \times (\Omega_{ssrad12} - \pi/2) - (0.505 + 0.0261 \times (\Omega_{ssrad12} - \pi/2)) \times \cos((2 \times K_{T12}) - 1.8))$$

{Calculation of Monthly Average beam component B_h }

$$B_{h1} = H_{h1} - D_{h1}$$

$$B_{h2} = H_{h2} - D_{h2}$$

$$B_{h3} = H_{h3} - D_{h3}$$

$$B_{h4} = H_{h4} - D_{h4}$$

$$B_{h5} = H_{h5} - D_{h5}$$

$$B_{h6} = H_{h6} - D_{h6}$$

$$B_{h7} = H_{h7} - D_{h7}$$

$$B_{h8} = H_{h8} - D_{h8}$$

$$B_{h9} = H_{h9} - D_{h9}$$

$$B_{h10} = H_{h10} - D_{h10}$$

$$B_{h11} = H_{h11} - D_{h11}$$

$$B_{h12} = H_{h12} - D_{h12}$$

{Calculation of Beam, Diffuse and Mixed or ground surface reflected radiation tilt factor due to inclination}

$$\Omega_{sr1} = -\arccos((- \tan(L)) \times \tan(\delta_1))$$

$$\Omega_{sr2} = -\arccos((- \tan(L)) \times \tan(\delta_2))$$

$$\Omega_{sr3} = -\arccos((- \tan(L)) \times \tan(\delta_3))$$

$$\Omega_{sr4} = -\arccos((- \tan(L)) \times \tan(\delta_4))$$

$$\Omega_{sr5} = -\arccos((- \tan(L)) \times \tan(\delta_5))$$

$$\Omega_{sr6} = -\arccos((- \tan(L)) \times \tan(\delta_6))$$

$$\Omega_{sr7} = -\arccos((- \tan(L)) \times \tan(\delta_7))$$

$$\Omega_{sr8} = -\arccos((- \tan(L)) \times \tan(\delta_8))$$

$$\Omega_{sr9} = -\arccos((- \tan(L)) \times \tan(\delta_9))$$

$$\begin{aligned}\Omega_{sr10} &= -\arccos((-\tan(L)) * \tan(\delta_{10})) \\ \Omega_{sr11} &= -\arccos((-\tan(L)) * \tan(\delta_{11})) \\ \Omega_{sr12} &= -\arccos((-\tan(L)) * \tan(\delta_{12}))\end{aligned}$$

$$\begin{aligned}\Omega_{srad1} &= -\arccos((-\tan(L)) * \tan(\delta_1)) * (\pi/180) \\ \Omega_{srad2} &= -\arccos((-\tan(L)) * \tan(\delta_2)) * (\pi/180) \\ \Omega_{srad3} &= -\arccos((-\tan(L)) * \tan(\delta_3)) * (\pi/180) \\ \Omega_{srad4} &= -\arccos((-\tan(L)) * \tan(\delta_4)) * (\pi/180) \\ \Omega_{srad5} &= -\arccos((-\tan(L)) * \tan(\delta_5)) * (\pi/180) \\ \Omega_{srad6} &= -\arccos((-\tan(L)) * \tan(\delta_6)) * (\pi/180) \\ \Omega_{srad7} &= -\arccos((-\tan(L)) * \tan(\delta_7)) * (\pi/180) \\ \Omega_{srad8} &= -\arccos((-\tan(L)) * \tan(\delta_8)) * (\pi/180) \\ \Omega_{srad9} &= -\arccos((-\tan(L)) * \tan(\delta_9)) * (\pi/180) \\ \Omega_{srad10} &= -\arccos((-\tan(L)) * \tan(\delta_{10})) * (\pi/180) \\ \Omega_{srad11} &= -\arccos((-\tan(L)) * \tan(\delta_{11})) * (\pi/180) \\ \Omega_{srad12} &= -\arccos((-\tan(L)) * \tan(\delta_{12})) * (\pi/180)\end{aligned}$$

{Calculation of Radiation tilt factor}
{tilt angle of panel in degree Beta}

$$\begin{aligned}\text{Beta}_1 &= -0.00002 * \delta_1^3 - 0.0009 * \delta_1^2 - 1.0647 * \delta_1 + 33.515 \\ \text{Beta}_2 &= -0.00002 * \delta_2^3 - 0.0009 * \delta_2^2 - 1.0647 * \delta_2 + 33.515 \\ \text{Beta}_3 &= -0.00002 * \delta_3^3 - 0.0009 * \delta_3^2 - 1.0647 * \delta_3 + 33.515 \\ \text{Beta}_4 &= -0.00002 * \delta_4^3 - 0.0009 * \delta_4^2 - 1.0647 * \delta_4 + 33.515 \\ \text{Beta}_5 &= -0.00002 * \delta_5^3 - 0.0009 * \delta_5^2 - 1.0647 * \delta_5 + 33.515 \\ \text{Beta}_6 &= -0.00002 * \delta_6^3 - 0.0009 * \delta_6^2 - 1.0647 * \delta_6 + 33.515 \\ \text{Beta}_7 &= -0.00002 * \delta_7^3 - 0.0009 * \delta_7^2 - 1.0647 * \delta_7 + 33.515 \\ \text{Beta}_8 &= -0.00002 * \delta_8^3 - 0.0009 * \delta_8^2 - 1.0647 * \delta_8 + 33.515 \\ \text{Beta}_9 &= -0.00002 * \delta_9^3 - 0.0009 * \delta_9^2 - 1.0647 * \delta_9 + 33.515 \\ \text{Beta}_{10} &= -0.00002 * \delta_{10}^3 - 0.0009 * \delta_{10}^2 - 1.0647 * \delta_{10} + 33.515 \\ \text{Beta}_{11} &= -0.00002 * \delta_{11}^3 - 0.0009 * \delta_{11}^2 - 1.0647 * \delta_{11} + 33.515 \\ \text{Beta}_{12} &= -0.00002 * \delta_{12}^3 - 0.0009 * \delta_{12}^2 - 1.0647 * \delta_{12} + 33.515\end{aligned}$$

$$\begin{aligned}R_{b1} &= (\cos(L - \text{Beta}_1) * \cos(\delta_1) * \sin(\Omega_{sr1}) + \Omega_{srad1} * \sin(L - \text{Beta}_1) * \sin(\delta_1)) / (\cos(L) * \cos(\delta_1) * \sin(\Omega_{sr1}) + \Omega_{srad1} * \sin(L) * \sin(\delta_1)) \\ R_{b2} &= (\cos(L - \text{Beta}_2) * \cos(\delta_2) * \sin(\Omega_{sr2}) + \Omega_{srad2} * \sin(L - \text{Beta}_2) * \sin(\delta_2)) / (\cos(L) * \cos(\delta_2) * \sin(\Omega_{sr2}) + \Omega_{srad2} * \sin(L) * \sin(\delta_2)) \\ R_{b3} &= (\cos(L - \text{Beta}_3) * \cos(\delta_3) * \sin(\Omega_{sr3}) + \Omega_{srad3} * \sin(L - \text{Beta}_3) * \sin(\delta_3)) / (\cos(L) * \cos(\delta_3) * \sin(\Omega_{sr3}) + \Omega_{srad3} * \sin(L) * \sin(\delta_3)) \\ R_{b4} &= (\cos(L - \text{Beta}_4) * \cos(\delta_4) * \sin(\Omega_{sr4}) + \Omega_{srad4} * \sin(L - \text{Beta}_4) * \sin(\delta_4)) / (\cos(L) * \cos(\delta_4) * \sin(\Omega_{sr4}) + \Omega_{srad4} * \sin(L) * \sin(\delta_4)) \\ R_{b5} &= (\cos(L - \text{Beta}_5) * \cos(\delta_5) * \sin(\Omega_{sr5}) + \Omega_{srad5} * \sin(L - \text{Beta}_5) * \sin(\delta_5)) / (\cos(L) * \cos(\delta_5) * \sin(\Omega_{sr5}) + \Omega_{srad5} * \sin(L) * \sin(\delta_5)) \\ R_{b6} &= (\cos(L - \text{Beta}_6) * \cos(\delta_6) * \sin(\Omega_{sr6}) + \Omega_{srad6} * \sin(L - \text{Beta}_6) * \sin(\delta_6)) / (\cos(L) * \cos(\delta_6) * \sin(\Omega_{sr6}) + \Omega_{srad6} * \sin(L) * \sin(\delta_6)) \\ R_{b7} &= (\cos(L - \text{Beta}_7) * \cos(\delta_7) * \sin(\Omega_{sr7}) + \Omega_{srad7} * \sin(L - \text{Beta}_7) * \sin(\delta_7)) / (\cos(L) * \cos(\delta_7) * \sin(\Omega_{sr7}) + \Omega_{srad7} * \sin(L) * \sin(\delta_7)) \\ R_{b8} &= (\cos(L - \text{Beta}_8) * \cos(\delta_8) * \sin(\Omega_{sr8}) + \Omega_{srad8} * \sin(L - \text{Beta}_8) * \sin(\delta_8)) / (\cos(L) * \cos(\delta_8) * \sin(\Omega_{sr8}) + \Omega_{srad8} * \sin(L) * \sin(\delta_8)) \\ R_{b9} &= (\cos(L - \text{Beta}_9) * \cos(\delta_9) * \sin(\Omega_{sr9}) + \Omega_{srad9} * \sin(L - \text{Beta}_9) * \sin(\delta_9)) / (\cos(L) * \cos(\delta_9) * \sin(\Omega_{sr9}) + \Omega_{srad9} * \sin(L) * \sin(\delta_9)) \\ R_{b10} &= (\cos(L - \text{Beta}_{10}) * \cos(\delta_{10}) * \sin(\Omega_{sr10}) + \Omega_{srad10} * \sin(L - \text{Beta}_{10}) * \sin(\delta_{10})) / (\cos(L) * \cos(\delta_{10}) * \sin(\Omega_{sr10}) + \Omega_{srad10} * \sin(L) * \sin(\delta_{10})) \\ R_{b11} &= (\cos(L - \text{Beta}_{11}) * \cos(\delta_{11}) * \sin(\Omega_{sr11}) + \Omega_{srad11} * \sin(L - \text{Beta}_{11}) * \sin(\delta_{11})) / (\cos(L) * \cos(\delta_{11}) * \sin(\Omega_{sr11}) + \Omega_{srad11} * \sin(L) * \sin(\delta_{11})) \\ R_{b12} &= (\cos(L - \text{Beta}_{12}) * \cos(\delta_{12}) * \sin(\Omega_{sr12}) + \Omega_{srad12} * \sin(L - \text{Beta}_{12}) * \sin(\delta_{12})) / (\cos(L) * \cos(\delta_{12}) * \sin(\Omega_{sr12}) + \Omega_{srad12} * \sin(L) * \sin(\delta_{12}))\end{aligned}$$

$$\begin{aligned}R_{d1} &= (1 + \cos(\text{Beta}_1)) / 2 \\ R_{d2} &= (1 + \cos(\text{Beta}_2)) / 2 \\ R_{d3} &= (1 + \cos(\text{Beta}_3)) / 2 \\ R_{d4} &= (1 + \cos(\text{Beta}_4)) / 2 \\ R_{d5} &= (1 + \cos(\text{Beta}_5)) / 2 \\ R_{d6} &= (1 + \cos(\text{Beta}_6)) / 2 \\ R_{d7} &= (1 + \cos(\text{Beta}_7)) / 2 \\ R_{d8} &= (1 + \cos(\text{Beta}_8)) / 2 \\ R_{d9} &= (1 + \cos(\text{Beta}_9)) / 2 \\ R_{d10} &= (1 + \cos(\text{Beta}_{10})) / 2 \\ R_{d11} &= (1 + \cos(\text{Beta}_{11})) / 2 \\ R_{d12} &= (1 + \cos(\text{Beta}_{12})) / 2 \\ \text{roh} &= 0.2 \text{ {diffuse reflectance for grass and concrete surface when solar panel is monted near the ground}} \\ R_{r1} &= (\text{roh} * (1 - \cos(\text{Beta}_1))) / 2 \\ R_{r2} &= (\text{roh} * (1 - \cos(\text{Beta}_2))) / 2 \\ R_{r3} &= (\text{roh} * (1 - \cos(\text{Beta}_3))) / 2\end{aligned}$$

$$\begin{aligned}R_{r4}&=(\rho_h*(1-\cos(\text{Beta}_4)))/2 \\R_{r5}&=(\rho_h*(1-\cos(\text{Beta}_5)))/2 \\R_{r6}&=(\rho_h*(1-\cos(\text{Beta}_6)))/2 \\R_{r7}&=(\rho_h*(1-\cos(\text{Beta}_7)))/2 \\R_{r8}&=(\rho_h*(1-\cos(\text{Beta}_8)))/2 \\R_{r9}&=(\rho_h*(1-\cos(\text{Beta}_9)))/2 \\R_{r10}&=(\rho_h*(1-\cos(\text{Beta}_{10}))/2 \\R_{r11}&=(\rho_h*(1-\cos(\text{Beta}_{11}))/2 \\R_{r12}&=(\rho_h*(1-\cos(\text{Beta}_{12}))/2\end{aligned}$$

{Calculation of the Long term beam, Diffuse and Diffuse-reflected radiation component on tilted surface}

$$\begin{aligned}B_{c1}&=R_{b1}*B_{h1} \\B_{c2}&=R_{b2}*B_{h2} \\B_{c3}&=R_{b3}*B_{h3} \\B_{c4}&=R_{b4}*B_{h4} \\B_{c5}&=R_{b5}*B_{h5} \\B_{c6}&=R_{b6}*B_{h6} \\B_{c7}&=R_{b7}*B_{h7} \\B_{c8}&=R_{b8}*B_{h8} \\B_{c9}&=R_{b9}*B_{h9} \\B_{c10}&=R_{b10}*B_{h10} \\B_{c11}&=R_{b11}*B_{h11} \\B_{c12}&=R_{b12}*B_{h12}\end{aligned}$$

$$\begin{aligned}D_{c1}&=R_{d1}*D_{h1} \\D_{c2}&=R_{d2}*D_{h2} \\D_{c3}&=R_{d3}*D_{h3} \\D_{c4}&=R_{d4}*D_{h4} \\D_{c5}&=R_{d5}*D_{h5} \\D_{c6}&=R_{d6}*D_{h6} \\D_{c7}&=R_{d7}*D_{h7} \\D_{c8}&=R_{d8}*D_{h8} \\D_{c9}&=R_{d9}*D_{h9} \\D_{c10}&=R_{d10}*D_{h10} \\D_{c11}&=R_{d11}*D_{h11} \\D_{c12}&=R_{d12}*D_{h12}\end{aligned}$$

$$\begin{aligned}Dr_1&=R_{r1}*(D_{h1}+B_{h1}) \\Dr_2&=R_{r2}*(D_{h2}+B_{h2}) \\Dr_3&=R_{r3}*(D_{h3}+B_{h3}) \\Dr_4&=R_{r4}*(D_{h4}+B_{h4}) \\Dr_5&=R_{r5}*(D_{h5}+B_{h5}) \\Dr_6&=R_{r6}*(D_{h6}+B_{h6}) \\Dr_7&=R_{r7}*(D_{h7}+B_{h7}) \\Dr_8&=R_{r8}*(D_{h8}+B_{h8}) \\Dr_9&=R_{r9}*(D_{h9}+B_{h9}) \\Dr_{10}&=R_{r10}*(D_{h10}+B_{h10}) \\Dr_{11}&=R_{r11}*(D_{h11}+B_{h11}) \\Dr_{12}&=R_{r12}*(D_{h12}+B_{h12})\end{aligned}$$

{Total irradiation on tilted surface in MJ/m²/day}

$$\begin{aligned}H_{c1}&=(B_{c1}+D_{c1}+Dr_1)/10^6 \\H_{c2}&=(B_{c2}+D_{c2}+Dr_2)/10^6 \\H_{c3}&=(B_{c3}+D_{c3}+Dr_3)/10^6 \\H_{c4}&=(B_{c4}+D_{c4}+Dr_4)/10^6 \\H_{c5}&=(B_{c5}+D_{c5}+Dr_5)/10^6 \\H_{c6}&=(B_{c6}+D_{c6}+Dr_6)/10^6 \\H_{c7}&=(B_{c7}+D_{c7}+Dr_7)/10^6 \\H_{c8}&=(B_{c8}+D_{c8}+Dr_8)/10^6 \\H_{c9}&=(B_{c9}+D_{c9}+Dr_9)/10^6 \\H_{c10}&=(B_{c10}+D_{c10}+Dr_{10})/10^6 \\H_{c11}&=(B_{c11}+D_{c11}+Dr_{11})/10^6 \\H_{c12}&=(B_{c12}+D_{c12}+Dr_{12})/10^6\end{aligned}$$

{Assumed values based on LONGi solar panel type}

$$\begin{aligned}Q_{deg}&=0.9035 \quad \{\text{module degradation co-efficient}\} \\C_{Temp}&=-0.35 \quad \{\text{temperature co-efficient for } P_{max} \text{ \%/degree celcius}\} \\T_{NOCT}&=293 \quad \{\text{Nominal Operating cell temperature in K}\} \\U_o&=30.2 \quad \{\text{is the constant heat transfer coefficient } W/m^2.K\} \\U_1&=6.28 \quad \{\text{is the wind speed coefficient of heat transfer } Ws/m^3.K\} \\Eta_r&=0.192 \quad \{\text{Refrence efficiency of the panel}\} \\P_{STC}&=350 \quad \{\text{standard testing condition power in W}\} \\G_{STC}&=1000 \quad \{\text{is the irradiance at the standard test condition } W/m^2\} \\Tau&=0.9 \quad \{\text{transmissivity of the galss assumed to be 90 \% from literature}\} \\A&=1.823 \quad \{\text{Area of Longi solar panel in } m^2 \text{ where dimension is } 1.755 \text{ m x } 1.038 \text{ m}\}\end{aligned}$$

{The maximum monthly ambient temperature of study area in Kelvin }

T_a1=23.1+273
 T_a2=24.2+273
 T_a3=24.7+273
 T_a4=25.2+273
 T_a5=23.8+273
 T_a6=22.7+273
 T_a7=18.7+273
 T_a8=18.30+273
 T_a9=20.0+273
 T_a10=21.50+273
 T_a11=21.2+273
 T_a12=21.7+273
 T_aMean=22.09+273

{Montly solar irradiation of the study area in W/m²}

H_cMean=311.82

{Monthly average Wind speed in m/s }

v_m1=6.12*(10/36)
 v_m2=6.12*(10/36)
 v_m3=6.12*(10/36)
 v_m4=6.12*(10/36)
 v_m5=6.12*(10/36)
 v_m6=4.68*(10/36)
 v_m7=4.32*(10/36)
 v_m8=4.32*(10/36)
 v_m9=5.76*(10/36)
 v_m10=7.92*(10/36)
 v_m11=7.92*(10/36)
 v_m12=6.12*(10/36)
 v_Mean=5.97*(10/36)

{The Operating temperature of the cell in degree celcius}

T_c1=(T_a1+(H_c1/(U_o+(U_1*v_m1))))-273
 T_c2=(T_a2+(H_c1/(U_o+(U_1*v_m2))))-273
 T_c3=(T_a3+(H_c1/(U_o+(U_1*v_m3))))-273
 T_c4=(T_a4+(H_c1/(U_o+(U_1*v_m4))))-273
 T_c5=(T_a5+(H_c1/(U_o+(U_1*v_m5))))-273
 T_c6=(T_a6+(H_c1/(U_o+(U_1*v_m6))))-273
 T_c7=(T_a7+(H_c1/(U_o+(U_1*v_m7))))-273
 T_c8=(T_a8+(H_c1/(U_o+(U_1*v_m8))))-273
 T_c9=(T_a9+(H_c1/(U_o+(U_1*v_m9))))-273
 T_c10=(T_a10+(H_c1/(U_o+(U_1*v_m10))))-273
 T_c11=(T_a11+(H_c1/(U_o+(U_1*v_m11))))-273
 T_c12=(T_a12+(H_c1/(U_o+(U_1*v_m12))))-273
 T_cMean=(T_aMean+(H_cMean/(U_o+(U_1*v_Mean))))-273

{Loss Calculation due to Temperature }

P_Tloss1=P_STC*(H_c1/G_STC)*Q_deg*C_Temp*(25-T_c1)
 P_Tloss2=P_STC*(H_c2/G_STC)*Q_deg*C_Temp*(25-T_c2)
 P_Tloss3=P_STC*(H_c3/G_STC)*Q_deg*C_Temp*(25-T_c3)
 P_Tloss4=P_STC*(H_c4/G_STC)*Q_deg*C_Temp*(25-T_c4)
 P_Tloss5=P_STC*(H_c5/G_STC)*Q_deg*C_Temp*(25-T_c5)
 P_Tloss6=P_STC*(H_c6/G_STC)*Q_deg*C_Temp*(25-T_c6)
 P_Tloss7=P_STC*(H_c7/G_STC)*Q_deg*C_Temp*(25-T_c7)
 P_Tloss8=P_STC*(H_c8/G_STC)*Q_deg*C_Temp*(25-T_c8)
 P_Tloss9=P_STC*(H_c9/G_STC)*Q_deg*C_Temp*(25-T_c9)
 P_Tloss10=P_STC*(H_c10/G_STC)*Q_deg*C_Temp*(25-T_c10)
 P_Tloss11=P_STC*(H_c11/G_STC)*Q_deg*C_Temp*(25-T_c11)
 P_Tloss12=P_STC*(H_c12/G_STC)*Q_deg*C_Temp*(25-T_c12)
 P_TlossMean=P_STC*(H_cMean/G_STC)*Q_deg*C_Temp*(25-T_cMean)

{Loss of the pannel due to temperature}

Temp_Loss1=P_STC+P_Tloss1
 Temp_Loss2=P_STC+P_Tloss2
 Temp_Loss3=P_STC+P_Tloss3
 Temp_Loss4=P_STC+P_Tloss4
 Temp_Loss5=P_STC+P_Tloss5
 Temp_Loss6=P_STC+P_Tloss6
 Temp_Loss7=P_STC+P_Tloss7
 Temp_Loss8=P_STC+P_Tloss8
 Temp_Loss9=P_STC+P_Tloss9
 Temp_Loss10=P_STC+P_Tloss10
 Temp_Loss11=P_STC+P_Tloss11
 Temp_Loss12=P_STC+P_Tloss12

$$\text{Temp_LossMean} = P_STC + P_TlossMean$$

{Loss percentage of the pannel due to temperature}

$$\text{Loss_percent1} = (P_Tloss1 * 100) / P_STC * (0-1)$$

$$\text{Loss_percent2} = (P_Tloss2 * 100) / P_STC * (0-1)$$

$$\text{Loss_percent3} = (P_Tloss3 * 100) / P_STC$$

$$\text{Loss_percent4} = (P_Tloss4 * 100) / P_STC$$

$$\text{Loss_percent5} = (P_Tloss5 * 100) / P_STC * (0-1)$$

$$\text{Loss_percent6} = (P_Tloss6 * 100) / P_STC * (0-1)$$

$$\text{Loss_percent7} = (P_Tloss7 * 100) / P_STC * (0-1)$$

$$\text{Loss_percent8} = (P_Tloss8 * 100) / P_STC * (0-1)$$

$$\text{Loss_percent9} = (P_Tloss9 * 100) / P_STC * (0-1)$$

$$\text{Loss_percent10} = (P_Tloss10 * 100) / P_STC * (0-1)$$

$$\text{Loss_percent11} = (P_Tloss11 * 100) / P_STC * (0-1)$$

$$\text{Loss_percent12} = (P_Tloss12 * 100) / P_STC * (0-1)$$

$$\text{Loss_percentMean} = (\text{Temp_LossMean} * 100) / P_STC * (0-1)$$

Unit Settings: SI C kPa kJ mass deg

A = 1.823	a ₁ = 0.2733	a ₁₀ = 0.2539	a ₁₁ = 0.2728	a ₁₂ = 0.2634	a ₂ = 0.2565	a ₃ = 0.2398
a ₄ = 0.2417	a ₅ = 0.2372	a ₆ = 0.2021	a ₇ = 0.1795	a ₈ = 0.1934	a ₉ = 0.2467	β ₁ = 55.57
β ₁₀ = 43.67	β ₁₁ = 53.46	β ₁₂ = 57.82	β ₂ = 47.2	β ₃ = 36.08	β ₄ = 23.39	β ₅ = 13.06
β ₆ = 8.21	β ₇ = 10.37	β ₈ = 18.98	β ₉ = 31.15	b ₁ = 0.4863	b ₁₀ = 0.5103	b ₁₁ = 0.4869
b ₁₂ = 0.4985	b ₂ = 0.5071	b ₃ = 0.5277	b ₄ = 0.5254	b ₅ = 0.531	b ₆ = 0.5744	b ₇ = 0.6024
b ₈ = 0.5852	b ₉ = 0.5193	B _{c1} = 2.660E+07	B _{c10} = 2.111E+07	B _{c11} = 2.406E+07	B _{c12} = 2.430E+07	B _{c2} = 2.181E+07
B _{c3} = 1.915E+07	B _{c4} = 1.843E+07	B _{c5} = 1.822E+07	B _{c6} = 1.604E+07	B _{c7} = 1.401E+07	B _{c8} = 1.491E+07	B _{c9} = 1.917E+07
B _{h1} = 2.132E+07	B _{h10} = 2.041E+07	B _{h11} = 2.002E+07	B _{h12} = 1.869E+07	B _{h2} = 2.007E+07	B _{h3} = 2.019E+07	B _{h4} = 2.090E+07
B _{h5} = 2.037E+07	B _{h6} = 1.740E+07	B _{h7} = 1.543E+07	B _{h8} = 1.695E+07	B _{h9} = 2.103E+07	C _{Temp} = -0.35	δ ₁ = -20.92
δ ₁₀ = -9.599	δ ₁₁ = -18.91	δ ₁₂ = -23.05	δ ₂ = -12.95	δ ₃ = -2.418	δ ₄ = 9.415	δ ₅ = 18.79
δ ₆ = 23.09	δ ₇ = 21.18	δ ₈ = 13.45	δ ₉ = 2.217	Dr ₁ = 1.234E+06	Dr ₁₀ = 764022	Dr ₁₁ = 1.082E+06
Dr ₁₂ = 1.160E+06	Dr ₂ = 866447	Dr ₃ = 529079	Dr ₄ = 238362	Dr ₅ = 74014	Dr ₆ = 25231	Dr ₇ = 35530
Dr ₈ = 128542	Dr ₉ = 416609	D _{c1} = 5.539E+06	D _{c10} = 6.206E+06	D _{c11} = 5.362E+06	D _{c12} = 4.694E+06	D _{c2} = 5.845E+06
D _{c3} = 6.675E+06	D _{c4} = 7.759E+06	D _{c5} = 8.154E+06	D _{c6} = 7.183E+06	D _{c7} = 6.286E+06	D _{c8} = 6.512E+06	D _{c9} = 7.296E+06
D _{h1} = 7.077E+06	D _{h10} = 7.203E+06	D _{h11} = 6.722E+06	D _{h12} = 6.126E+06	D _{h2} = 6.960E+06	D _{h3} = 7.384E+06	D _{h4} = 8.091E+06
D _{h5} = 8.261E+06	D _{h6} = 7.220E+06	D _{h7} = 6.337E+06	D _{h8} = 6.694E+06	D _{h9} = 7.863E+06	η _r = 0.192	G _{sc} = 1367
G _{STC} = 1000	h = 2.581	H _{c1} = 33.38	H _{c10} = 28.08	H _{c11} = 30.51	H _{c12} = 30.16	H _{c2} = 28.52
H _{c3} = 26.36	H _{c4} = 26.42	H _{c5} = 26.45	H _{c6} = 23.25	H _{c7} = 20.33	H _{c8} = 21.55	H _{c9} = 26.88
H _{cMean} = 311.8	H _{h1} = 2.840E+07	H _{h10} = 2.761E+07	H _{h11} = 2.674E+07	H _{h12} = 2.482E+07	H _{h2} = 2.703E+07	H _{h3} = 2.758E+07
H _{h4} = 2.900E+07	H _{h5} = 2.863E+07	H _{h6} = 2.462E+07	H _{h7} = 2.177E+07	H _{h8} = 2.365E+07	H _{h9} = 2.889E+07	H _{o1} = 4.102E+07
H _{o10} = 4.606E+07	H _{o11} = 4.216E+07	H _{o12} = 4.019E+07	H _{o2} = 4.472E+07	H _{o3} = 4.825E+07	H _{o4} = 5.038E+07	H _{o5} = 5.056E+07
H _{o6} = 5.039E+07	H _{o7} = 5.027E+07	H _{o8} = 5.056E+07	H _{o9} = 4.936E+07	K _{T1} = 0.6923	K _{T10} = 0.5996	K _{T11} = 0.6343
K _{T12} = 0.6174	K _{T2} = 0.6045	K _{T3} = 0.5716	K _{T4} = 0.5755	K _{T5} = 0.5663	K _{T6} = 0.4886	K _{T7} = 0.433
K _{T8} = 0.4677	K _{T9} = 0.5854	L = 9.62	Loss _{percent1} = 1.144	Loss _{percent10} = 2.435	Loss _{percent11} = 2.934	Loss _{percent12} = 2.368

Losspercent2= -0.0149	Losspercent3= 0.4305	Losspercent4= 0.8493	Losspercent5= 0.3207	Losspercent6= 1.051	Losspercent7= 3.482	Losspercent8= 3.964
Losspercent9= 3.545	LosspercentMean= -147	LST ₁ = 12	LST ₂ = 18	nd ₁ = 17	nd ₁₀ = 15	nd ₁₁ = 14
nd ₁₂ = 10	nd ₂ = 16	nd ₃ = 16	nd ₄ = 15	nd ₅ = 15	nd ₆ = 11	nd ₇ = 17
nd ₈ = 16	nd ₉ = 15	NL ₁ = 11.5	NL ₁₀ = 11.78	NL ₁₁ = 11.56	NL ₁₂ = 11.45	NL ₂ = 11.7
NL ₃ = 11.95	NL ₄ = 12.21	NL ₅ = 12.44	NL ₆ = 12.55	NL ₇ = 12.5	NL ₈ = 12.31	NL ₉ = 12.05
N ₁ = 17	N ₁₀ = 288	N ₁₁ = 318	N ₁₂ = 344	N ₂ = 47	N ₃ = 75	N ₄ = 105
N ₅ = 135	N ₆ = 162	N ₇ = 198	N ₈ = 228	N ₉ = 258	ω _{sr1} = -86.29	ω _{sr10} = -88.36
ω _{sr11} = -86.67	ω _{sr12} = -85.86	ω _{sr2} = -87.77	ω _{sr3} = -89.59	ω _{sr4} = -91.61	ω _{sr5} = -93.31	ω _{sr6} = -94.14
ω _{sr7} = -93.77	ω _{sr8} = -92.32	ω _{sr9} = -90.38	ω _{srad1} = -1.506	ω _{srad10} = -1.542	ω _{srad11} = -1.513	ω _{srad12} = -1.499
ω _{srad2} = -1.532	ω _{srad3} = -1.564	ω _{srad4} = -1.599	ω _{srad5} = -1.629	ω _{srad6} = -1.643	ω _{srad7} = -1.637	ω _{srad8} = -1.611
ω _{srad9} = -1.577	ω _{ss1} = 86.29	ω _{ss10} = 88.36	ω _{ss11} = 86.67	ω _{ss12} = 85.86	ω _{ss2} = 87.77	ω _{ss3} = 89.59
ω _{ss4} = 91.61	ω _{ss5} = 93.31	ω _{ss6} = 94.14	ω _{ss7} = 93.77	ω _{ss8} = 92.32	ω _{ss9} = 90.38	ω _{ssrad1} = 1.506
ω _{ssrad10} = 1.542	ω _{ssrad11} = 1.513	ω _{ssrad12} = 1.499	ω _{ssrad2} = 1.532	ω _{ssrad3} = 1.564	ω _{ssrad4} = 1.599	ω _{ssrad5} = 1.629
ω _{ssrad6} = 1.643	ω _{ssrad7} = 1.637	ω _{ssrad8} = 1.611	ω _{ssrad9} = 1.577	P _{STC} = 350	P _{Tloss1} = -4.002	P _{Tloss10} = -8.522
P _{Tloss11} = -10.27	P _{Tloss12} = -8.29	P _{Tloss2} = 0.05214	P _{Tloss3} = 1.507	P _{Tloss4} = 2.973	P _{Tloss5} = -1.123	P _{Tloss6} = -3.679
P _{Tloss7} = -12.19	P _{Tloss8} = -13.87	P _{Tloss9} = -12.41	P _{TlossMean} = 164.5	Q _{deg} = 0.9035	roh = 0.2	R _{b1} = 1.248
R _{b10} = 1.034	R _{b11} = 1.202	R _{b12} = 1.3	R _{b2} = 1.087	R _{b3} = 0.9484	R _{b4} = 0.8814	R _{b5} = 0.8945
R _{b6} = 0.9218	R _{b7} = 0.908	R _{b8} = 0.8796	R _{b9} = 0.9113	R _{d1} = 0.7827	R _{d10} = 0.8617	R _{d11} = 0.7977
R _{d12} = 0.7663	R _{d2} = 0.8397	R _{d3} = 0.9041	R _{d4} = 0.9589	R _{d5} = 0.9871	R _{d6} = 0.9949	R _{d7} = 0.9918
R _{d8} = 0.9728	R _{d9} = 0.9279	R _{r1} = 0.04347	R _{r10} = 0.02767	R _{r11} = 0.04047	R _{r12} = 0.04675	R _{r2} = 0.03206
R _{r3} = 0.01918	R _{r4} = 0.008221	R _{r5} = 0.002585	R _{r6} = 0.001025	R _{r7} = 0.001632	R _{r8} = 0.005436	R _{r9} = 0.01442
sn ₁ = 8.56	sn ₁₀ = 7.98	sn ₁₁ = 8.58	sn ₁₂ = 8.13	sn ₂ = 8.03	sn ₃ = 7.51	sn ₄ = 7.76
sn ₅ = 7.71	sn ₆ = 6.26	sn ₇ = 5.26	sn ₈ = 5.77	sn ₉ = 7.86	τ = 0.9	TempLoss ₁ = 346

TempLoss10 = 341.5	TempLoss11 = 339.7	TempLoss12 = 341.7	TempLoss2 = 350.1	TempLoss3 = 351.5	TempLoss4 = 353	TempLoss5 = 348.9
TempLoss6 = 346.3	TempLoss7 = 337.8	TempLoss8 = 336.1	TempLoss9 = 337.6	TempLossMean = 514.5	T _{a1} = 296.1	T _{a10} = 294.5
T _{a11} = 294.2	T _{a12} = 294.7	T _{a2} = 297.2	T _{a3} = 297.7	T _{a4} = 298.2	T _{a5} = 296.8	T _{a6} = 295.7
T _{a7} = 291.7	T _{a8} = 291.3	T _{a9} = 293	T _{aMean} = 295.1	T _{c1} = 23.92	T _{c10} = 22.26	T _{c11} = 21.96
T _{c12} = 22.52	T _{c2} = 25.02	T _{c3} = 25.52	T _{c4} = 26.02	T _{c5} = 24.62	T _{c6} = 23.57	T _{c7} = 19.58
T _{c8} = 19.18	T _{c9} = 20.83	T _{cMean} = 29.77	T _{NOCT} = 293	U ₁ = 6.28	U _o = 30.2	v _{m1} = 1.7
v _{m10} = 2.2	v _{m11} = 2.2	v _{m12} = 1.7	v _{m2} = 1.7	v _{m3} = 1.7	v _{m4} = 1.7	v _{m5} = 1.7
v _{m6} = 1.3	v _{m7} = 1.2	v _{m8} = 1.2	v _{m9} = 1.6	v _{Mean} = 1.658	W ₁ = 0	W ₂ = 90

156 potential unit problems were detected.

Check Units

Calculation time = .0 sec.